The Dissertation Committee for John Yang Certifies that this is the approved version of the following dissertation:

Pharmacokinetics and Cytoprotective Evaluation of Caffeic Acid Phenethyl Amide and Fluorinated Derivatives Against Oxidative Stress

Committee:

Salomon Stavchansky, Supervisor

Phillip D. Bowman

Sean M. Kerwin

Robert O. Williams III

James W. McGinity

Pharmacokinetics and Cytoprotective Evaluation of Caffeic Acid Phenethyl Amide and Fluorinated Derivatives Against Oxidative Stress

by

John Yang, B.S. Bioch.

Dissertation

Presented to the Faculty of the GraduateSchool of

The University of Texas at Austin

in Partial Fulfillment

of the Requirements

for the Degree of

Doctor of Philosophy

The University of Texas at Austin

December 2012

Dedication

To my family

Acknowledgements

I would like to acknowledge and thank my advising professor Dr. Salomon Stavchansky for his guidance as a mentor. I am extremely grateful for his teachings as well as his sharing of his knowledge and experiences; these are lessons that I will remember and carry with me long after I have completed my studies. I would also like to thank Dr. Phillip Bowman for his support and advice. I received considerable amounts of training from him in cell and molecular biology, but more importantly he taught me to think critically and approach problems in different ways. I am also grateful for the guidance of Dr. Sean M. Kerwin, who had the patience to mentor me, a student with no initial organic chemistry background, through an entire synthesis project. I am thankful for the help and support of my committee members Dr. Robert O. Williams III and Dr. James W. McGinity as well. Their valuable advice during my qualifying exam and their review of this dissertation is very much appreciated. I would also like to thank former and current staff members of the College of Pharmacy, namely Mickie Sheppard, Stephanie Crouch and Yolanda Abasta, for their assistance in various matters throughout my graduate studies. I would also like to acknowledge my colleagues. I am thankful for the friendship and advice of Ashish Rastogi, who taught me about the finer points in graduate study. Thanks to James Bynum and Adam Meledeo as well for their assistance in showing me how to use nearly every piece of lab equipment I know how to operate today. Lastly I would like to thank my family for their love, support and encouragement throughout this process.

Pharmacokinetics and Cytoprotective Evaluation of Caffeic Acid Phenethyl Amide and Fluorinated Derivatives Against Oxidative Stress

John Yang, Ph.D.

The University of Texas at Austin, 2012

Supervisor: Salomon Stavchansky

Ischemic injury occurs when the flow of blood is reduced or blocked to an area of the body and can cause significant tissue damage by generation of reactive oxygen species (ROS), activation of apoptotic pathways and through induction of the inflammatory response. Restoration of blood flow and reperfusion of the blocked site, while essential, can generate a second injury that itself needs to be controlled. Together the two injuries are termed ischemia/reperfusion (I/R) injury. This type of injury is frequently encountered in medicine and is a major medical problem. Therapeutic strategies to combat I/R injury include the introduction of compounds that can scavenge ROS or can induce metabolic pathways with the effect of inhibiting apoptosis. Caffeic Acid Phenethyl Ester (CAPE), a polyphenolic compound found in propolis, has been shown to protect a variety of cells types against ROS in vitro and has also been shown to induce a variety of genes including hemeoxygenase 1 (HMOX-1) , an enzyme that has been implicated in a cytoprotective pathway. Despite showing significant cytoprotection

of cells against oxidant stress in vitro, CAPE is readily hydrolyzed in plasma and is also quickly removed from circulation. This result may explain the limited cytoprotective effects of CAPE in vivo. We have synthesized a series of CAPE amide derivatives, including Caffeic Acid Phenethyl Amide (CAPA), with the aim of improving CAPE's stability properties while maintaining the cytoprotective effects of the parent compound. We found that CAPA, in addition to 2 other amide derivatives, were able to protect human umbilical vein endothelial cells (HUVEC) against ROS to a similar degree as CAPE. In addition, we have observed significant improvement in plasma stability of CAPA over CAPE at multiple temperatures. The elimination half-life of CAPA from the systemic circulation was also seen to be significantly improved over CAPE following intravenous administration to male Sprague-Dawley rats. The longer residence time of CAPA over CAPE in circulation may potentially result in greater cytoprotection *in vivo*.

Table of Contents

List of Tables

List of Figures

Statement of Objectives and Significance of Research

Ischemia reperfusion (I/R) injury describes a dysfunctional physiological state that results from tissue hypoxia followed by reoxygenation. I/R injury can manifest following a variety of routine surgical procedures and is a broad underlying mechanism of cellular damage in a number of conditions including cardiovascular disease. Clinical implications of I/R injury are diverse and can include reperfusion arrhythmia, impairment of brain function, or systemic inflammatory response syndrome that may progress to multiple organ dysfunction syndrome. A large body of experimental data supports the claim that reactive oxygen species (ROS) produced during reperfusion play a significant role in the development of I/R injury. Radical scavengers and antioxidants have been administered in attempts to ameliorate the damage caused by I/R injury with varying degrees of success in animal models. One such compound is Caffeic Acid Phenethyl Ester (CAPE), which has been found to reduce the effects of I/R when administered pre injury in rats and rabbits. CAPE is also cited to have numerous other beneficial effects including antioxidant, anti-viral, anti-inflammatory and immuno-modulatory activities. It was also shown however that CAPE is quickly hydrolyzed *in vitro* and removed rapidly from the circulation *in vivo*. If the half-life of CAPE in the circulation were to be significantly increased without compromising the desirable activities of the compound, the beneficial effects of CAPE might be extended and/or improved. This dissertation is a summary of research activities aimed at structurally altering CAPE such that *in vitro* stability and *in vivo* half-life would be significantly increased while maintaining the cytoprotective properties of CAPE. Listed below are the specific objectives followed during the course of this research project.

1) Synthesize an amide derivative of CAPE, Caffeic Acid Phenethyl Amide (CAPA), along with five additional fluorinated amide analogues.

2) Develop a cytoprotection assay against oxidative stress using human umbilical vein endothelial cells (HUVEC) to compare the protective activities of CAPE with the newly synthesized analogues.

3) Attempt to establish structure activity relationships between the CAPA derivatives and cytoprotective activity against oxidative stress

4) Investigate the chemical stability of CAPE and CAPA in rat plasma to determine whether amide derivatization increased *in vitro* stability.

5) Develop a liquid chromatography mass spectrometry (LCMS) method for the quantitative determination of CAPE and CAPA in blood plasma.

6) Characterize the pharmacokinetic profile of CAPE and CAPA in male Sprague-Dawley rats following intravenous bolus to see whether derivatization improved *in vivo* half-life

Chapter 1 – Background and Literature Review

1.1 – Mechanism of Ischemia / Reperfusion Injury

Ischemia is characterized by hypoperfusion of vascular beds resulting in a shortage of oxygen and other nutrients being supplied to the tissues as well as the accumulation of waste products and is an underlying pathological event in a variety of clinical conditions including cardiovascular disease, the global leading cause of death [1-2]. As a function of age, the endothelial lining of the vasculature is less well able to provide a nonthrombogenic surface, leading to the formation of blood clots that block vessels in the heart or brain leading to myocardial infarction or stroke. This oxygen shortage additionally occurs when there is a reduction of blood flow to a tissue or an organ during procedures such as organ transplantation and cardiovascular and orthopedic surgeries [3]. Other events that can result in arterial blockage and subsequent ischemia include traumatic injury and tourniquet application. Interruption of blood flow resulting from these conditions can lead to deficiency of nutrients and oxygen, as well as reduced ability to remove waste products from the affected area. Inability to supply sufficient oxygen to meet metabolic demands can result in cell death and irreversible tissue damage if prolonged. Hypoxia impairs the process of oxidative phosphorylation in the cells of effected tissues leading to a marked decrease in the production of ATP and the interruption of multiple cellular processes [3]. Other consequences of reduced ATP in the

cell include increased glycolysis, decreased pH, clumping of nuclear chromatin, reduced function of the sodium potassium pump, detachment of ribosomes and lipid deposition [4]. Ischemia can also result in loss of calcium homeostasis in the cell, causing increased calcium levels and activation of enzymes such as phospholipases, proteases and endonucleases [3, 5]. The increased activity of these enzymes can work to disrupt membranes and proteins, and possibly cause nuclear chromatin damage [6-7]. In addition, the loss of calcium ion homeostasis can lead to mitochondrial membrane permeability and the loss of function of the electron transport chain. If the mitochondrion is severely compromised, cytochrome c may be released leading to the induction of apoptosis [8]. Prolonged interruptions to these cellular mechanisms can cause permanent tissue or organ injury, making the re-introduction of oxygen vital for restoring function. This reperfusion, however, initiates a complex cascade of events leading to inflammatory and oxidative damage both locally and systemically [9-10]. This phenomenon is known as ischemia / reperfusion (I/R) injury.

The concept of reperfusion injury was first introduced by Hearse in 1977 [11-12]. It was thought previously that the increase in apoptotic and necrotic cells upon oxygen re-introduction was due to irreversible injury sustained to those cells prior to reperfusion. More recent experimental evidence however suggests that these cells damaged during reperfusion were indeed viable before re-oxygenation [13]. The reperfusion of a previously ischemic organ restores the possibility of aerobic metabolism and is essential for recovery, but will also result in an inflammatory response that can extend tissue damage beyond the original area of ischemia [14]. This inflammatory state can

potentially persist for several days and may induce apoptosis on vascular structures [15-17]. Studies have shown that I/R injury can trigger the activation of the complement system in different organs [3, 18]. The inflammatory response induced by complement activation, namely C5a and C5b, can include neutrophil mobilization, NFκB induction and release of inflammatory mediators such as TNF-α, IL-1 and IL-6 [19-22]. The release of reactive oxygen species (ROS) as a result of this inflammatory response is thought to contribute significantly to the damage caused in the event of an I/R injury [11, 23].

A large body of experimental evidence implicates the activity of ROS in the exacerbation of tissue injury following reperfusion [11, 24-27]. This group of unstable and highly reactive oxygen derived compounds includes hydrogen peroxide (H_2O_2), superoxide anion (O_2^-) and hydroxyl radical (OH●). These ROS accumulate in substantial amounts under I/R conditions and can significantly damage tissues if untreated [11, 24-26, 28]. Under normal conditions, these oxygen free radicals are produced in small amounts. The majority of oxygen (95%) is safely reduced to H_2O in the mitochondria under normal conditions, whereas the remaining 5% undergoes univalent reduction to superoxide (O_2^-). The cell can normally control the small amount of superoxide generated through the activity of the antioxidant enzymes superoxide dismutase and catalase, which convert superoxide to hydrogen peroxide and subsequently to water [28-31]. Under I/R conditions however, there is excessive production of ROS that the cell cannot sufficiently inactivate. During ischemia, there are inadequate amounts of oxygen available, which leads to ATP deficiency as well as the loss of sodium, calcium, and potassium ion regulation within the cell [5]. Without oxygen to serve as the final electron acceptor in

the electron transport chain (ETC), mitochondria are unable to produce ATP and the oxidative phosphorylation pathway begins to form increased amounts of ROS intermediates. In addition, high amounts of calcium caused by the loss of ionic homeostasis may induce the mitochondrial permeability transition [32-33]. This transition causes the formation of permeable pores from the inner membrane to the outer membrane of the mitochondria and allows the efflux of ROS and calcium, propagating and exacerbating the oxidative stress. Another consequence of mitochondrial permeability is the movement of cytochrome c out of the mitochondrial inner membrane into the cytosol. Cytochrome c is a vital component of the ETC, and its removal may result in the further production of ROS intermediates due to a disturbed oxidative phosphorylation pathway [34-35]. When cytochrome c is present in the cytosol, the caspase pathway becomes activated and apoptosis is induced [36-38]. Cytochrome c movement may also be induced by the translocation of the bax protein from the cytosol to the outer mitochondrial membrane. Bax is a pro-apoptotic member of the bcl2 protein family, and promotes mitochondrial membrane permeability as well as cytochrome c movement when translocated [34]. This induction of apoptosis is an additional mechanism through which I/R injury manifests.

Ischemic conditions and increased intracellular calcium levels promote the conversion of xanthine dehydrogenase to xanthine oxidase, an enzyme capable of generating ROS [5]. Evidence suggests that the activity of xanthine oxidase (XO) is another significant source of ROS production within the cell. Depletion of ATP by ischemia results in the formation of hypoxanthine. Xanthine oxidase then uses O_2 as a

substrate to convert hypoxanthine to xanthine upon re-introduction of oxygen, generating the ROS superoxide anion in the process [39-40]. The proposed mechanism for this pathway of ROS generation is outlined in Figure 1.1 [41-42].

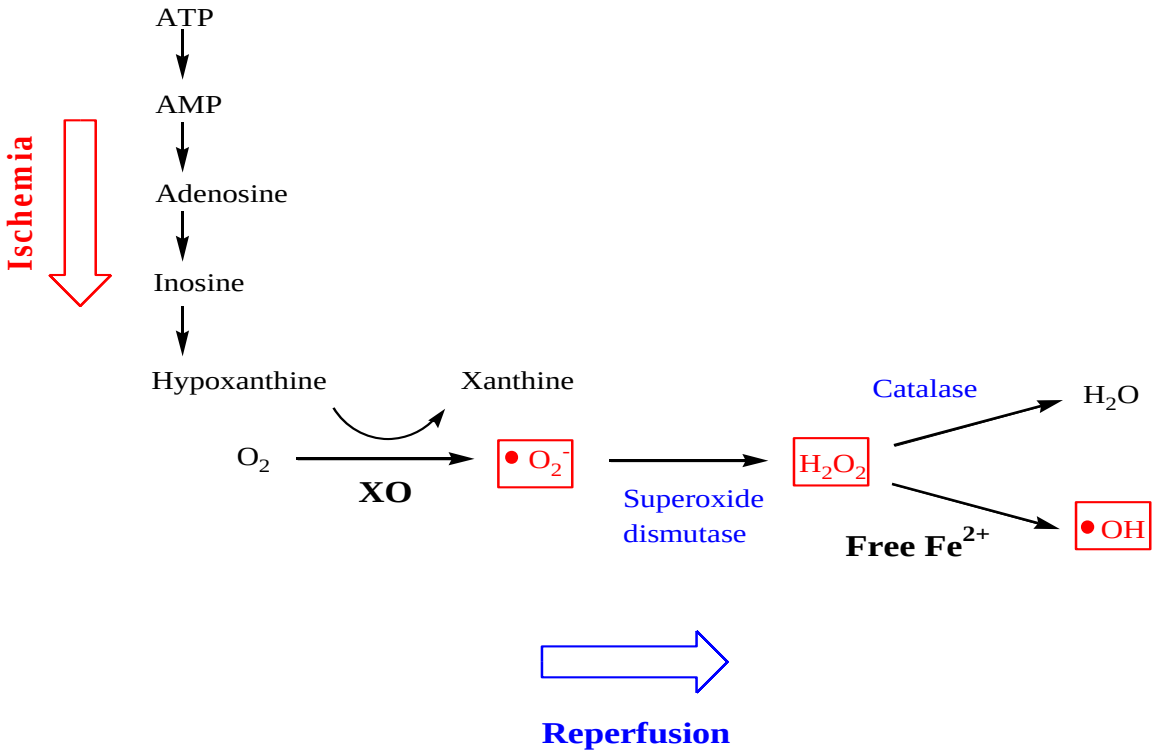

Figure 1.1 – Proposed mechanism of I/R injury, modified [43-44].

These radicals generate an oxidative stress on the cell that can result in a number of consequences, such as lipid peroxidation and modification of a number of cellular proteins [6, 43, 45-47]. These changes can cause cellular defects such as interruption of the Ca^{2+} pump ATPase and the Na^{+}/K^{+} pump ATPase [48]. If the activity of ROS is allowed to proceed unchecked in the cell, irreversible damage may be caused to cellular structures, leading to potential apoptosis as described earlier, or necrosis. On a larger scale, this ROS induced oxidative stress can manifest into a variety of clinical conditions. It has been shown that ROS induced cytotoxicity in the myocardium can contribute to myocardial stunning [22, 49]. I/R injury resulting from head trauma or stroke can lead to disruption of the blood brain barrier, allowing for the infiltration of leukocytes. The ROS generated from these leukocytes can irreversibly damage potentially salvageable cells, which may result in worsened sensory or motor functions [50]. I/R injuries sustained in skeletal muscle are met with local ROS generation, leading to the sequestration of polymorphnuclear leukocytes within the skeletal muscle. These leukocytes further secrete ROS into the surrounding area, initiating a type of positive feedback loop of ROS release. The cytotoxicity caused by this burst in ROS can result in endothelial dysfunction and edema of the skeletal muscle [51-52].

1.2 – Role of Antioxidants in I/R Injury Treatment

The onset of ischemia will always result in irreversible damage to a group of cells in the affected area. Another group of cells will be potentially salvageable upon successful reperfusion of the tissue. Treatment of I/R injury revolves around maximizing the chance of recovery for this group of potentially salvageable cells. A worst case scenario arises when 100% of the salvageable cells experiences cell death. The ideal situation would be 100% recovery of the cells in the salvageable group. Treatment strategies for I/R injury vary in effectiveness and fall between the two extremes.

The role of ROS in the pathology of I/R injury is significant and has prompted a number of studies investigating the use of radical scavengers as potential therapeutic options. These antioxidants and radical scavengers react with the ROS generated by an I/R episode and prevent their interaction with biological macromolecules. Melatonin, a naturally occurring antioxidant and radical scavenger, has been shown to attenuate cardiac [53] and renal [54] I/R injury in rats. When pre-treated with ascorbic acid, the extent of I/R damage in the kidneys of male rats was less severe [55]. N-acetylcysteine (NAC), an antioxidant thiol used for treatment of paracetamol poisoning, can also function as a radical scavenger and works to increase the amount of cellular glutathione, an endogenous anti-oxidant compound. NAC has been shown to protect against hepatic I/R injury in rats [56]. When administered to knee surgery patients, it was found that NAC and propofol both reduce the extent of I/R injury [57]. There has been recent interest in the use of plant derived compounds to attenuate I/R tissue damage. Many of

these metabolite compounds contain antioxidant phenolic groups and have been shown to reduce the effects of I/R injury in a variety of applications. The flavonoids rutin [58] and pycnogenol [59] have been reported to protect against renal I/R damage in rats. In addition, quercetin showed improved tissue conditions over control following cerebral [60], renal [61], and cardiac [62] I/R episodes. Resveratrol [63] and curcumin [64] have also been shown to protect against myocardial I/R injury in rats.

The cytoprotection against I/R injury provided by these compounds is attributed to direct antioxidant and radical scavenging activity, though experimental data have shown that the induction of antioxidant activating genes as well as signal pathway modulation may play a role as well. A number of mitogen activated protein kinases (MAPKs) have been correlated to downstream effects of cellular oxidative stress and may be involved in the apoptosis pathway. These MAPKs include extracellular signal regulated kinases (ERKs), p38 kinase, and the c-Jun N-terminal kinases (JNKs) [65]. ROS exposure has been found to induce the phosphorylation activity of p38 and increase apoptosis in cardiomyocytes [66]. ERKs are also involved in the cellular response to oxidative stress, as ROS exposure leads to up-regulation of ERKs [67]. In addition, these kinases play a role in the cascade of signals upstream from mitochondrial cytochrome-c release [68]. JNKs are other enzymes that are also involved in the cellular stress response, although it has been reported that JNK can act in a pro- or anti-apoptotic manner, depending on the cell type, nature of the stimulus, and duration of activity [69]. The transcriptional pathway of NF-κB is another signaling route involved in the cellular response to oxidative stress. Epigallocatechin gallate is able to cytoprotect against I/R

induced injury when administered to rats, and has also been found to inhibit the NF-κB pathway.

Due to the complexity of I/R injury, a multitude of treatment strategies have been investigated. Although anti-oxidant treatment has seen some success in animal models in attenuating I/R injury as described earlier, the results have been less conclusive in clinical trials. Some investigators have observed protective effects by direct antioxidants such as vitamin E against I/R injury [70-71], while other investigators did not observe such results [46, 72-73]. Superoxide dismutase has also been shown to improve graft acceptance in patients receiving renal transplants [74], but failed to provide any benefit in myocardial function when administered to patients who had experienced myocardial infarction [75]. Despite equivocal experimental results such as these, there is a considerable data that supports the significance of oxidative stress in I/R injury and the importance of antioxidants in protecting against this type of damage. Findings from the animal studies discussed earlier in addition to the positive results from various clinical trials warrant further investigation into the use of antioxidants as well as compounds that can induce antioxidant enzymes as treatments strategies against I/R injury.

1.3 – CAFFEIC ACID PHENETHYL ESTER (CAPE)

CAPE is a naturally occurring antioxidant compound produced by plants and found in honeybee propolis. Propolis is a resinous substance used by bees to seal spaces in the hive. Natural medicine practitioners from many cultures have recommended propolis as a remedy for inflammation, intestinal disorders and burns. Flavonoids derived from propolis have been shown to protect against I/R injury in animal models in a variety of organs [76-78]. The components of propolis include resins from various plants and wax produced from the body of the bees. Propolis is typically aromatic and has a color ranging from light green to dark brown, depending on the types of constituents that comprise it. Chemical analysis estimates that propolis contains over 300 different compounds and is composed of primarily resin (50%), wax (30%), essential oils, (10%) pollen (5%) and other organic compounds (5%) [79-80]. The components of propolis vary depending on the source of plant resin, climate and other environmental conditions. CAPE has been found to be concentrated in propolis located in temperate climates.

CAPE has the form of an off-white powder with molecular weight 284.31 and empirical formula $C_{17}H_{16}O_4$. CAPE is soluble in most organic solvents including ethyl acetate, DMSO, ethanol and methanol. The structure of CAPE is shown in Figure 1.2. CAPE is susceptible to photo-oxidation and should be protected from light when stored or handled.

\

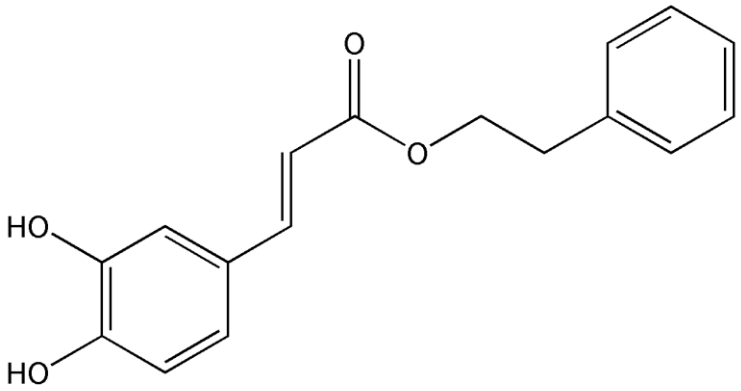

Figure 1.2 – Structure of Caffeic Acid Phenethyl Ester (CAPE), MW = 284.31 g/mol, MP = 173.38°C

Numerous animal studies have investigated CAPE as a protectant against I/R injury. When 50 μM/kg of CAPE was administered to rats prior to a coronary occlusion, it was found that myocardial infarct size was reduced from an average of 23 cm^3 for control rats to an average of 9 cm^3 for CAPE treated rats [81]. Another study reports that rats treated with 1 μg/kg of CAPE prior to coronary occlusion resulted in significantly fewer incidents of ventricular fibrillation and lower mortality rates than control rats [82]. CAPE was administered to rats at 10 μM/kg concentration prior to an intraocular ischemic event and it was found that the CAPE treated rats had significantly fewer apoptotic cells in the retina than did non treated rats [83]. The effects of CAPE were also investigated in rats that experienced I/R injury of the kidneys. It was reported that CAPE treated rats experienced significantly reduced amounts of tubular necrosis in the kidneys than did rats that were treated only with negative control [84]. CAPE has also been shown to be protective in other types of I/R injury including ischemic episodes in the spinal cord, testis and intestines [85-87].

CAPE is well documented as being an inhibitor of pro-inflammatory mediators. Natarajan *et al*. report that CAPE is a specific inhibitor of NFκB activation [88], a result that is consistent with findings from numerous other studies [89-92]. CAPE's anti-inflammatory properties have also been attributed to its activity as an inhibitor of tumor necrosis factor alpha (TNF-α) and Il-8 both *in vitro* and *in vivo* [93-95]. Other pro-inflammatory mediators that CAPE has been shown to inhibit include Il-1 alpha and beta, and Il-6 [95-97]. CAPE has also been implicated as an inhibitor of cyclooxygenase-2

both *in vitro* and *in vivo*, another possible mechanism through which CAPE exerts its anti-inflammatory activity [65, 98].

CAPE has received recent interest as an anti-tumor agent and has been found to inhibit growth of a number of tumor cell lines [99]. Grunberger *et al*. report that CAPE exerts higher cytotoxicity in tumor cells than in analogous normal cells [100]. CAPE is also cited to have anti-metastatic action on various tumor cell lines due to its inhibition of matrix metalloproteinase-2 and -9 [101]. CAPE is implicated in inducing apoptosis in human pancreatic cancer cells, human prostate adenocarcinomas, and in inhibiting proliferation of C6 glioma cells as well among others [99, 102-105] .

The activity of CAPE as a potent radical scavenger and antioxidant is well documented. Chen *et al*. reported a 57% radical inhibition of 0.1 mM 1,1-diphenyl-2-picrylhydrazyl (DPPH) by 20 μM CAPE. It was also found that CAPE inhibited lipid oxidation by 18 hours over control in the Rancimat antioxidant assay [106]. Göcer *et al*. report similar concentrations for CAPE in DPPH inhibition, in addition to significant reducing ability in the ferric ion reducing power and cupric ion reducing power assays [107]. The antioxidant ability of CAPE is thought to be attributed to the two hydroxyl groups located on the catechol ring of the compound [108]. The antioxidant and radical scavenging properties of CAPE have also been investigated in the context of cellular protection. Wang *et al*. report CAPE is a protective against the oxidative damage caused by 2,2'-azobis(2-methylpropionamidine) dihydrochloride (AAPH) and H_2O_2 in multiple cellular structures. Specifically, CAPE showed significant inhibitory effects against lipid peroxidation, DNA strand breakage and protein fragmentation when compared to control

[109]. CAPE has also shown protection against isoniazid induced oxidative stress in red blood cells and against 12-O-tetradecanoylphorbol 13-acetate (TPA) induced oxidative stress in HeLa cells [110-111]. Our laboratories have also previously shown CAPE to be cytoprotective against menadione induced oxidative stress in human umbilical vein endothelial cells (HUVEC) [112]. It is likely that this antioxidant activity contributes to the ability of CAPE to protect against I/R injury to some degree, since the generation of ROS is one of the primary mechanisms of damage through which I/R injury occurs. If CAPE is able to scavenge these ROS prior to their interaction with cellular structures the damage caused may be attenuated.

The mechanism through which CAPE is able to exert its beneficial properties is not fully understood. While it is believed that antioxidant activity is important in the treatment of I/R injury, the nature of the injury is complex and many pathways are affected. When a stress event such as I/R occurs, there are cellular defense mechanisms in place to respond to the stressor. Activation of these stress response systems prior to injury has shown to be effective in attenuating the damage caused. Ischemic preconditioning is one such method to activate these stress response enzymes and involves subjecting tissue to a short period of hypoxia prior to the ischemic event. Ischemic preconditioning has been reported to be consistently effective in reducing infarct size in myocardial I/R injuries in various animal models [113]. Preconditioned tissues have also been shown to have fewer ROS released and reduced amount of apoptotic cells following reperfusion when compared to non-preconditioned controls [114]. Heme oxygenase-1 (HO-1) is one such stress response enzyme that is up-regulated during ischemic preconditioning and has

been implicated as a cytoprotectant against the oxidative stress caused by I/R injury [115]. CAPE has been shown to be a strong inducer of HO-1 expression. CAPE's cytoprotective properties may very well be a combination of its antioxidant properties and its ability to induce the expression of cytoprotective systems such as HO-1.

1.4 – HEME OXYGENASE-1

Heme oxygenase-1 (HO-1) is a stress response enzyme that is induced in response to harmful stimuli such as ROS, hypoxia and acidosis [116-117]. HO-1 induction in response to ROS induced oxidative stress has been attributed to transcriptional activation by Nuclear factor (erythroid-derived 2)-like 2 (Nrf-2). Under normal conditions, Nrf-2 is bound in the cytosol to Kelch like-ECH-associated protein 1 (Keap1). ROS induced oxidative stress promotes the dissociation of Nrf-2 from Keap1, allowing it to move into the nucleus and bind to the promoter region of the antioxidant response element (ARE); inducing the transcription of HO-1 [118-119].

Initially, HO-1 was recognized as the enzyme involved in the metabolism of heme. HO-1 breaks down heme into equimolar amounts of carbon monoxide (CO), biliverdin, and iron (Fe), and is encoded by the heme oxygenase 1 gene (HMOX-1). However it has been recently discovered that upon induction, HO-1 exhibits broad cytoprotective properties [120-122]. Our interest in HO-1 revolves around the enzyme system's involvement in protection against I/R injury and oxidative stress [123-126]. Amersi *et al*. reported that upregulation of HO-1 prior to an ischemic event protected rat livers from reperfusion injury [127]. Katori *et al*. found that overexpression of HO-1 protected rat hearts from I/R injury [128]. I/R injury induced from transplantation procedures also appear to be attenuated by the induction of HO-1 expression [129-131].

A number of possible explanations for HO-1's protective activity have been offered. Under oxidative stress conditions, heme may be released from hemoproteins allowing them to catalyze the production of free radicals through Fenton chemistry [132]. The ability of HO-1 to catabolize free heme and therefore preventing it from inducing radical production is one possible explanation for the cytoprotection against oxidative stress that HO-1 provides. Many of the studies investigating the cytoprotection mechanism of HO-1 have done so in the context of apoptosis [118]. HO-1 induction has been found to inhibit TNF-mediated apoptosis [133] through cooperation with the anti-apoptotic actions of NF-κB signaling [134]. HO-1 has also been reported to act through the akt/PI3K transduction pathway, inducing the expression of Bcl-xl and Bcl-2, two anti-apoptotic genes with activity in the mitochondria [128]. In addition to the enzymatic action of HO-1, there is evidence that the end products of HO-1 activity; CO, Fe, and biliverdin, may also contribute to the cytoprotective effects. The presence of CO leads to the degradation of the p38α isoform while maintaining the anti-apoptotic isoform p38β, suppressing caspase activation and apoptosis [135]. Biliverdin can be converted to bilirubin, a potent antioxidant compound [136]. Iron has also been linked to suppression of TNF mediated apoptosis through its induction of ferritin, an iron sequestering compound [137]. To further study the involvement of HO-1, investigators have utilized compounds to inhibit the expression of HMOX-1 to determine whether or not cytoprotection is compromised. Inhibition of HMOX-1 by small interfering RNA (siRNA) has been shown to remove the cytoprotective effect initially provided by HO-1 against *in vivo* I/R injury [124, 138] as well as *in vitro* oxidative stress [138-139]. The

addition of tin protoporphyrin IX, another inhibitor of HO-1, has likewise shown removal of cytoprotection both *in vivo* [140] and *in vitro* [141]. The results from these studies suggest that HO-1 activity is necessary for cytoprotection against the oxidative stress and inflammatory response resulting from I/R injury. The pathways discussed earlier are correlated with the induction of HO-1 and are all possible mechanistic explanations for the cytoprotection provided. There is however, no single definitive pathway fully accounting for the manner in which HO-1 provides protection against oxidative stress, though there is strong correlation between induction of HO-1 and cytoprotective activity.

Compounds that are able to up-regulate the expression of HO-1 have garnered interest as potential therapeutic agents for combating the effects of I/R injury. The up-regulation of HMOX-1 in HUVEC has been observed following incubation of CAPE, and is consistent with reports in the literature concerning the relationship between cytoprotection and HMOX-1 expression. In addition, when suppressing HO-1 with tin protoporphyrin IX, it was found that the cytoprotection against menadione provided by CAPE is removed [142].

Chapter 2 – Synthesis of Caffeic Acid Phenethyl Amide (CAPA) and Fluorinated Derivatives

2.1 – INTRODUCTION

We believe that CAPE is a promising therapeutic compound due to the effectiveness it has shown in combating I/R injury in animal models and for its cytoprotective activity against oxidative stress both *in vivo* and *in vitro*; properties that were discussed earlier. We have previously conducted a number of studies aimed at investigating CAPE's properties. Wang *et al*. treated HUVEC with 5 μg/ml of CAPE prior to exposing the cells to 25 μM menadione and was able to observe 60% cell viability vs the 8% viability of the untreated cells [112]. It was seen that CAPE highly upregulated the HMOX-1 gene and also significantly increased the amount of HO-1 protein in HUVEC as well [142]. Despite showing significant activity, it was found that CAPE is readily hydrolyzed in plasma ($t_{1/2}$ = 0.35h at 37 °C) [143] and that it is removed quickly from circulation ($t_{1/2}$ = 26 minutes) [144].

Structural modification of CAPE was done previously in the form of fluorine introduction to the catechol ring at various positions in efforts to promote stability of the compound [112]. CAPE fluorinated at the 6' position (FCAPE) was found to exhibit similar cytoprotective properties against menadione in HUVEC to CAPE. FCAPE was then tested for stability in rat plasma and in circulation in male Sprague-Dawley rats. FCAPE showed a 1.31 fold increase in half-life at 37°C in rat plasma over CAPE and no significant difference in circulation half-life ($P > 0.05$) [143-144].

The purpose of this research project was to significantly increase the circulation half-life of CAPE without compromising its desirable cytoprotective properties. FCAPE derivatization was successful such that the cytoprotective activity against menadione induced oxidative stress was maintained, however the compound showed no improvements in circulation half-life. We hypothesized that the activity of esterase enzymes in circulation was responsible for the rapid decomposition of CAPE. We therefore decided to synthesize CAPA, a CAPE derivative that contained an amide bond in place of the ester. The lack of an ester bond would prevent the decomposition of the compound by esterases in the serum. The structures of CAPA and the CAPA derivatives are shown in Figure 2.1. Hydroxyl groups were methylated at various positions on the catechol ring. This was done to determine the effect that the hydroxyls had on cytoprotective activity. Fluorine was also placed at varying positions on the catechol ring to see if cytoprotective activity would be affected.

Fluorination of potential drug candidates is a popular practice that has seen much success in imparting desirable properties to compounds. Fluorine is the most electronegative element in the periodic table and has a strong electron withdrawing effect on neighboring functional groups. The inductive effect of fluorine is significant and can alter a number of physicochemical properties such as affecting the pKa of acidic groups as far as 4 carbons away [145]. Fluorine has been introduced to compounds to improve metabolic stability and to enhance potency. The C-F bond is more resistant to attack than the C-H bond and may prevent oxidative metabolism. Substitution may also alter the conformation or electrostatic properties of the compound. Fluorine substitution significantly enhanced the potencies of the drug candidates that eventually became the marketed drugs Ezetimibe® and Sitagliptin®. Enhanced duration of action was also seen following a fluorine substitution in a candidate compound that eventually became

Aprepitant®. Another example is that of Taranabant®, a drug that had reduced potential for covalent protein binding compared to a non-fluorinated derivative [146-147]. We were interested in fluorinating the catechol ring because of its purported importance in radical scavenging and cytoprotective activity [148-149]. This modification was done in attempt to improve the protective activities of the CAPA derivatives.

CAPA has been previously synthesized and described [150-151]. Previous work on CAPA has described its ability to act as an antioxidative against lipid peroxidation [152] as well as a potential anti-inflammatory agent through its inhibition of 5-lipoxygenase [151]. CAPA has also been shown to exhibit significant radical scavenging activity using a 2,2-diphenyl-1-picrylhydrazyl (DPPH) assay [150] Although various CAPA analogues have been investigated for both radical scavenging activity as well as α-glucosidase inhibition [153] no catechol ring fluorinated CAPA analogs have been studied. The cytoprotectant ability of CAPA in vitro has also not been previously addressed.

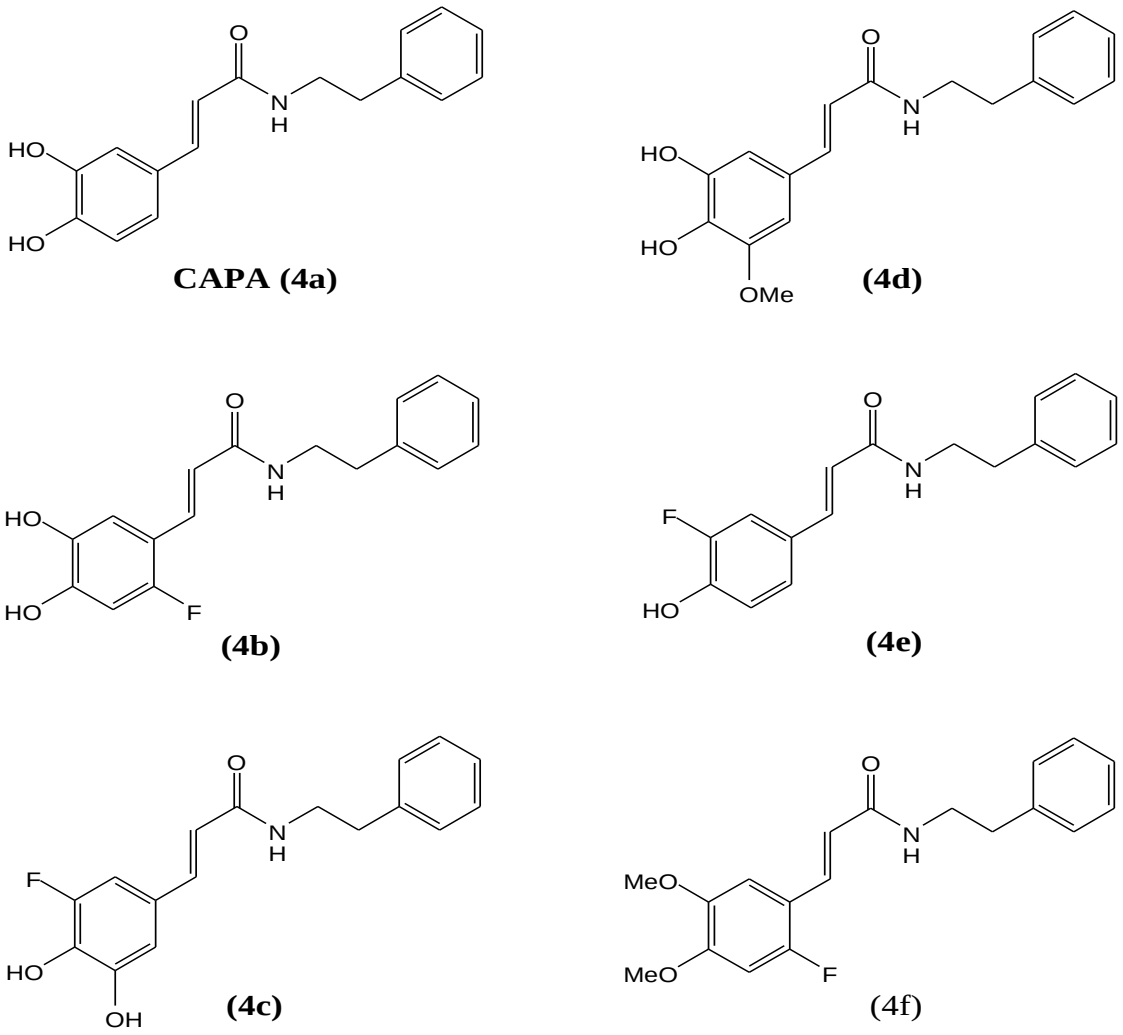

Figure 2.1 – Structures of CAPA (4a) and CAPA derivatives (4b-4f)

2.2 – MATERIALS AND METHODS

2.2.1 – Materials and Instrumentation

The reagents chloroacetyl chloride, phenethylamine, chloro-*tert*-butyldimethyl-silane (TBDMSCl), 3,4-dihydroxybenzaldehyde, 2-fluoro-4,5-dimethoxy-benzaldehyde, 3-fluoro-4-methoxy-benzaldehyde, 3-fluoro-4-hydroxy-5-methoxy-benzaldehyde, tetra-butyl-ammonium-fluoride (TBAF), hydrogen peroxide, and boron tribromide were purchased from Sigma Aldrich (St Louis, MO) and used without further purification. All solvents were distilled prior to use. Nuclear magnetic resonance (NMR) spectroscopy was performed with a Varian Unity+ 300 (300 MHz). Melting points were obtained using a Buchi B-540 apparatus and are uncorrected. Mass spectrometry services were provided by the Mass Spectrometry Facility at the University of Texas at Austin. Carbon, hydrogen, and nitrogen (CHN) elemental analysis was conducted by Quantitative Technologies Inc (Whitehouse, NJ). HPLC was performed on a Varian Prostar 320 system. Purity of the final compounds was assessed by both normal and reverse phase HPLC at λ=320 nm. Normal phase isocratic elution was conducted with a Varian Microsorb 100-5 Silica HPLC column (250x4.6 mm) running for 30 minutes at 75% ethyl acetate and 25% hexane. Reverse phase isocratic elution was conducted with an Alltech Partisil C8 HPLC column (250x4.6 mm, 5 μm) running for 30 minutes at 60% methanol 40% water.

2.2.2 – General Synthesis Pathway

CAPA and five additional fluorinated amide analogues of CAPE were prepared using a Wittig coupling approach. The known chloroacetamide **1** [154-155] was reacted with triphenyl phosphine to give the phosphonium chloride **2** (Figure 2.2). Wittig coupling of **2** with unprotected hydroxybenzaldehydes **3a-e** (Figure 2.3) proved problematic, in contrast to previous studies employing the analogous ester phosphonium chloride [112]. Thus, the hydroxybenzaldehydes **3a-e**, which were either commercially available or obtained via demethylation of the corresponding methoxybenzaldehydes with boron tribromide, were first transiently protected as the *t*-butyldimethylsilyl ethers by treatment with TBDMSCl and imidazole prior to Wittig coupling (Figure 2.3). The resulting α,β-unsaturated amides were subjected to deprotection with TBAF, to afford CAPA and the desired amides **4b-e** in modest overall yields. The dimethoxybenzaldehyde **3f** was used directly in the Wittig coupling to afford **4f** in reasonable yield. With the exception of amide **4e** which was isolated as a ~3:1 mixture of (*E*)-/(*Z*)- isomers after column chromatography, the amides **4** were obtained as >90% pure (*E*)-isomers after column chromatography and, for **4a-c** and **4f**, recrystallization.

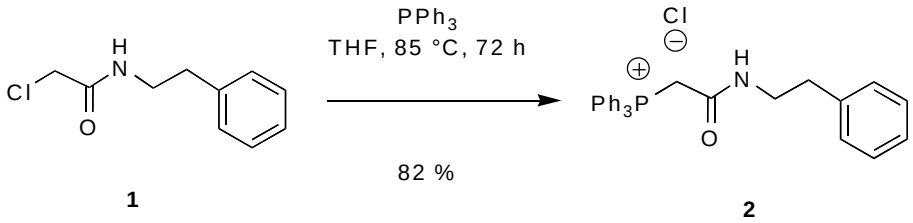

Figure 2.2 – Synthesis of the Wittig reagent

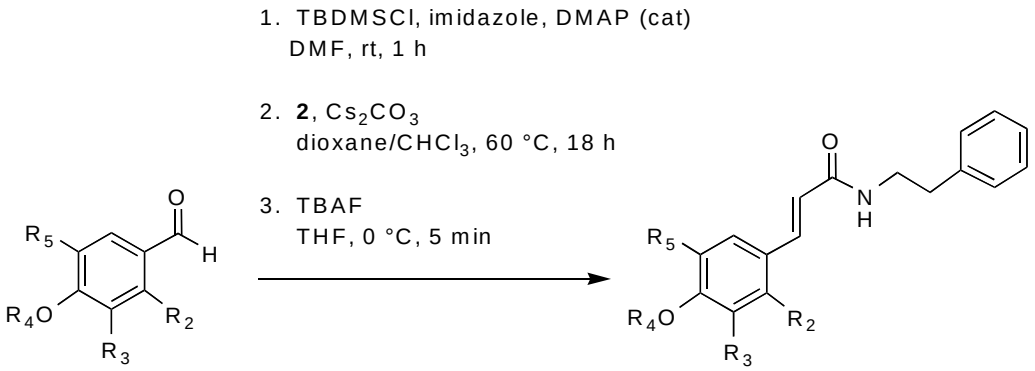

3a-f **4a-f**

Compound	R_2 =	R_3 =	R_4 =	R_5 =	Yield[a]
4a (CAPA)	H	H	H	OH	14%
4b	F	H	H	OH	7%
4c	H	OH	H	F	15%
4d	H	OMe	H	F	22%
4e	H	H	H	F	8% [b]
4f	F	H	Me	OMe	63% [c]

a. Isolated overall yield from benzaldehyde **3** after column chromatography and recrystallization.
b. Isolated as ~3:1 mixture of (*E*)-/(*Z*)-isomers.
c. Step 2 only.

Figure 2.3 – Synthesis of CAPA and CAPA derivatives

2.2.3 – Experimental

2-Chloro-N-phenethyl-acetamide (1). To a solution of phenethylamine (20 mmol, 2.52 mL) in CH_2Cl_2 (40 mL) was added K_2CO_3 (24 mmol, 3.32 g). Chloroacetylchloride (22 mmol, 1.75 mL) was slowly added to the reaction mixture. The reaction mixture was stirred at 45 ˚C under argon for 18 hours. The mixture was diluted with CH_2Cl_2, washed with water and brine, and then dried over Na_2SO_4. The resulting solution was concentrated under a rotary evaporator and the resulting solid filtered to give 2.93 g of white crystals (74% yield); mp 63.6-64.6 ˚C (lit [154], 65 °C); ^{1}H-NMR spectrum matches literature [154].

Phenethylcarbamoylmethyl-triphenylphosphonium chloride (2). To a solution of triphenylphosphine (18.9 mmol, 4.96 g) in THF (50 mL) was added 2-chloro-*N*-phenethylacetamide **1** (12.6 mmol, 2.5g. The mixture was stirred at 85˚C for 72 hours under argon. The reaction mixture was diluted with diethyl ether and filtered, giving 4.75 g of white solid (82% yield); mp 220.9–222.8 ˚C; 1H-NMR δ ($CDCl_3$): 2.67 (2H, t, J = 8.1 Hz), 3.31 (2H, q), 5.05 (2H, d, J = 14.4 Hz), 7.15-7.25 (5H, m), 7.59-7.68 (5H, m), 7.72-7.88 (10H, m).

General Procedure for the Demethylation of Benzaldehydes

2-Fluoro-4,5-dihydroxy-benzaldehyde. 2-Fluoro-4,5-dimethoxy-benzaldehyde (4 mmol, 736.64 mg) was dissolved in 10 mL of CH_2Cl_2. The mixture was placed in a -78˚C acetone and dry ice bath and 10 mL of a 1 M solution of BBr_3 in CH_2Cl_2 was added slowly under argon. The reaction mixture was allowed to warm to room temperature and stirred for 18 hours. Methanol was added to the resulting mixture, and the solvent evaporated. This process was repeated three times. Column chromatography (5:1 CH_2Cl_2/EtOAc) afforded 590 mg (94.5% yield) of 2-fluoro-4,5-dihydroxy-benzaldehyde as a white solid which was carried forward without further purification.

General Procedure for the Wittig reaction

3-(3,4-Dihydroxy-phenyl)-*N*-phenethyl-acrylamide (4a, CAPA). A mixture of 3,4-dihydroxybenzaldehyde (3 mmol, 414.36 mg), imidazole (9 mmol, 612.72 mg), TBDMSCl (9 mmol, 1356.48 mg), and DMAP (0.3 mmol, 36.65 mg) were dissolved in 5 mL of DMF and allowed to react at room temperature under argon for 1 hour. The reaction mixture was extracted with diethyl ether, washed with deionized water, and then dried over Na_2SO_4. Column chromatography (2% EtOAc in hexane) of the residue after evaporation of the solvent afforded 540 mg of the protected benzaldehyde, which was

combined with the phosphonium chloride **2** (1.8 mmol, 828 mg) and Cs_2CO_3 (3.9 mmol, 1651.65 mg) and then 5 mL of dioxane and 5 mL of $CHCl_3$. The resulting mixture was heated to 60˚C and for 18 hours. Extraction was performed with $CHCl_3$, and the reaction mixture was washed with water and dried over Na_2SO_4. Column chromatography (3:1 hexane/EtOAc) gave 550 mg of yellow oil. The oil was dissolved in 5 mL of THF and TBAF (2.5 mL, 1M in THF) was then added and the mixture was stirred for 5 minutes at 0˚C. The reaction mixture was concentrated on a rotary evaporator and subjected to chromatography on a silica gel column (4:3 EtOAc/hexane). Recrystallization (CH_2Cl_2 and hexane) afforded 115 mg of **4a** as a white solid: mp 145 ˚C (lit [150], 138-140 ˚C); ^{1}H NMR matches literature [150]; ^{13}C NMR ($CDCl_3$) δ 35.48, 41.09, 113.89, 115.30, 117.17, 120.95, 126.2, 127.13, 128.35, 128.65, 139.39, 141.07, 145.56, 147.60, 168.14. CI-MS *m/z* 284 (MH^+, 100). HRCI-MS: Calculated for $C_{17}H_{18}NO_3$; 284.1287. Found: 284.1288. ^{1}H NMR spectra is shown on Figure 2.3. ^{13}C NMR spectra is shown Figure 2.4. Normal and Reverse phase HPLC chromatograms are shown on Figure 2.5.

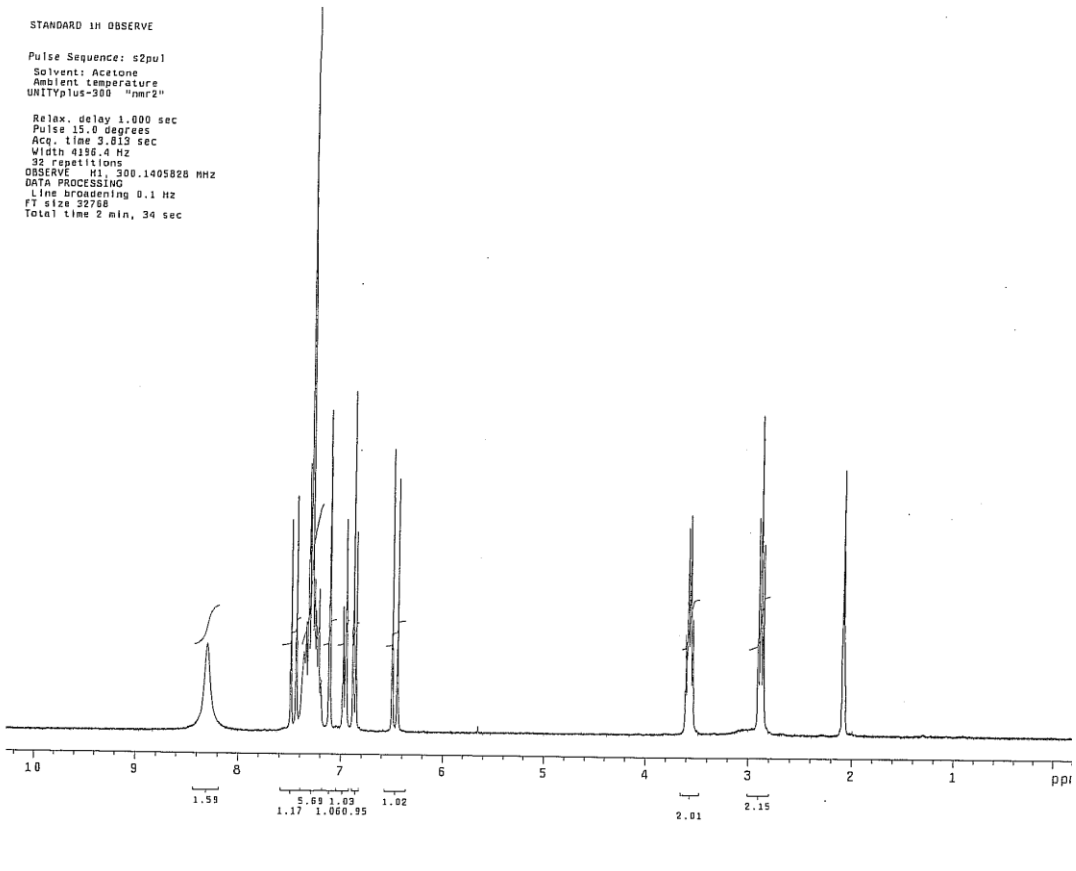

Figure 2.3 – ^{1}H NMR spectra of CAPA **4a**

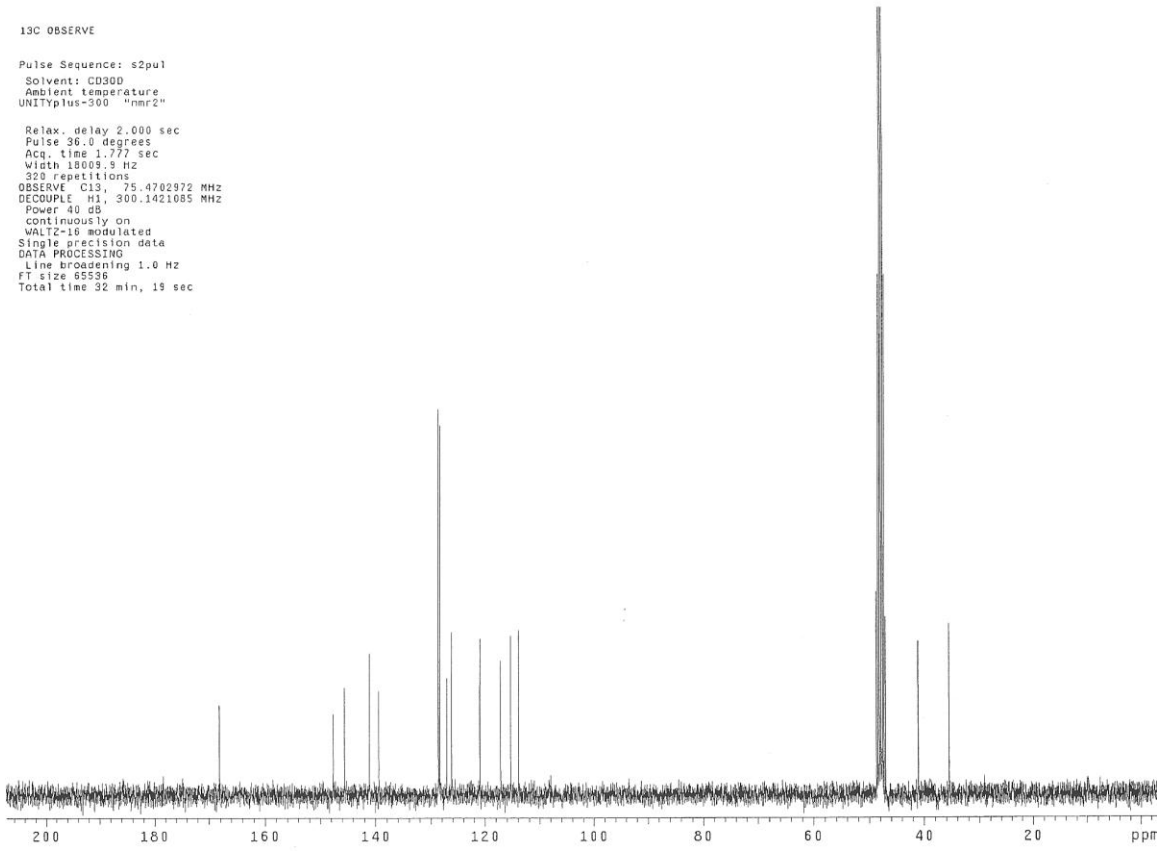

Figure 2.4 – ^{13}C NMR spectra of CAPA **4a**

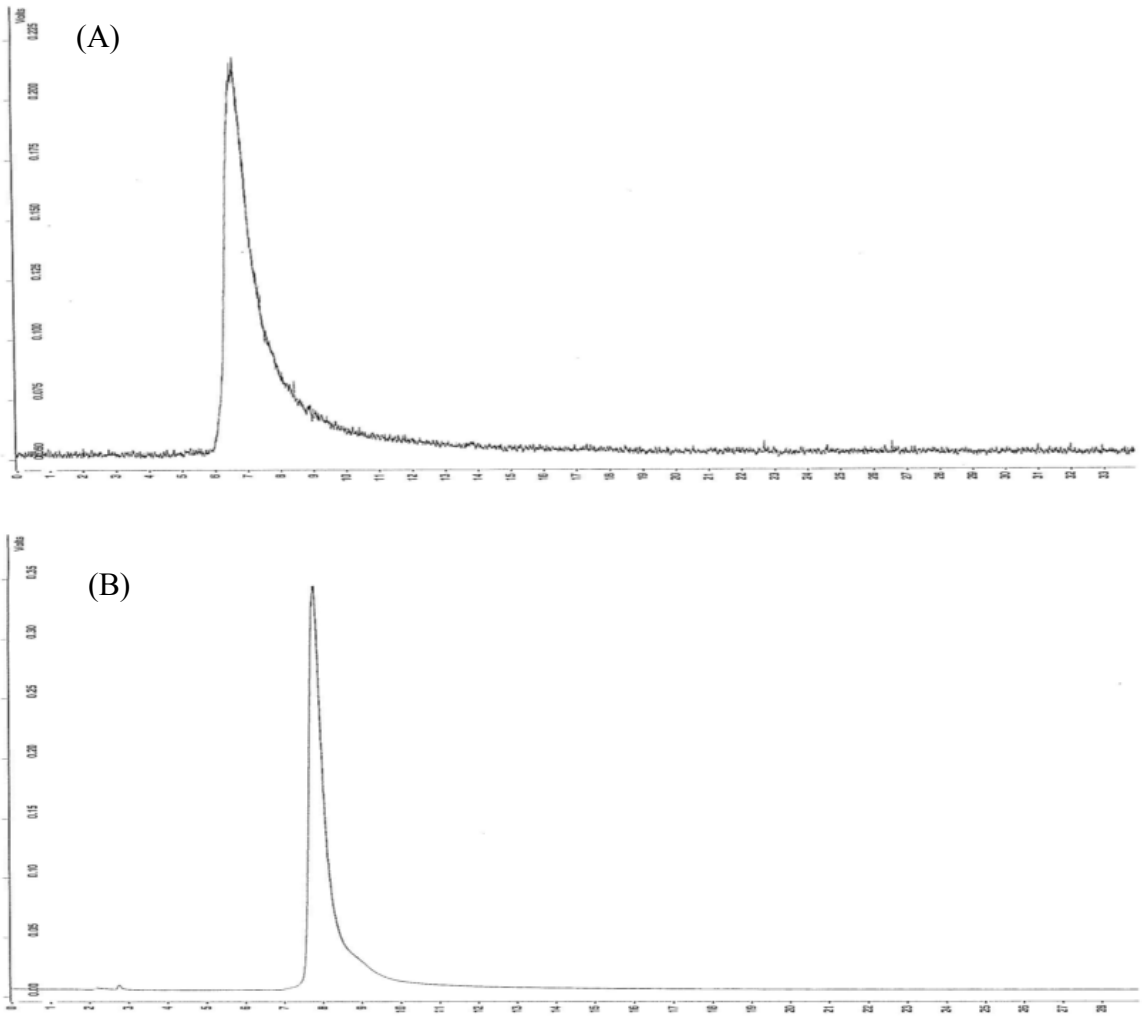

Figure 2.5 – Normal phase (A) and reverse phase (B) HPLC chromatograms of CAPA **4a**

The following compounds were prepared following the procedure described above:

3-(2-Fluoro-4,5-dihydroxyphenyl)-*N*-phenethyl-acrylamide (**4b**). Recrystallization (CH_2Cl_2 and hexane) afforded 80 mg of **4b** as a white solid: mp 145 ˚C; ^{1}H NMR (d_6-DMSO) δ (ppm): 2.77 (t, J = 6.9 Hz, 2H), 3.39 (q, J = 6.6 Hz, 2H), 6.40 (d, J = 15.9 Hz, 1H), 6.60 (d, J = 12.3 Hz, 1H), 6.91 (d, J = 7.8 Hz, 1H), 7.28 (m, 5H), 8.18 (s, 1H), 9.17 (s, 1H), 9.89 (s, 1H); ^{13}C NMR (d_6-DMSO) δ: 35.44, 41.11, 102.81 (J_{C-F} = 26 Hz), 113.07 (J_{C-F} = 5 Hz), 113.29, 119.27 (J_{C-F} = 6 Hz), 126.20, 128.35, 128.64, 133.36, 139.37, 142.09, 148.67 (JC-F =11.55 Hz), 155.77 (J_{C-F} = 243 Hz), 167.88; CI-MS m/z 302 (MH^+, 100). HRCI-MS: Calculated for $C_{17}H_{17}NO_3F$; 302.1192. Found: 302.1194. ^{1}H NMR spectra is shown on Figure 2.6. ^{13}C NMR spectra is shown Figure 2.7. Normal and Reverse phase HPLC chromatograms are shown on Figure 2.8.

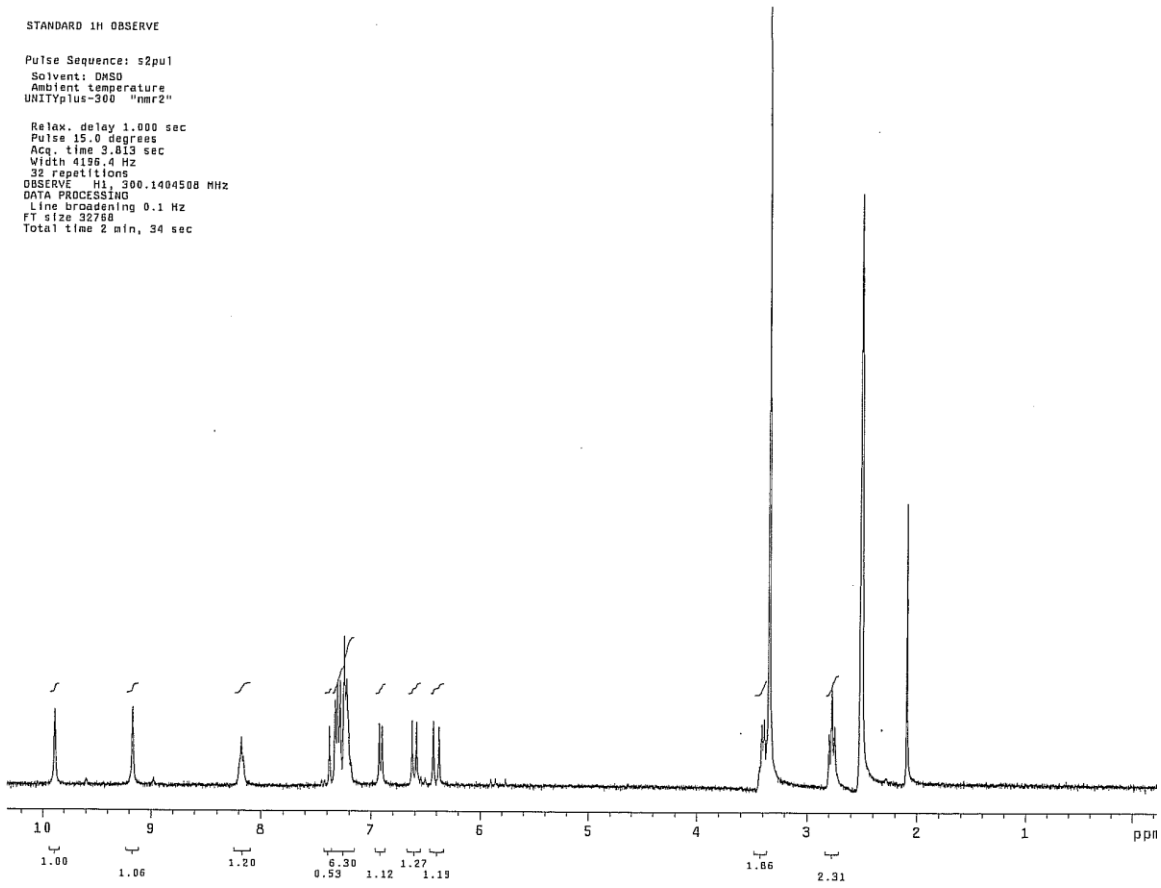

Figure 2.6 – ^{1}H NMR spectra of **4b**

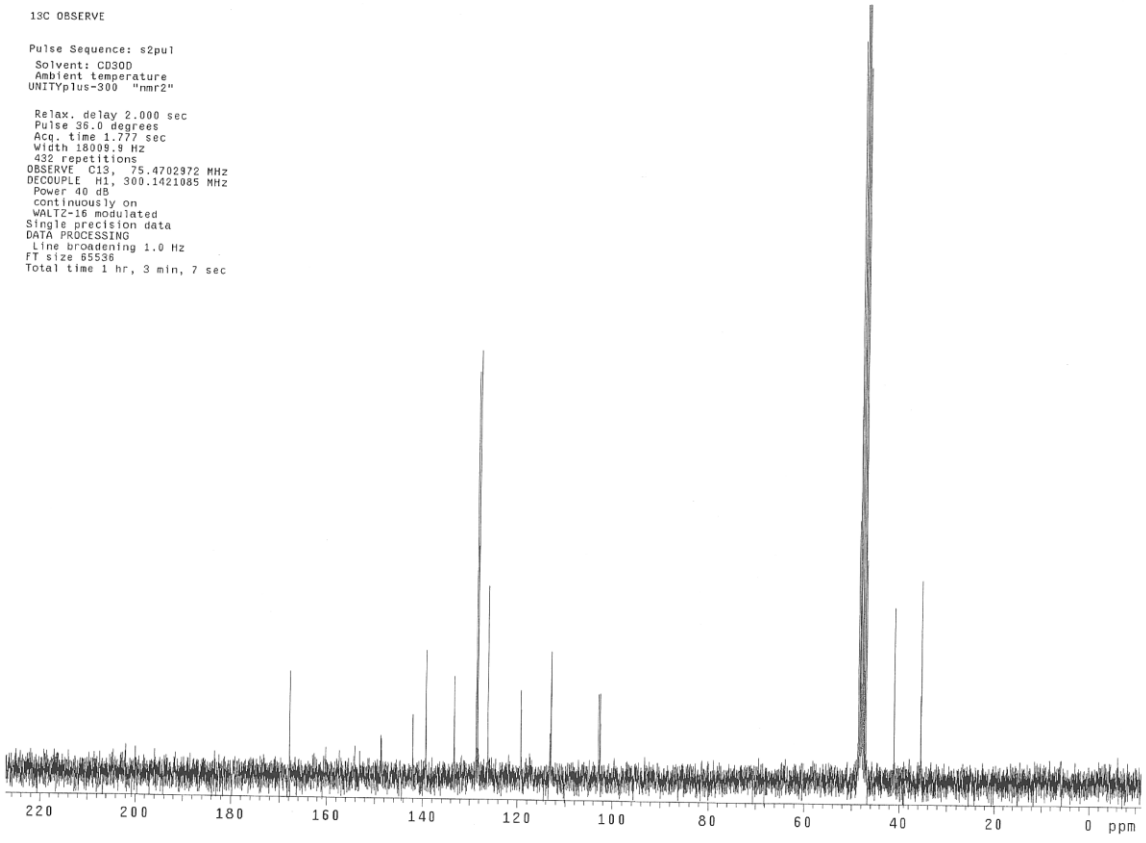

Figure 2.7 – ^{13}C NMR spectra of **4b**

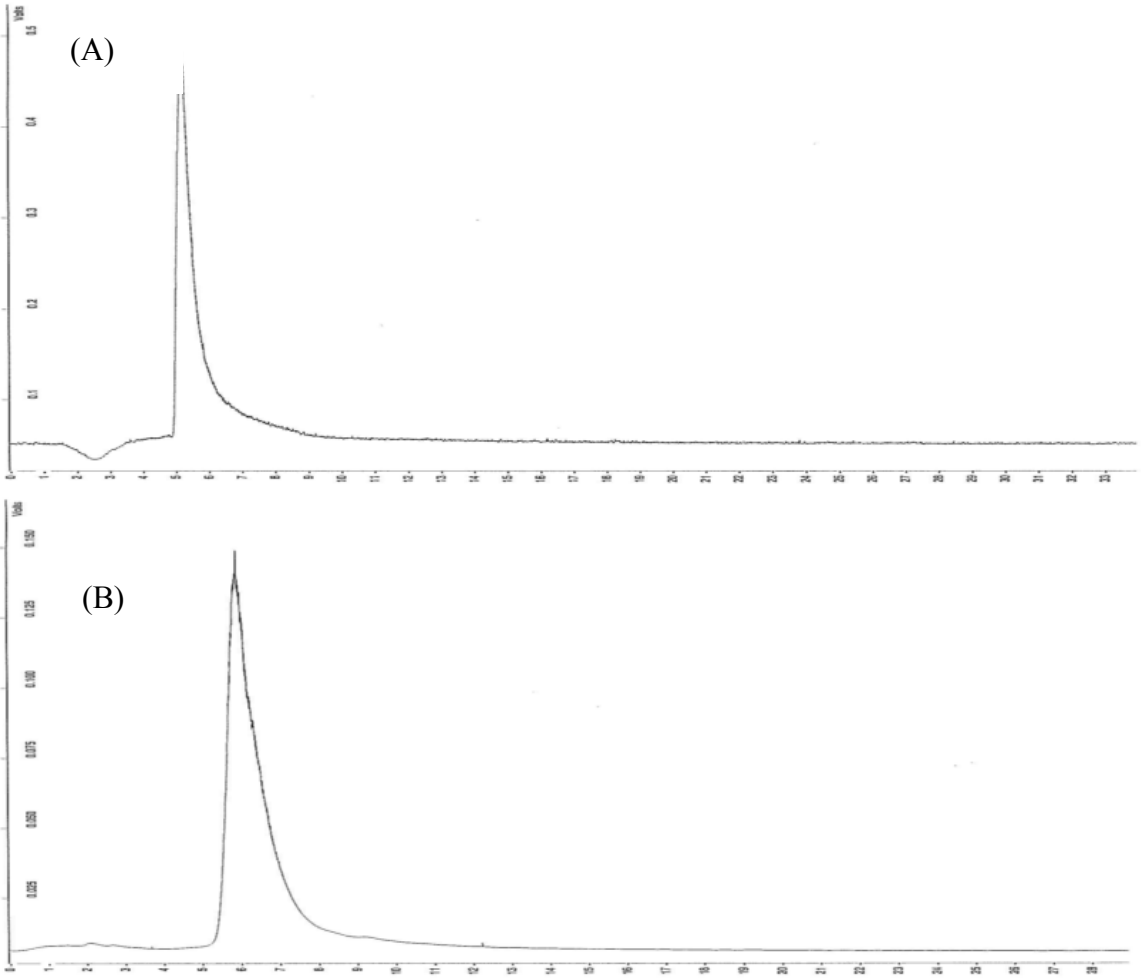

Figure 2.8 – Normal phase (A) and reverse phase (B) HPLC chromatograms of **4b**

3-(3-Fluoro-4,5-dihydroxyphenyl)-*N*-phenethyl-acrylamide (4c). Recrystallization (CH_2Cl_2 and hexane) afforded 135 mg of **4c** as a white solid: mp 154 ˚C; ^{1}H NMR (d_6-DMSO) δ (ppm): 2.76 (d, J = 7.2 Hz, 2H), 3.39 (d, J = 6.6 Hz, 2H), 6.36 (d, J = 15.6 Hz, 1H), 6.81 (d, J = 6 Hz, 1H), 6.86 (s, 1H), 7.23 (m, 5H), 8.09 (t, J = 5.1 Hz, 1H), 9.46 (s, 1H), 9.71 (s, 1H); ^{13}C NMR (d_6-DMSO) δ: 35.43, 41.1, 106.41 (J_{C-F} = 20 Hz), 110.59, 118.79, 126.10, 126.22, 128.36, 128.64, 135.23, 139.34, 140.06, 147.57 (J_{C-F} = 6 Hz), 152.28 (J_{C-F} = 238 Hz), 167.67; CI-MS m/z 302 (MH+ , 100). HRCI-MS: Calculated for $C_{17}H_{17}NO_3F$; 302.1192. Found: 302.1188. ^{1}H NMR spectra is shown on Figure 2.9. ^{13}C NMR spectra is shown Figure 2.10. Normal and Reverse phase HPLC chromatograms are shown on Figure 2.11.

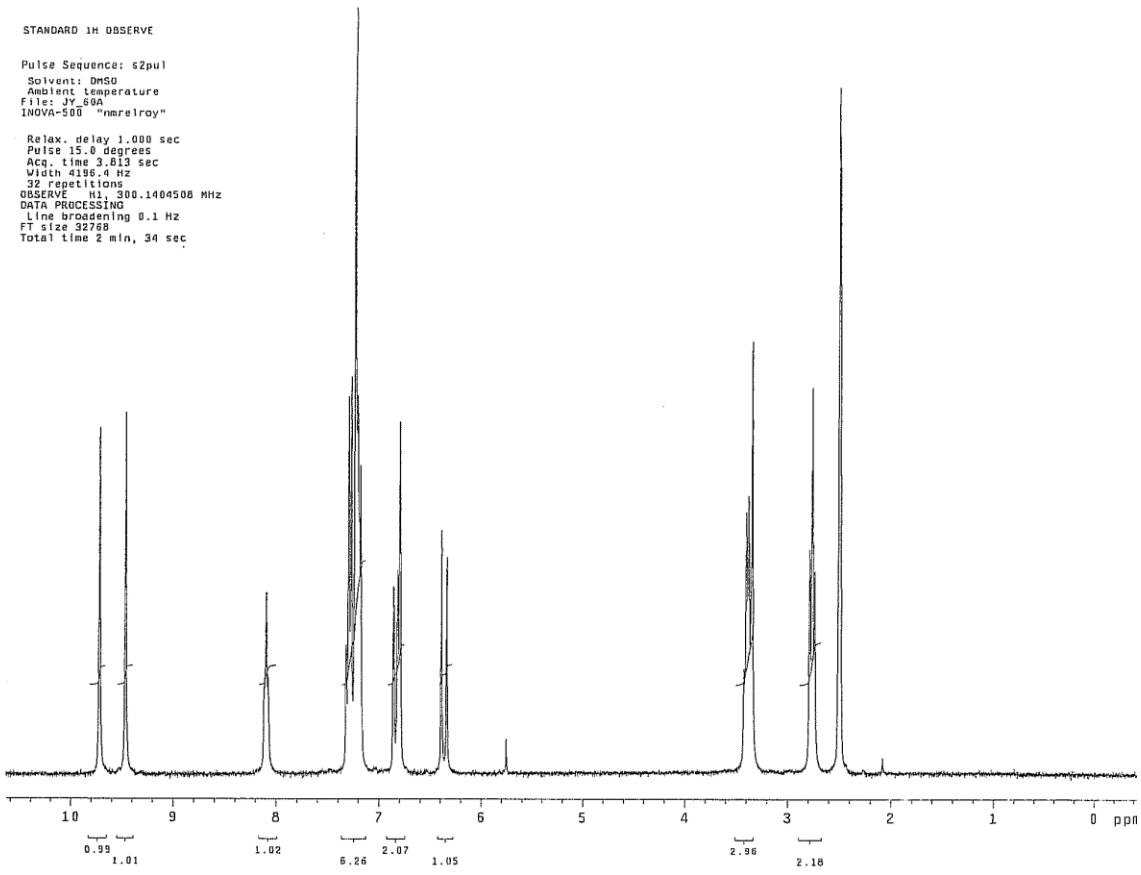

Figure 2.9 – ^{1}H NMR spectra of **4c**

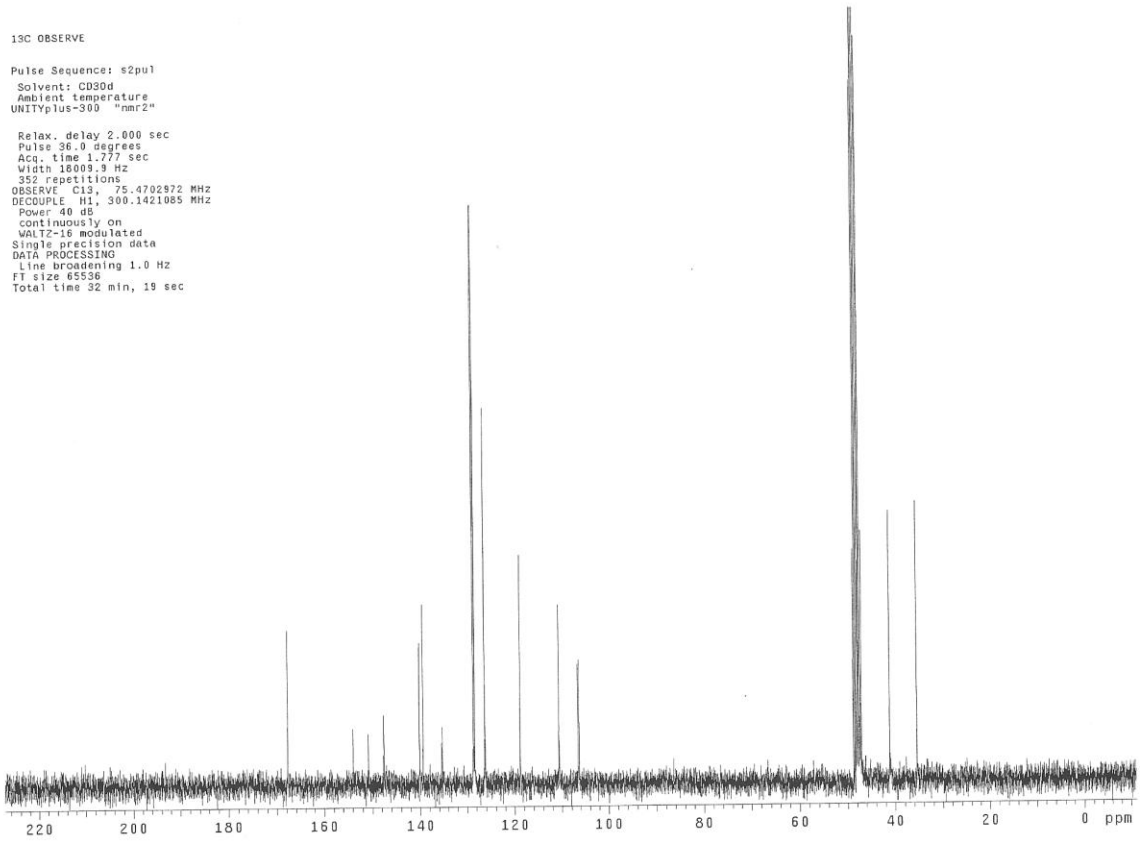

Figure 2.10 – ^{13}C NMR spectra of **4c**

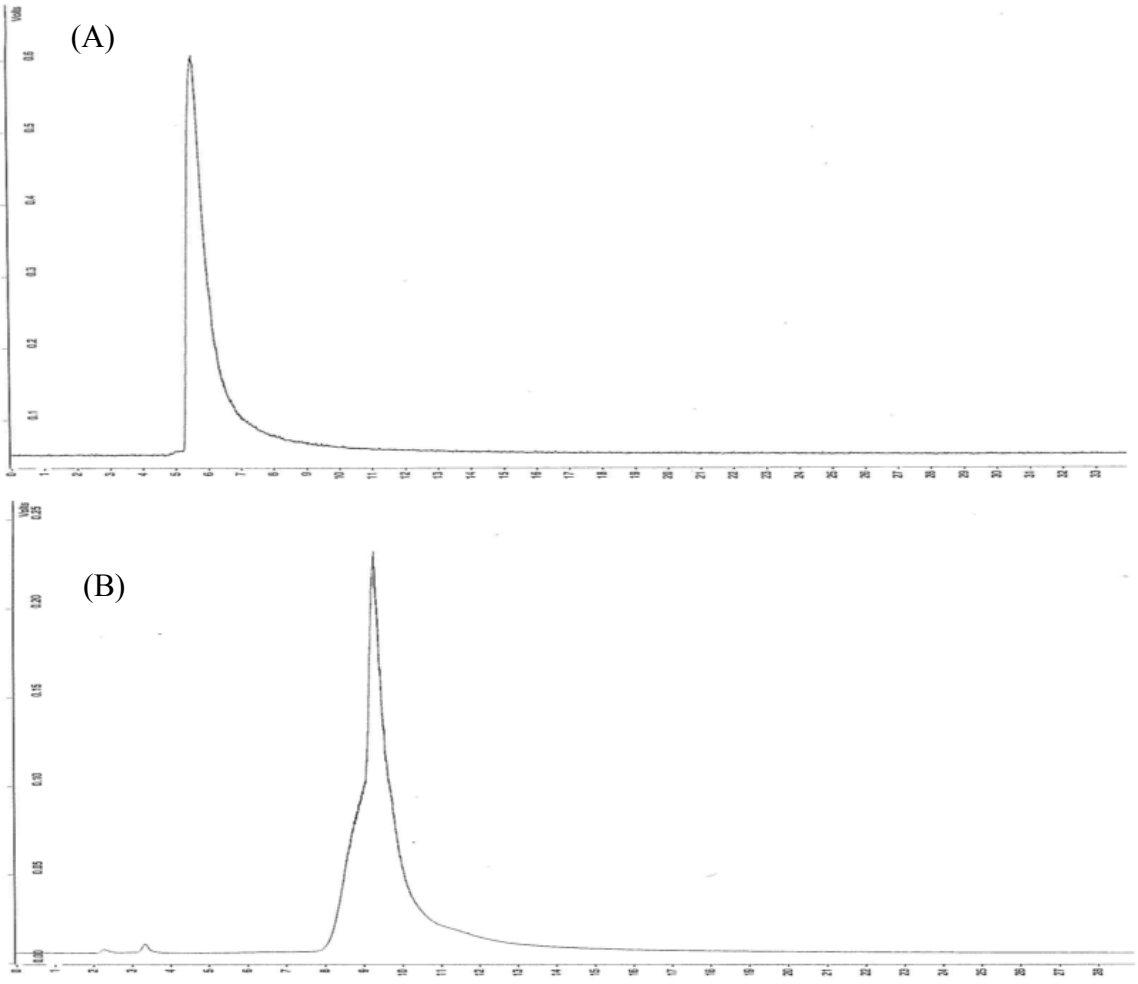

Figure 2.11 – Normal phase (A) and reverse phase (B) HPLC chromatograms of **4c**

3-(3-Fluoro-4-hydroxy-5-methoxyphenyl)-*N*-phenethyl-acrylamide (4d). An additional column chromatography purification (1:1.5 EtOAc/hexane) to remove traces of the Z isomer, afforded 100 mg of **4d** as a white foam: ^{1}H NMR ($CDCl_3$) δ (ppm): 2.91 (t, J = 6.9 Hz, 2H), 3.68 (q, J = 6.2 Hz, 2H), 5.68 (s, 1H), 5.82 (s, 1H), 6.20 (d, J = 15.4 Hz, 1H), 6.79 (s, 1H), 6.65 (dd, J = 1.6 Hz, J = 10.8 Hz, 1H), 7.28 (m, 5H), 7.50 (d, J = 15.4 Hz, 1H); ^{13}C NMR ($CDCl_3$) δ: 31.92, 37.13, 52.74, 102.72, 104.76 (J_{C-F} = 19 Hz), 115.81, 122.65 (J_{C-F} = 9 Hz),122.87, 125.00, 125.09, 131.72 (J_{C-F} = 14 Hz), 135.13, 136.53, 144.69 (J_{C-F} = 6 Hz), 147.02 (J_{C-F} = 242 Hz), 162.22; CI-MS m/z 316 (MH^+, 100). HRCI-MS: Calculated for $C_{18}H_{19}NO_3F$; 316.1349. Found: 316.1351. ^{1}H NMR spectra is shown on Figure 2.12. ^{13}C NMR spectra is shown Figure 2.13. Normal and Reverse phase HPLC chromatograms are shown on Figure 2.14.

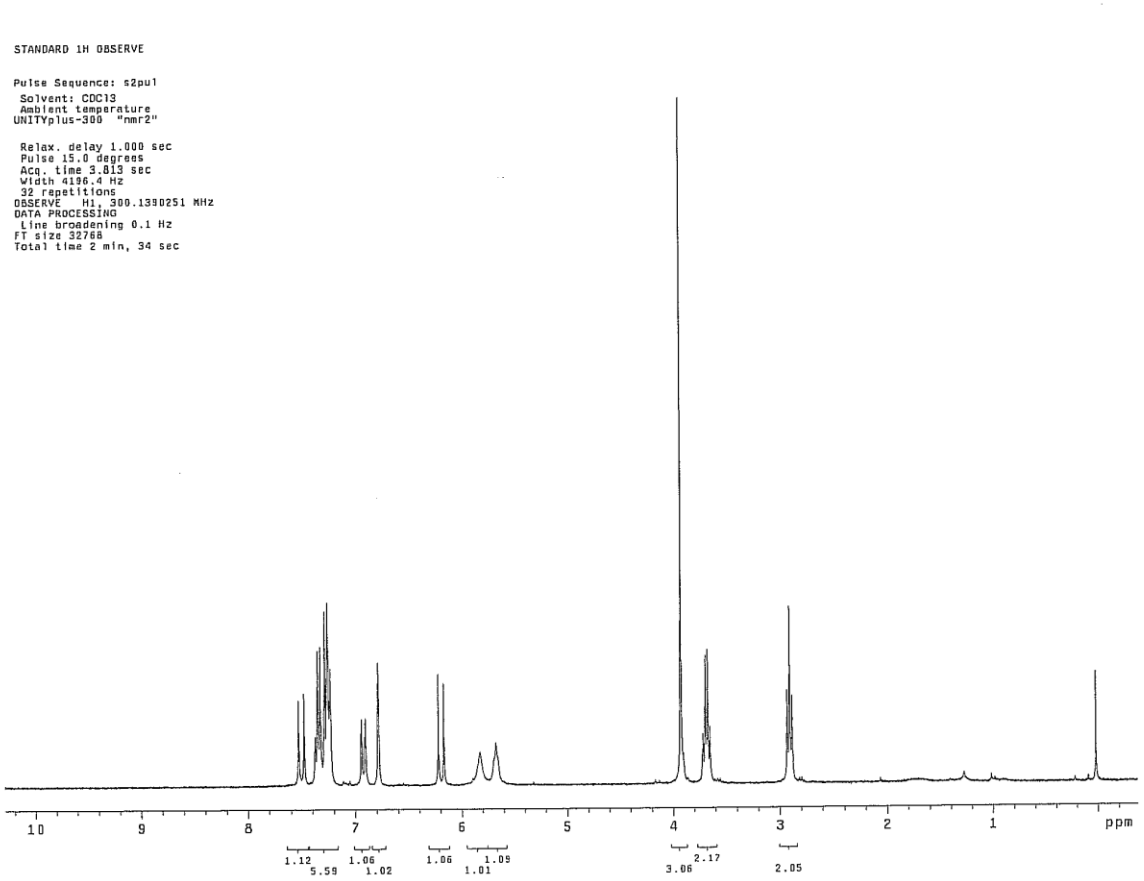

Figure 2.12 – ^{1}H NMR spectra of **4d**

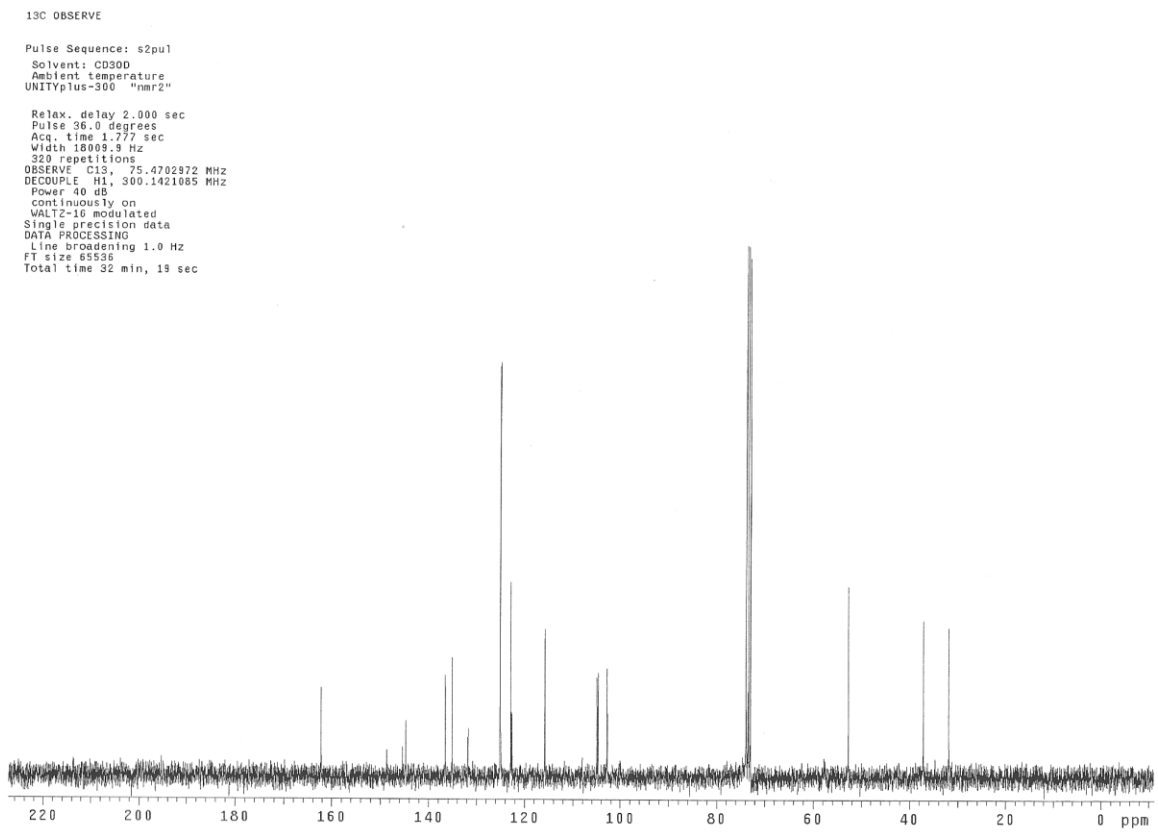

Figure 2.13 – ^{13}C NMR of **4d**

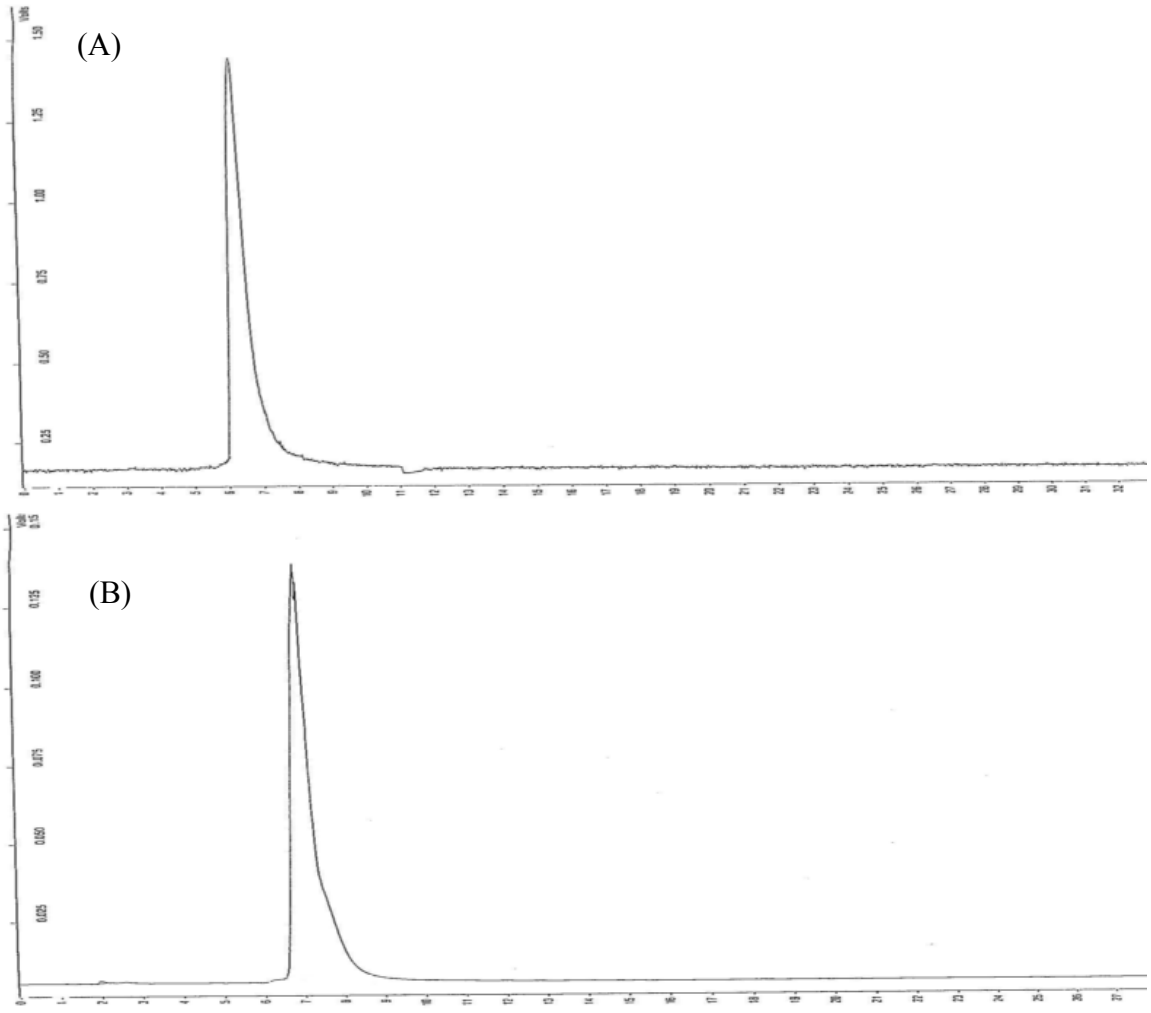

Figure 2.14 – Normal phase (A) and reverse phase (B) HPLC chromatograms of **4d**

3-(3-Fluoro-4-hydroxyphenyl)-*N*-phenethyl-acrylamide (4e). This process afforded 90 mg of **4e** as a yellow foam with a 3:1 (*E*)-/(*Z*)-isomer ratio by ^{1}H NMR: ^{1}H NMR ($CDCl_3$) δ (ppm) major isomer: 2.91 (t, J = 6.9 Hz, 2H), 3.68 (q, J = 6.1 Hz, 2H), 5.66 (s, 1H), 6.18 (d, J = 15.6 Hz, 1H), 7.00 (t, J = 8.5 Hz, 1H), 7.12 (d, J = 8.5 Hz, 1H), 7.18 (d, J = 1.8 Hz, 1H), 7.28 (m, 5H), 7.52 (d, J = 15.6 Hz, 1H); ^{13}C NMR (CDCl3) δ: 35.80, 41.30, 114.85 (J_{C-F} = 19 Hz), 118.31, 118.66, 125.50, 126.95 (J_{C-F} = 20 Hz), 127.18, 128.92, 128.99, 138.89, 140.85, 146.99 (J_{C-F} = 14 Hz), 151.86 (J_{C-F} = 241 Hz), 167.13; CI-MS m/z 286 (MH^+, 100). HRCI-MS: Calculated for $C_{17}H_{17}NO_2F$; 286.1243. Found: 286.1242. ^{1}H NMR spectra is shown on Figure 2.15. ^{13}C NMR spectra is shown Figure 2.16. Normal and Reverse phase HPLC chromatograms are shown on Figure 2.17.

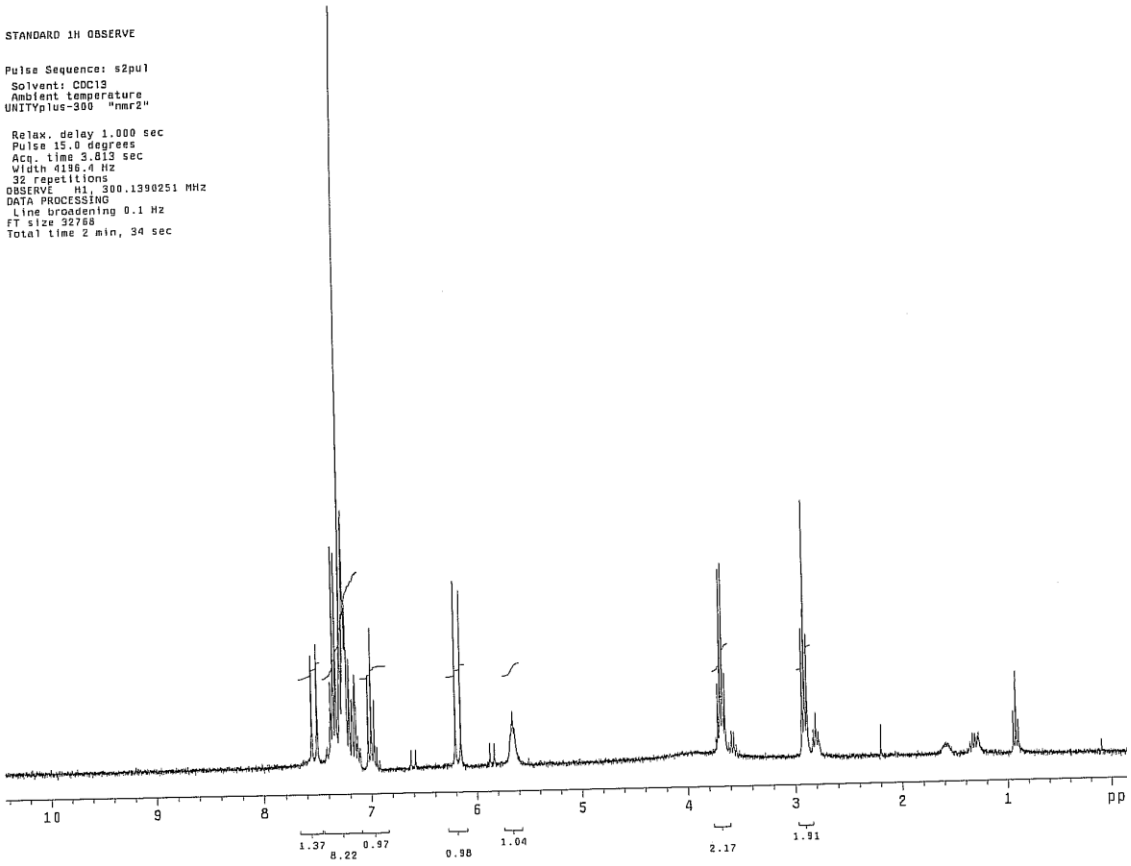

Figure 2.15 – ^{1}H NMR spectra of **4e**

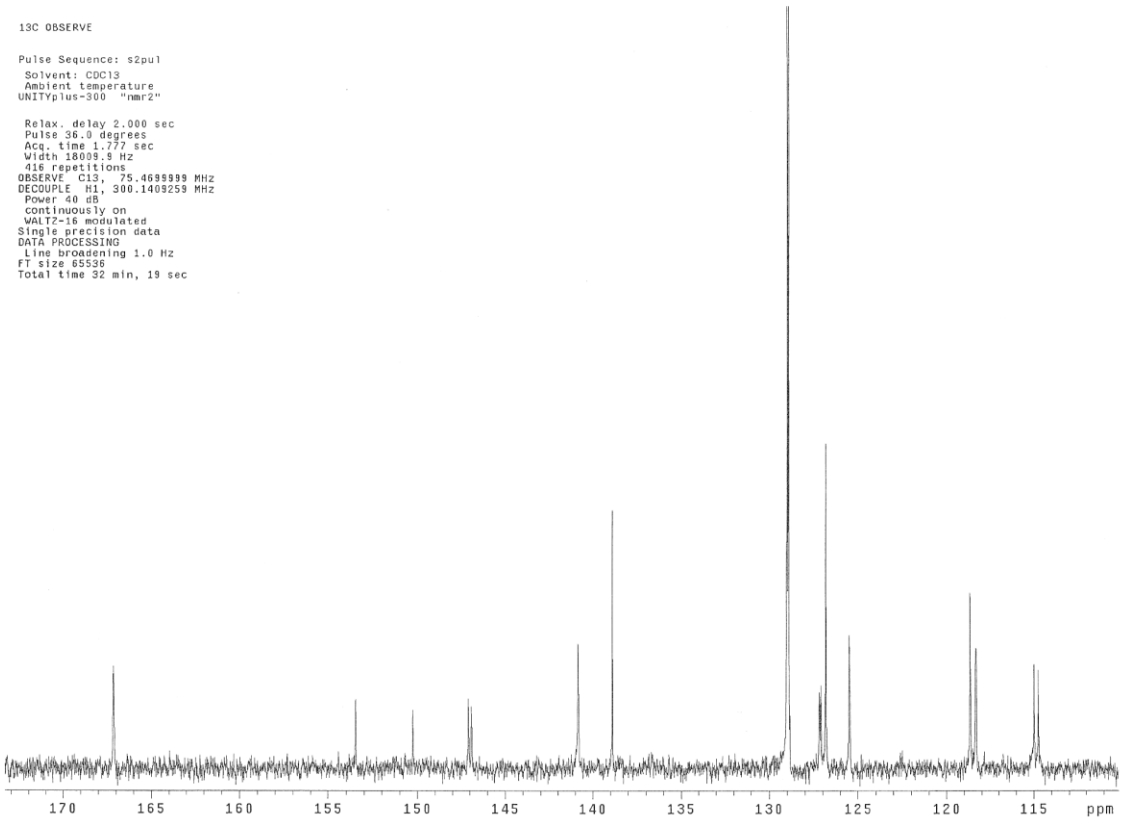

Figure 2.16 – ^{13}C NMR spectra of **4e**

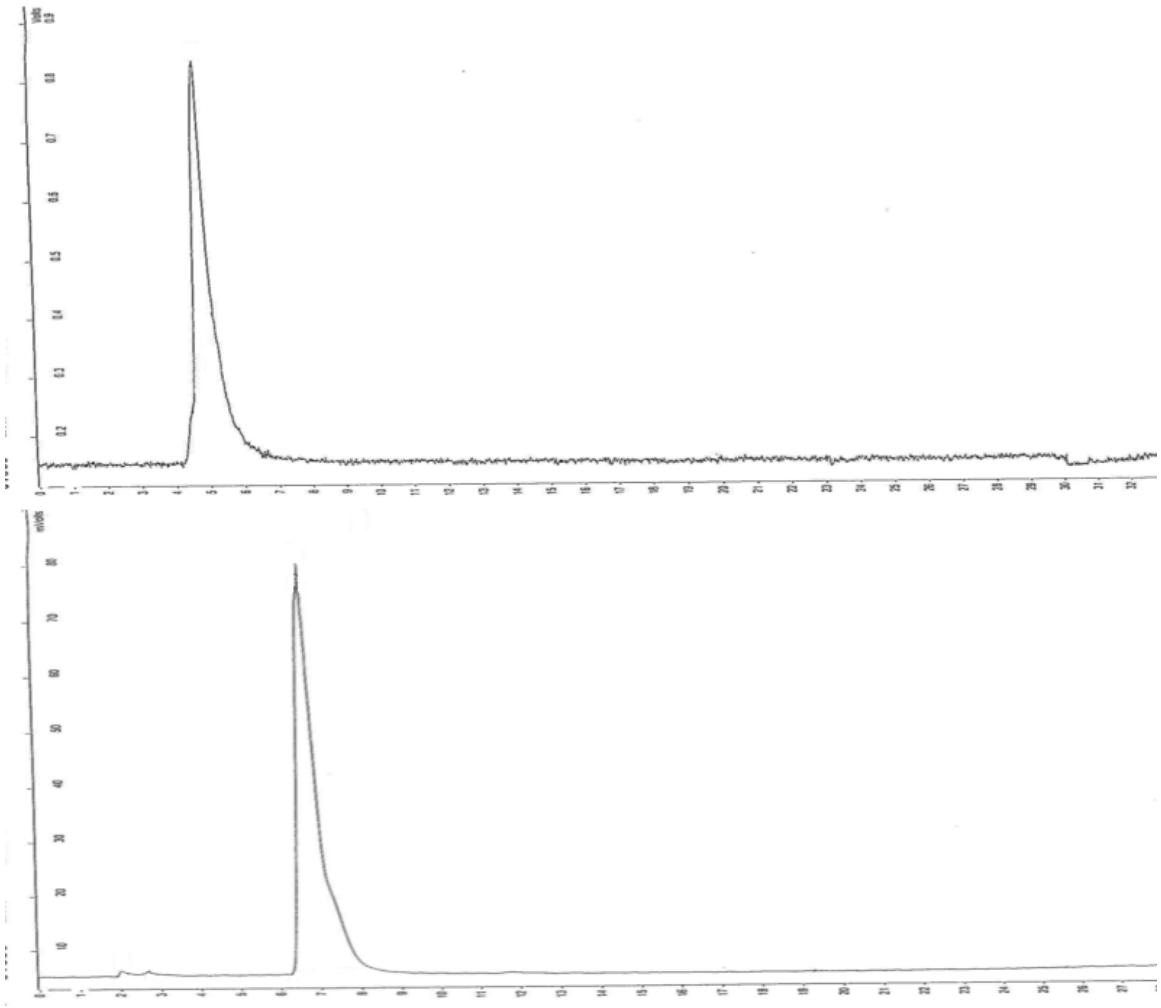

Figure 2.17 – Normal phase (A) and reverse phase (B) HPLC chromatograms of **4e**

3-(2-Fluoro-4,5-dimethoxyphenyl)-N-phenethyl-acrylamide (4f). Recrystallization from EtOAc and hexane gave 48 mg of **4f** as white crystals: mp 149 ˚C; ^{1}H NMR ($CDCl_3$) δ (ppm): 2.92 (t, J = 6.9 Hz, 2H), 3.68 (q, J = 6.5, 2H), 3.88 (d, J = 8.7, 6H), 5.90 (bs, 1H), 6.38 (d, J = 15.6 Hz, 1H), 6.64 (d, J = 12.0, 1H), 6.90 (d, J = 7.20 Hz, 1H), 7.29 (m, 5H), 7.66 (d, J = 15.6 Hz, 1H); ^{13}C NMR ($CDCl_3$) δ 35.93, 41.09, 56.53 (JC-F = 9.96 Hz), 100.45 (J_{C-F} = 28 Hz), 110.54 (J_{C-F} = 4 Hz), 114.01 (J_{C-F} = 13 Hz), 121.15 (J_{C-F} =7 Hz), 126.77, 128.99 (J_{C-F} = 11 Hz), 134.03, 139.15, 145.67, 151.41 (J_{C-F} = 10 Hz), 156.54 (J_{C-F} = 248 Hz), 166.40; CI-MS m/z 330 (MH^+, 100). HRCI-MS: Calculated for $C_{19}H_{21}NO_3F$; 330.1505. Found; 330.1506; Elemental analysis calculated for $C_{19}H_{20}NO_3F$: C, 69.29; H, 6.12; N, 4.25. Found: C, 69.03; H, 6.12; N, 4.21. ^{1}H NMR spectra is shown on Figure 2.15. ^{13}C NMR spectra is shown Figure 2.16.

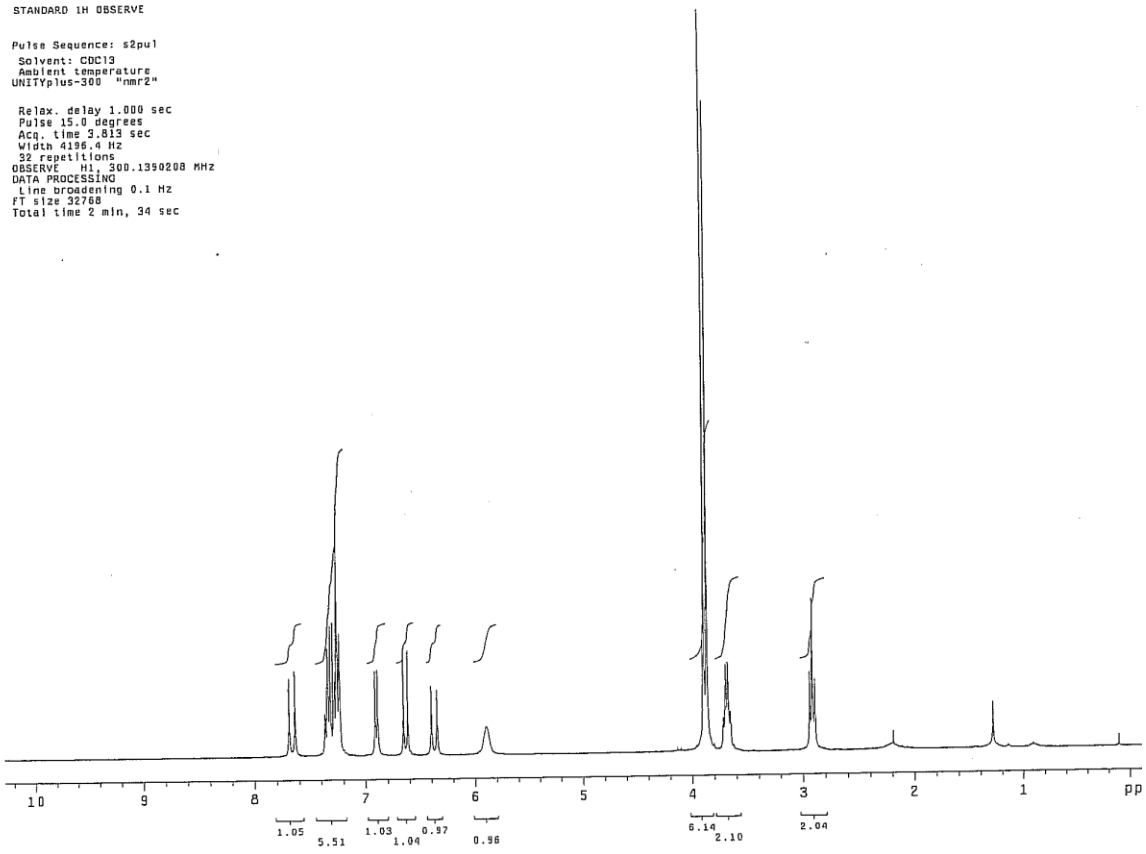

Figure 2.18 – ^{1H} NMR spectra for **4f**

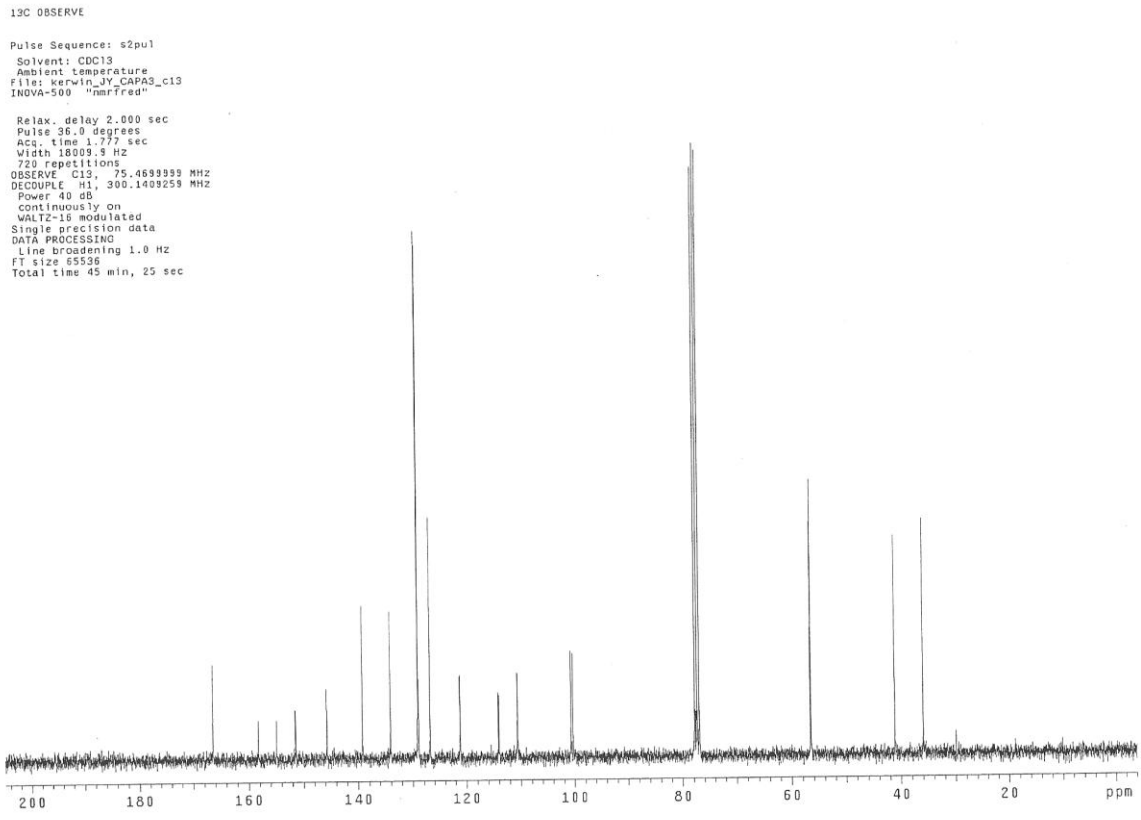

Figure 2.19 – ^{13}C NMR spectra for **4f**

2.3 – Discussion and Conclusions

Caffeic Acid Phenethyl Amide and five catechol ring fluorinated analogues were synthesized, purified and characterized by mass spectrometry, ^{1}H NMR and ^{13}C NMR.

Chapter 3 – Cytoprotective Activity of CAPA and CAPA derivatives in HUVEC

3.1 – INTRODUCTION

Endothelial cells comprise the inner layer of arteries, veins and capillaries and play a key role in the propagation of I/R injury [156]. In addition to providing a protective barrier between the lumen and the smooth muscle of a blood vessel, these cells contribute to regulation of immune cells, blood flow and overall function of the tissue being perfused. The endothelium is also important in modulating the inflammatory response that occurs following an I/R episode [157-158]. Upon reperfusion following an ischemic insult, these endothelial cells produce the previously discussed ROS rapidly in large amounts [159-160]. Major sources of ROS production from the endothelium have been reported to be from cytosolic xanthine oxidase and from complexes I and III of the electron transport chain [161-162]. Recruitment of neutrophils and other immune cells are also responses to I/R injury and can exacerbate the damage caused by the endogenous ROS. Injury to the endothelium can result in interferences with the performance of homeostatic functions such as maintenance of local blood flow, control of fluid exchange with the surrounding tissues and regulation of immune cells. If the damage caused is severe enough, endothelial dysfunction can manifest as inadequate perfusion, leak of vascular fluids or inflammation [163]. Since these endothelial cells are the first to experience the consequences of I/R injury, they serve as an appropriate model for studying the effects of the oxidative stress that follows reperfusion. Damage to the

endothelium has also been shown to correlate with function of neighboring tissues [164-165].

Human Umbilical Vein Endothelial Cells (HUVEC) were chosen as a model cell line because of the previously discussed significance of the endothelium in I/R injury. Endothelial cells are both targets and producers of ROS following an ischemic event and therefore are useful for studying the effects of cytoprotectants against oxidative stress. HUVEC are harvested from umbilical cords and pooled before distribution to minimize variability. HUVEC have been used extensively in a wide array of research activities and have also been utilized in studies simulating I/R conditions *in vitro* [166-168]. Hydrogen peroxide was employed as the inducer of oxidant stress in this study. H_2O_2 is commonly used as an exogenous stressor and has been used to induce oxidative damage and apoptosis in a variety of cell types in cytoprotection studies [169-173]. H_2O_2 is also one of the ROS produced endogenously by endothelial cells in I/R conditions.

CAPA and the fluorinated CAPA analogues were synthesized to improve the stability of CAPE and to determine whether derivatization affected the desirable cytoprotective activity of the parent compound. CAPE has been shown to be a potent antioxidant and cytoprotectant against oxidative stress in addition to being a protectant against I/R injury. CAPE has also been shown to be a potent inducer of the HMOX-1 gene and the HO-1 enzyme, a cytoprotective response system discussed earlier [142]. The purpose of the following series of experiments was to evaluate the protective activity of CAPA and the fluorinated derivatives in comparison to CAPE by way of cytoprotection assay against H_2O_2 in HUVEC and by evaluation of HO-1 induction.

3.2 – MATERIALS AND METHODS

3.2.1 – Materials and Instrumentation

Human umbilical vein endothelial cells (HUVEC) were obtained from Lifeline Technologies (Walkersville, MD) and cultivated on 75 cm^2 1% gelatin coated culture flasks using MCDB 131 cell culture media (Invitrogen, Carlsbad CA) supplemented with 2% fetal bovine serum, ascorbic acid, heparin, VEGF, hydrocortisone bFGF and heparin (Lifeline Technologies). The cells were grown to confluency at 37 ˚C in humidified atmosphere with 5% CO_2. HUVEC were then treated with Trypsin/EDTA and subcultivated onto gelatin coated 96 well and 24 well multi-plates and used when confluent. Population doubling levels 2 through 5 were used in the described experiments. CellTiter-Blue® Blue solution ordered from Promega (Madison WI). Spectrophotometry was performed on a Spectramax M2 microplate reader (Molecular Devices, Sunnyvale CA). Western blot E-PAGE gels, iBlot apparatus, nitrocellulose transfer stacks and loading buffers were ordered from Invitrogen (Carlsbad, CA). Rabbit polyclonal HO-1 antibodies were obtained from Assay Designs (Ann Arbor, MI). Mouse polyclonal β-actin antibodies were obtained from Santa Cruz Biotechnology (Santa Cruz, CA). Donkey anti-mouse and donkey anti-rabbit secondary antibodies were obtained from Licor (Lincoln, NE).

3.2.2 – Cytotoxicity of compounds in HUVEC

CAPE and certain catechol ring-fluorinated CAPE analogs have been reported to be cytotoxic to HUVEC at higher concentrations [112]. CAPA and the CAPA derivatives were screened along with CAPE for toxicity in HUVEC. Stock CAPE, CAPA, and CAPA derivative solutions were dissolved in DMSO then diluted in MCDB 131 tissue culture media for use in the assays. Confluent HUVEC were treated with CAPE and the amide derivatives for 24 hours at 37 ˚C at concentrations ranging from 10 μM to 60μM. Following the 24 hour incubation, the media was replaced with 10 % CellTiter-Blue® Blue solution (Promega, Madison WI). HUVEC were incubated for 2 hours at 37 ˚C then analyzed for fluorescence. The readings were taken at 545 nm excitation and 590 nm emission wavelengths on a Spectramax M2 microplate reader (Molecular Devices, Sunnyvale CA). Cell viability was calculated from these fluorescence readings and compared to the DMSO vehicle control to obtain percent viability. Cell viability less than 90% of control was considered toxic.

3.2.3 – Cytotoxicity of H_2O_2 in HUVEC

Hydrogen peroxide is one of the principle reactive oxygen species produced in various vascular complications including ischemia reperfusion injury and has also been used in other *in vitro* models as an inducer of oxidative stress in endothelial cells [174-176]. To determine a suitable dose, HUVEC were treated with H_2O_2 at concentrations ranging from 0.01 mM to 5 mM for one hour. A stock solution of H_2O_2 (50% w/v, 14.7 M, Sigma Aldrich) was diluted to 1M with deionized water then subsequently diluted in MCDB131 buffer to obtain the desired concentrations.

Following the one hour period the culture media was replaced and the cells were allowed to recover for 18 hours. Cell viability was assessed with CellTiter-Blue® following the 18 hour period. The target dosage was one that reduced cell viability to approximately 20% of control.

3.2.4 – Cytoprotection Assay

Confluent HUVEC were treated with CAPE and the amide derivatives at 20 μM concentration for 5 hours at 37 ˚C. After the 5 hour incubation, the compounds were removed from the wells, and the cells were washed twice with MCDB 131 buffer. Stock hydrogen peroxide solution (50% w/v, Sigma Aldrich) was diluted in MCDB 131 buffer, and incubated in the cells following the buffer wash. HUVEC were incubated in the hydrogen peroxide for 1 hour at 37 ˚C. The hydrogen peroxide was then removed. The cells were washed once with MCDB 131 media, and were then incubated in complete MCDB 131 media for 18 hours at 37 ˚C. Following the 18 hour period, the cells were treated with 10% CellTiter-Blue® solution and analyzed for viability. In the dose response cytoprotection assay, percent cytoprotection for each compound was calculated by subtracting the average fluorescent reading of the negative control (HUVEC treated only with DMSO and hydrogen peroxide) from the fluorescent values of each well. This was then divided by the average fluorescence of the positive control (HUVEC treated only with DMSO) to obtain percent cytoprotection.

3.2.5 – HO-1 expression

HUVEC were treated with 5 µg/ml of CAPE and CAPA for 6 hours. At the 6 hour time point, the media was removed and the cells were exposed to 70 µl of lysis buffer. The lysis buffer was composed of 50 mM Tris(2-carboxyethyl) phosphine hydrochloride (TCEP) and 1x loading solution (Invitrogen, Carlsbad CA). A 48 well E-PAGE gel was then loaded with 15µl of the lysis buffer solution and run for 30 minutes. Protein was transferred to a nitrocellulose membrane via the iBlot apparatus (Invitrogen, Carlsbad CA). Upon successful transfer, the membrane was fixed in a solution of 50% methanol, 43% water and 7% acetic acid. The membrane was then washed in a solution of 50% water and 50% blocking buffer (Licor, Lincoln NE) for one hour. The HO-1 polyclonal antibody was diluted 1000x in blocking buffer and introduced to the membrane following the blocking phase. B-actin was used to normalize protein levels and was diluted 25,000x in blocking buffer before being introduced to the membrane. The membrane was exposed to the primary antibodies for 24 hours at 4 °C. Following this time period, the primary antibodies were removed and the membrane was washed 4x with a solution containing 0.1% tween 20 in PBS. The secondary antibodies were diluted 25,000x in blocking buffer and then introduced to the membrane for one hour after the wash. The membrane was then washed again with the 0.1% tween in PBS solution and read on the Licor Odyssey ® IR scanner using fluorescent antibody imaging for protein quantification. The signal obtained for HO-1 was divided by the signal for β-actin so that protein levels were normalized. Cells treated only with DMSO served as the control.

3.2.6 – Statistical analysis

Data are reported as means ± standard deviation as a percentage of the control. Differences between the groups were first analyzed by ANOVA, and then evaluated by the Tukey-Kramer post hoc analysis. O'Brien's and Bartlett's tests showed that variances were equal among groups. $P < 0.05$ was considered significant.

3.3 – RESULTS

3.3.1 – Cytotoxicity of compounds in HUVEC

The results, shown in Figure 3.1 demonstrate that CAPA and amides 4b and 4d-f showed no toxicity at any of the tested concentrations. CAPE exhibited cytotoxicity at 40 μM and 60 μM. The amide 4c showed cytotoxicity at all concentrations.

3.3.2 – Cytotoxicity of H_2O_2 in HUVEC

Cell viability as compared to control declined steadily as H_2O_2 concentration was increased. The target dosage for the cytoprotection study was one that reduced cell viability to approximately 20%. This was achieved with 2 mM H_2O_2. The results are shown in Figure 3.2

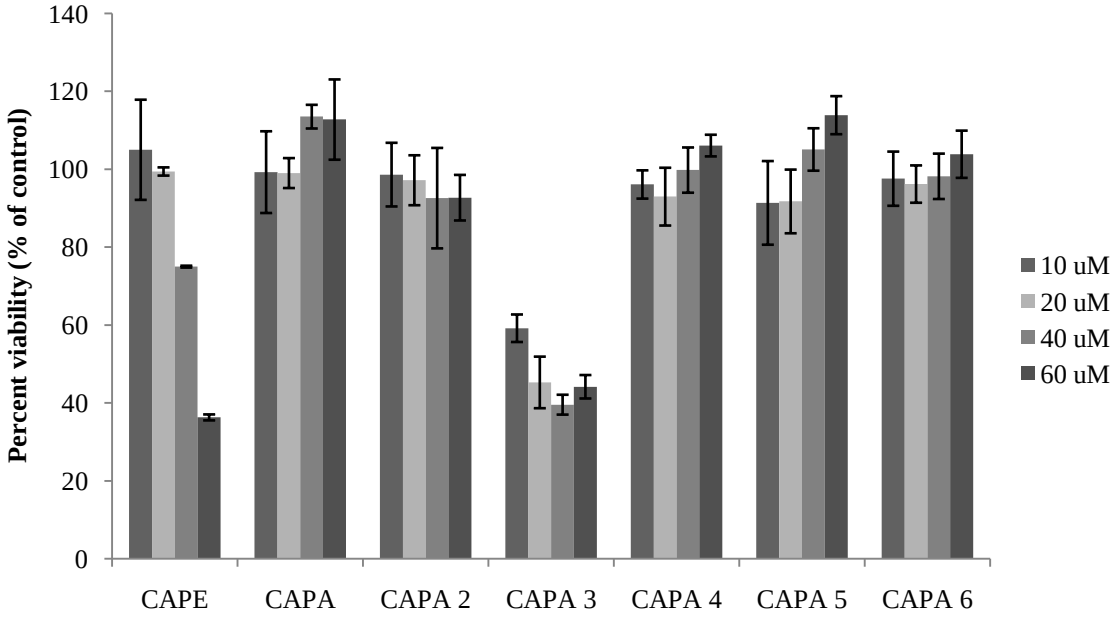

Figure 3.1 - Toxicity of CAPE, CAPA, and CAPA derivatives toward HUVEC. Compounds were incubated in HUVEC for 24 hours at 37 ˚C. Cell viability was determined by the Alamar Blue assay. Values are reported as a percentage of the vehicle control (0.1% DMSO).

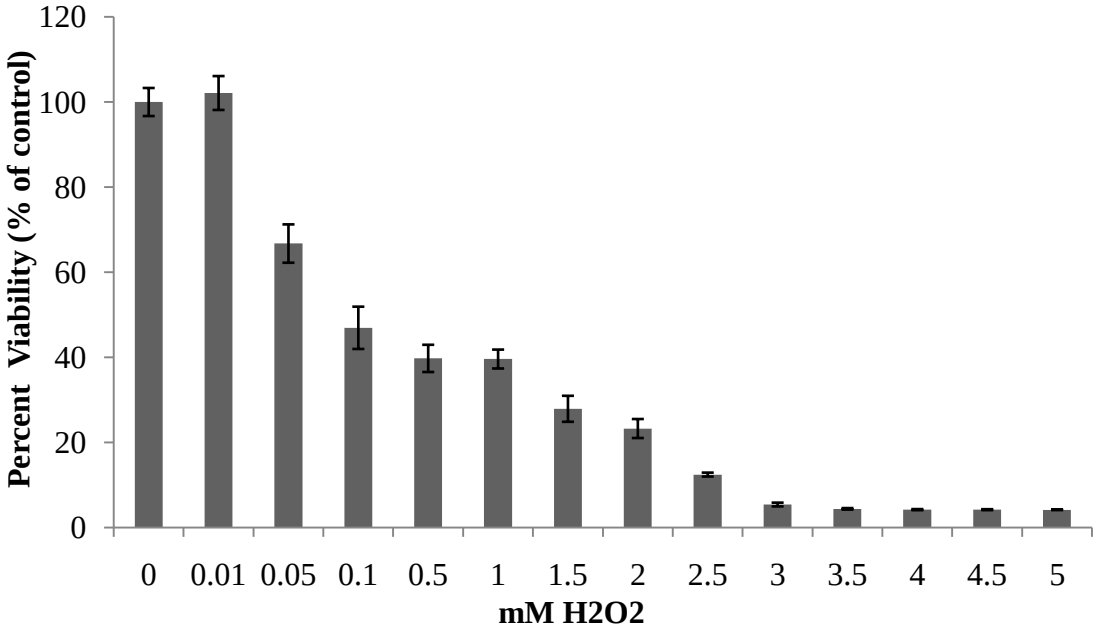

Figure 3.2 - Toxicity of H_2O_2 in HUVEC. HUVEC were incubated in culture media containing the indicated concentration of H_2O_2 for 1 hour at 37 ˚C. The culture media was replaced and cells were allowed 18 hours to recover, then were assessed for viability with the CellTiter-Blue®.

3.3.3 – Cytoprotection of HUVEC

To evaluate oxidative stress *in vitro*, we employed a model using H_2O_2 as the inducer of oxidative damage. HUVEC were treated with CAPE or the amide derivatives 4a-f at 20 μM concentration for 5 hours. The cells were rinsed and the then treated with 2 mM H_2O_2. After 1 hour, the H_2O_2 containing medium was replaced with cell culture media and the cells were allowed to recover for 18 hours. At the end of the 18 hour period, cell viability was assessed with the CellTiter-Blue® Cell Viability assay and compared to cells treated only with vehicle and H_2O_2, as well as with those that were not exposed to H_2O_2. The results are shown in Figure 3.3. CAPA and compounds 4b, 4c, and 4e exhibited significant cytoprotection against H_2O_2 when compared to vehicle only pre-treatment. CAPE was also significantly cytoprotective against H_2O_2. There was no significant difference in cytoprotective activity between CAPE and CAPA ($P > 0.05$).

In a dose dependent cytoprotection assay, HUVEC were treated with CAPE and CAPA at 1, 5, 20, 40, and 60 μM concentrations prior to the induction of oxidative stress with H_2O_2. The results are shown in Figure 3.4. The EC_{50} was calculated for both compounds by linear regression using the first 3 data points. The EC_{50} was found to be 8 μM for CAPE and 2 μM for CAPA.

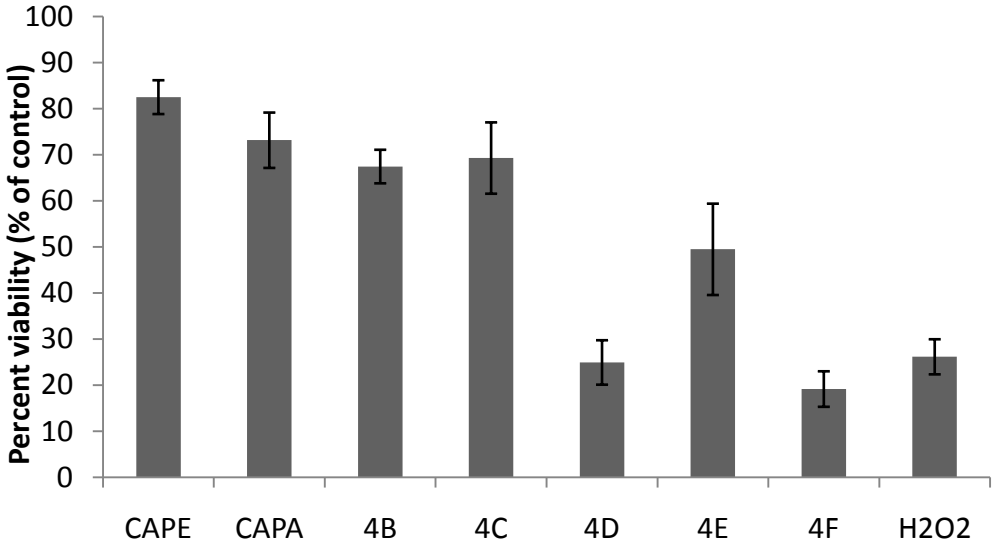

Figure 3.3 - Cytoprotection of HUVEC against 2 mM H_2O_2 by CAPE, CAPA, and CAPA analogues. All compound concentrations were at 20 μM. CAPE, CAPA, 4B, 4C and 4E all showed significant cytoprotection when compared to untreated (H_2O_2 only) ($P < 0.05$). CAPA derivatives 4D and 4F provided no cytoprotection.

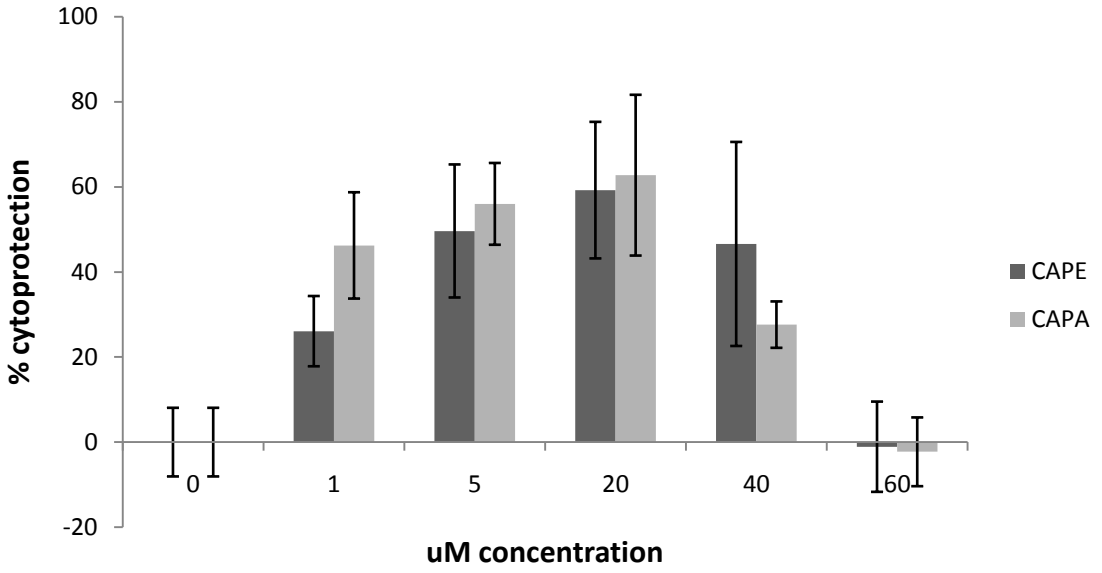

Figure 3.4 - Dose response cytoprotection relationship of CAPE and CAPA against 2 mM H_2O_2. Concentrations above 40 µM are cytotoxic for both CAPE and CAPA and gave lower cell viability than untreated HUVEC as shown. CAPE and CAPA showed significant cytoprotection at concentrations from 1 through 40 µM

3.3.4 – HO-1 expression

The induction of HO-1 expression was investigated for both CAPE and CAPA. Both compounds showed significant increases in HO-1 expression over the DMSO control. The western blot is shown in Figure 3.5. The quantified HO-1 expression data in shown in Figure 3.6

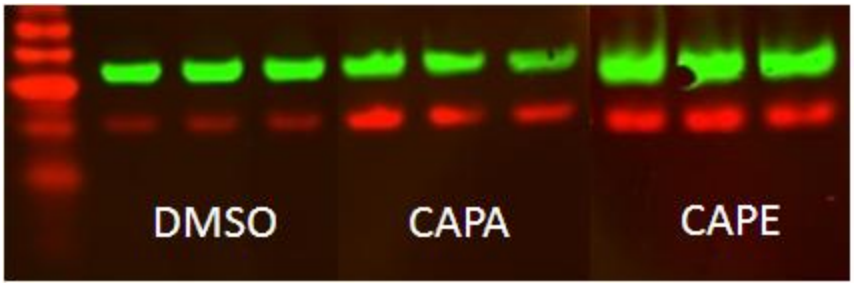

Figure 3.5 – Western blot of HO-1 expression following a 6 hour incubation of 5 μg/ml CAPE and CAPA. Protein extractions were performed at 6 hours. Fluorescent antibody imaging was used to quantitatively determine protein levels. Red = HO-1, green = β-actin

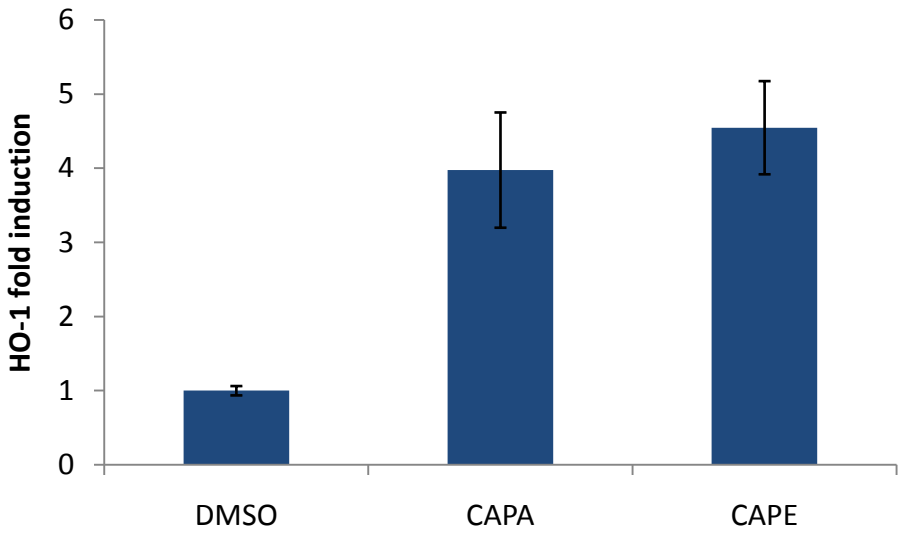

Figure 3.6 – HO-1 induction after a 6 hour incubation by 5 µg/ml CAPE and CAPA in HUVEC. Protein extractions performed at 6 hours for all samples. Values normalized against β-Actin. DMSO served as vehicle control.

3.4 – DISCUSSION AND CONCLUSIONS

Introducing a fluorine group on the catechol ring increases the electronic density of the conjugated system, can decrease the interaction with catechol methyltransferase, and may also have a significant effect on receptor binding or selectivity [177]. The hydroxyl groups on the CAPA catechol may contribute to the antioxidative activity of the compound. We were interested in seeing the effect of replacing one of these hydroxyls with a fluorine, hydrogen or methoxy group on the cytoprotective activity of the compound.

Prior to evaluating the cytoprotective activity of CAPE and the CAPA derivatives, each compound was screened for toxicity in HUVEC. CAPE was found to be toxic at 40 and 60 μM, in accord with previous studies [112]. There are interesting differences in cytotoxicity of the certain amide derivatives when compared to their corresponding ester analogues. Amides 4e and 4f were not cytotoxic at any concentration up to 60 μM, the highest concentration examined. The corresponding ester derivatives were similarly reported to be non-cytotoxic at concentrations up to 15 μg/mL (ca. 50 μM). Amide 4c was toxic at all the concentrations tested; similar to the corresponding ester analogue [112]. However, whereas CAPE and the esters corresponding to 4b and 4d are cytotoxic at concentrations greater than 40 μM, CAPA and the amides 4b and 4d are not cytotoxic even at concentrations as high as 60 μM. The origin of this difference in cytotoxicity between CAPE and certain fluorinated CAPE analogues versus CAPA and the corresponding fluorinated CAPA analogues is not clear.

CAPE was significantly cytoprotective against H_2O_2 induced oxidative stress in HUVEC. This was also demonstrated previously in a similar model [109] as well as a study which used menadione to generate an oxidative stress [112]. Four of the amide

derivatives of CAPE were also found to be significantly cytoprotective. These four compounds all contained either one or two hydroxyl groups on the cinnamic acid phenyl ring. Although compound 4c proved to be very cytotoxic in HUVEC over a 24 hour period, the toxicity is less apparent over a 5 hour incubation time, as the compound was found to be significantly cytoprotective against H_2O_2, and exhibited significantly higher cell viability over the vehicle control. While the mechanism behind this cytoprotective activity is not completely known, it is suggested that the anti-oxidative and radical scavenging properties of the catechol group are correlated with the protection against H_2O_2. The catechols CAPE, CAPA, 4b, and 4c all display cytoprotective effects; whereas, the monomethylated and dimethylated analogues 4d and 4f, respectively, were not cytoprotective. The *ortho*-fluorophenol 4e demonstrated intermediate cytoprotection, which may be due to the ability of the *ortho*-fluorine substituent to stabilize the phenol radical formed upon hydrogen atom donation [178]. Interestingly, the structure-activity relationship for cytoprotective effect for these amides is quite different from that reported for the corresponding esters.[112] The ester corresponding to 4c is not cytoprotective, despite the presence of the catechol functionality, and the ester corresponding to 4e is cytoprotective, despite the lack of any free phenolic hydroxyl groups. In the dose dependent cytoprotection assay, a biphasic response was observed for both CAPE and CAPA. The cytoprotection percentage increases from 1 μM up to 20 μM of CAPE and CAPA, then starts to decline at 40 μM. The drop off in cytoprotection at higher CAPE concentration had been attributed to CAPE's cytotoxicity above 20 μM [179] as indicated in Figure 3.1. However, a similar effect is observed for CAPA, even though it is not cytotoxic at 40 μM. It is unclear as to why this phenomenon occurs.

It is not well understood how cytoprotection is provided by pretreatment with these cytoprotective agents. Studies previously performed in our group have shown that

the cytoprotective activity of CAPE was correlated with the levels of the heme oxygenase 1 (HMOX 1) gene expression. CAPE is a potent inducer of the HMOX 1 gene transription and has been shown to up-regulate it as much as 8-fold over control [142]. Studies have also shown that when heme oxygenase activity is inhibited, the cytoprotective effect of CAPE against menadione induced oxidative stress is abolished [142]. The findings demonstrate that CAPA is less toxic than CAPE, and that there is no significant difference in cytoprotection between the two when tested at 5 and 20 μM concentrations against 2 mM hydrogen peroxide. Both CAPE and CAPA treated cells were able to significantly induce the expression of HO-1 over control with as little as 1 hour of exposure time. There were also no significant differences found in HO-1 expression between cells treated with CAPE and CAPA beyond 2 hours of exposure time. These findings suggest that the cells may not need to be continually exposed to CAPE or CAPA in order for a protective effect to be induced.

CAPA and catechol ring-fluorinated derivatives of CAPA were synthesized and investigated for cytoprotective activity against hydrogen peroxide induced oxidative stress in HUVEC. All but one of the CAPA derivatives synthesized were non-toxic up to the maximally tested concentration, with 4c being toxic at all tested concentrations. The results here also show that CAPA, 4b, 4c, and 4e are all significantly cytoprotective in this model ($P < 0.05$). The only two analogs which were not cytoprotective were the methylated compounds 4d and 4f. Although the mechanism of cytoprotection is not well understood, the antioxidative activity appears to be important as cytoprotection is correlated with the presence of free catechol hydroxyl groups. CAPA was less toxic in HUVEC when compared to CAPE, however, there was no significant difference found in cytoprotection between the two compounds. The lower toxicity exhibited by CAPA allows for higher concentrations of the compound when dosing.

Chapter 4 – Stability of CAPA in Male Sprague-Dawley Rat Plasma

4.1 – INTRODUCTION

CAPE's protective activities *in vitro* and *in vivo* have been well documented despite being labile in serum and in circulation [143]. Attempts to improve upon the stability of CAPE led to the synthesis of CAPA and 5 fluorinated derivatives of CAPA. Amides are generally associated with higher hydrolytic energies of activation. CAPA is also able to avoid hydrolysis via esterase enzymes due to lack of an ester bond. We therefore hypothesized that the amide derivatives would exhibit higher stability in serum. The previous cytoprotection study against H_2O_2 induced oxidative stress in HUVEC showed that there was no significant difference between CAPE and CAPA in protective ability. CAPA was also the most cytoprotective of the synthesized analogues so it was chosen as the candidate to be tested for stability alongside CAPE.

Plasma stability is an important consideration in drug development. Drug compounds that exhibit poor stability in plasma present high clearance, short half lives and minimized exposure *in vivo*, possibly resulting in poor efficacy. Extremely rapid plasma decompositions can also compromise the establishment of reliable pharmacokinetic profiles, since *ex vivo* hydrolysis of the compound becomes a significant variable [180]. Improved plasma stability could mean an extended half-life of the compound *in vivo*, longer exposure times in circulation and potentially increased efficacy. The purpose of these experiments was to determine whether amide derivatization improved the plasma stability of CAPE.

4.2 – MATERIALS AND METHODS

4.2.1 – Materials and Instrumentation

CAPE (≥ 98%) and *trans*-resveratrol (≥ 98%) were obtained from Cayman Chemical (Ann Arbor, MI). CAPA (≥ 95%) was synthesized and characterized previously in our laboratories [181]. Heparinized male Sprague-Dawley rat plasma was obtained from Innovative Research (Novi, MI). Water used in the experiments was passed through a Millipore (Billerica, MA) Milli-Q water purification system (18.2 MΩ). HPLC grade methanol was obtained from JT Baker (Mallinckrodt Baker, Phillipsburg, NJ). HPLC grade ethyl acetate was from Sigma Aldrich (St Louis, MO). An Agilent 1200 series HPLC (Santa Clara, CA) was used comprising a 1200 series pump, diode array detector, autosampler, and degasser. Separation was achieved with an Agilent ZORBAX C_{18} column (4.6 × 150 mm, 5μm) coupled to a cartridge guard column (4.6 × 12.5 mm) of the same material. The column was maintained at 25°C for the duration of the analysis. Autosampler temperature was maintained at 4°C. Instruments were controlled by the Agilent ChemStation software program. *Trans*-resveratrol was used as an internal standard (IS). It exhibits high absorbance at the λ_{max} of CAPA and CAPE (320 nm), and is easily separable from the analyte, decomposition products, and plasma contents with the mobile phase and column used. A gradient elution technique was used for the separation of both CAPA and CAPE from IS and plasma contents. The mobile phase used was ultrapure H_2O (solvent A) and MeOH (solvent B). Flow rate was set at 1 mL/min. The gradient elution program for CAPA and CAPE is described in Table 4.1. Detection wavelength was set to 320 nm.

CAPA

Time (min)	%A	%B
0	65	35
3	65	35
7	10	90
8	10	90
13	65	35
15	65	35

CAPE

Time (min)	%A	%B
0	75	25
1	75	25
5	15	85
8	15	85
12	75	25
15	75	25

Table 4.1 – HPLC gradients for CAPA and CAPE. Solvent A = H_2O, Solvent B = MeOH

4.2.2 – Sample preparation

CAPA, CAPE, and resveratrol working solutions were made in MeOH. Rat plasma samples (180 µL) were aliquoted into 1.5 mL microfuge tubes and spiked with CAPA or CAPE working solutions (10 µL). Working solutions of CAPA and CAPE were made at 0.05, 0.1, 0.2, 1, 2, and 5 mg/mL concentrations for construction of the calibration curve. At the time of extraction, 10 µL of resveratrol (400 ug/mL) was added to each sample. Ethyl acetate (600 µL) was subsequently added to each sample for extraction, followed by 5 minutes of vortexing and 5 minutes of centrifugation at 13,000 RCF under temperature control (4°C). The ethyl acetate layer was removed and transferred to a 2 mL microfuge tube. An additional 600 µL of ethyl acetate was added to the remaining plasma sample, and the extraction procedure was repeated. The ethyl acetate samples were pooled and evaporated under centrifugal vacuum via the SpeedVac Concentrator (Thermo Scientific, Waltham, MA). The dried samples were kept at -20°C until analysis. Prior to injection, the samples were reconstituted with 200 µL of MeOH, vortexed for 5 minutes, and centrifuged at 13,000 RCF for 2 minutes. The reconstituted samples were transferred to 300 µL glass HPLC vials (Agilent, Santa Clara, CA), inserted into the autosampler, and analyzed.

4.2.3 – Method Validation

Analyte response was expressed as CAPA vs resveratrol (IS) or CAPE vs resveratrol (IS) signal area ratio.

Selectivity

Selectivity of the assay was established by utilizing HPLC conditions such that analyte quantification was free from interference by endogenous plasma compounds or decomposition products.

Calibration curve and linearity

The concentrations of CAPA and CAPE used for modeling response vs concentration in rat plasma were 2.5, 5, 10, 50, 100, and 250 μg/mL. Calibration standards were analyzed in replicates of 5 per concentration and included 20 μg/mL of IS. Linear regression was performed to describe the analyte response vs concentration relationship. A correlation coefficient was also calculated for the linear fit curve.

Sensitivity

Sensitivity was determined by the limit of detection (LOD) and the lower limit of quantification (LLOQ). LOD was defined as the minimum concentration necessary to produce a signal to noise ratio of 3:1. The LLOQ is the lowest quantifiable concentration,

and is also defined as the lowest concentration on the calibration curve with a signal to noise ratio of at least 5:1.

Precision

Intra-day precision was evaluated by spiking blank plasma at 3 concentrations of CAPA and CAPE: the lowest and highest concentrations on the calibration curve (2.5 and 250 μg/mL) and an intermediate concentration (50 μg/mL), and then measuring analyte response. Five replicates at each concentration point were analyzed and the results were expressed as percent relative standard deviation (%RSD). Inter-day precision was evaluated at the same concentration levels (2.5, 50, and 250 μg/mL). Spiked plasma samples were processed and analyzed in replicates of five on three separate days. Results were expressed in %RSD. Precision determined at each concentration was considered acceptable if the %RSD did not exceed 15%, except for the lower limit of quantification (LLOQ), where the %RSD should not exceed 20%.

Accuracy

The accuracy of the method was evaluated as percentage deviation of the mean from the true value. Accuracy was determined at three concentration levels (2.5 (LLOQ), 50, 250 μg/mL). Mean values obtained were considered acceptable if within 15% of the true value, except for the LLOQ, where mean values under 20% deviation were accepted. True value was defined as the analyte response obtained from the calibration curve standards.

Recovery

Recovery was evaluated as absolute recovery and was calculated by comparing analyte peak area from plasma extracted samples to those of the corresponding concentrations of unextracted samples. The peak areas of the unextracted samples were considered to be 100% recovery, and were obtained by analyzing standards in MeOH that were directly injected into the HPLC. Recoveries of CAPA and CAPE were evaluated at three concentration levels (2.5 (LLOQ), 50, 250 μg/mL) with three replicates per concentration at 25 °C.

4.2.4 – Stability Study

This method was developed for the determination of CAPA and CAPE in rat plasma and was used to evaluate compound stability. Stability of CAPA in rat plasma was determined at 25, 37, and 60 °C and stability of CAPE was determined at 4, 25, and 37 °C. The concentration of the compounds was evaluated at a minimum of five time points for each temperature, with three replicates being analyzed at each time point. The decomposition of CAPA and CAPE was determined over a period of 2-5 half lives. The purpose of this stability study was to determine the half-life of CAPA and CAPE at each respective temperature and to calculate an energy of activation (E_a).

Blank rat plasma (4.75 mL) was spiked with 0.25 mL of a 2 mg/mL working solution of CAPA or CAPE. 190 µL aliquots of the plasma solutions were then placed in 1.5 mL micro-centrifuge tubes. The tubes were tightly capped and then incubated at the intended temperatures. The samples were allowed to incubate at their respective temperatures until the time of extraction. Immediately prior to extraction, 10 µL of 400 µg/mL resveratrol solution was added to each sample. This was subsequently followed by the ethyl acetate extraction procedure and HPLC quantification process described earlier. These steps were repeated at each time point and were done in triplicate.

The freeze thaw stability of CAPA was determined by subjecting plasma solutions of CAPA to three freeze/thaw cycles (FTC). Plasma solutions of CAPA were made in triplicate at 100 µg/mL concentration and frozen at -20°C for 24 hours. These solutions were then allowed to thaw unassisted at room temperature, upon which they were refrozen at -20°C for another 24 hours. This process was repeated three times. Following three FTCs, 10 µL of 400 µg/mL resveratrol was added. The samples were extracted using the ethyl acetate extraction procedure described earlier and then

quantitatively determined by HPLC. Analyte response of the FTC samples was compared to that of plasma samples that did not undergo the three FTCs. The freeze thaw stability of CAPA is reported as percent recovery. Long term stability was evaluated by storing three replicates of CAPA at 100 μg/mL concentration for 4 weeks at -20 °C. Following the 4 week period, 10 μL of 400 μg/mL resveratrol was added. The samples were then extracted and quantified on the HPLC. Long term stability is reported as percent recovery. CAPE and CAPA samples underwent the same method qualification procedures.

4.2.5 – Data analysis

The data from the stability studies for CAPA and CAPE were plotted as the natural logarithm of percent remaining vs time. The first order rate constant k was obtained from the slope of the linear regression line. The half-life of CAPA and CAPE was calculated from the rate constant k obtained from the linear regression lines at each of the tested temperatures using the following equation:

$$t_{1/2} = \frac{ln2}{k} \quad \textbf{(4.1)}$$

The energy of activation (Ea) was calculated for both CAPA and CAPE by fitting the obtained rate constants and the corresponding temperatures to the Arrhenius equation:

$$\ln k = \ln A \ - \left(\frac{Ea}{R}\right)\left(\frac{1}{T}\right) \quad \textbf{(4.2)}$$

k represents the first order decomposition rate constant, A is the pre-exponential factor which takes into account frequency of collisions, R is the universal gas constant and T is the absolute temperature in Kelvin.

4.3 – RESULTS

4.3.1 – Method Validation

The quantification of CAPE and CAPA was free from interferences by endogenous plasma compounds and decomposition products. The chromatograms for CAPE and CAPA are shown in Figure 4.1. Calibration curves for CAPA and CAPE were constructed by analyzing six concentrations (2.5, 5, 10, 50, 100, 250 µg/mL) of both compounds with five replicates assessed at each concentration level. Linear regression was performed to describe the relationship between CAPA concentration vs analyte response. The following are the linear regression parameters for the calibration curve of CAPA: Slope = 0.0235, Intercept = -0.0486, R^2 = 0.9988, and CAPE: Slope = 0.0217, Intercept = -0.0194, R^2 = 0.9998. The fitted line describes the linear relationship between analyte signal and nominal concentration in the range of 2.5 to 250 µg/mL. The LLOQ was defined as the lowest concentration on the calibration curve and was 2.5 µg/mL for both CAPA and CAPE. Analyte response at the LLOQ was greater than five times the blank response. The LOD was determined to be 1 µg/mL for both compounds and was at least three times the blank response. Inter-day and intra-day precision for the determination of CAPA did not exceed 7.41 %RSD. Precision values for CAPE did not exceed 9.34 %RSD. These values were considered acceptable. Accuracy values are reported as percent deviation (%Dev). The accuracy of CAPA determination was within 13.12% of the true value. These values are acceptable within the limits established by the FDA guidance. Recovery was calculated as the ratio of analyte response of plasma extracted samples to those of unextracted samples. Recovery is reported as absolute recovery. Inter-day precision values for CAPA and CAPE are listed in Tables 4.2 and 4.3

respectively. Assay qualification parameters are summarized in table 4.4 for both CAPA and CAPE

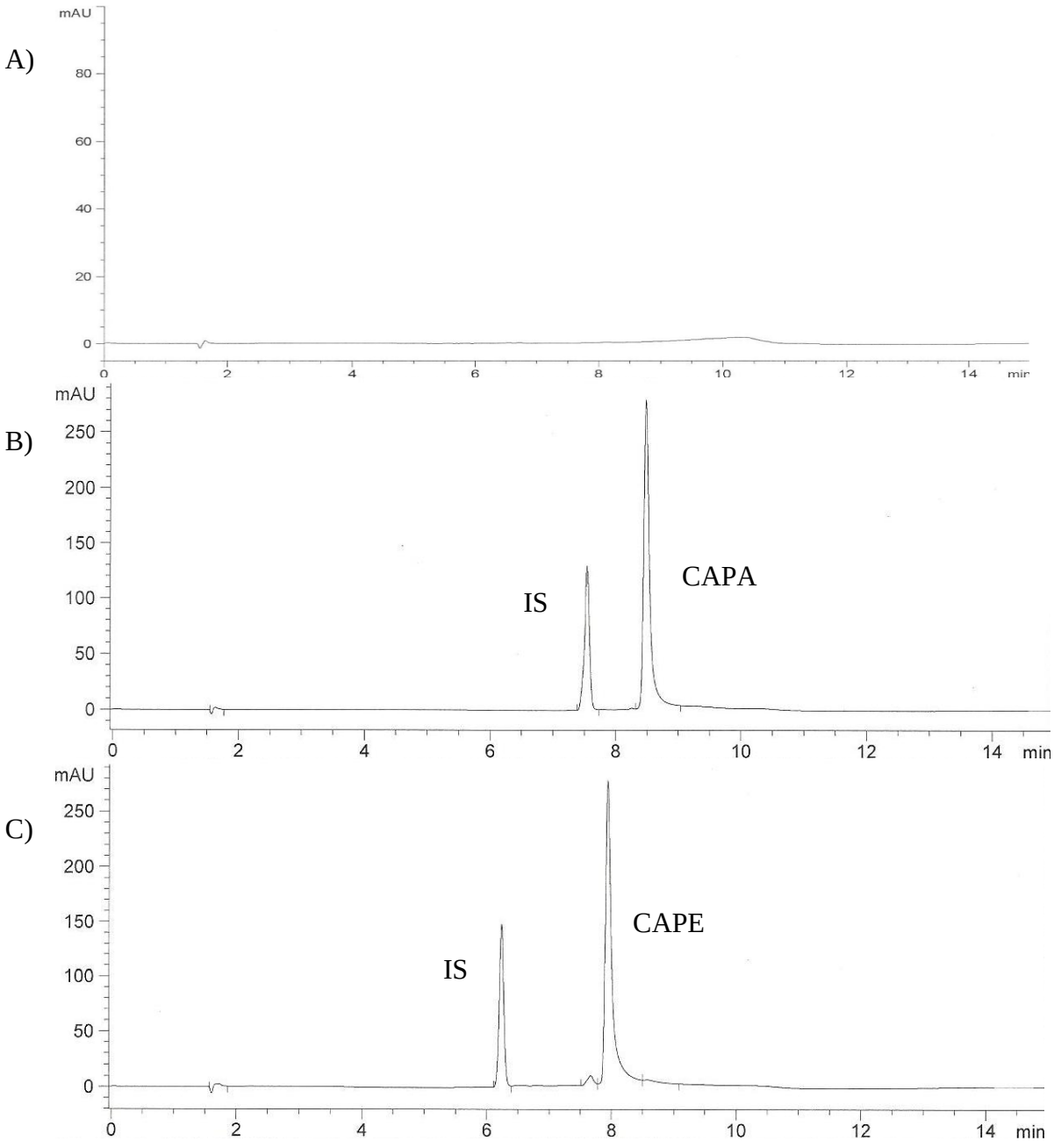

Figure 4.1 - Representative chromatograms of: (A) Blank rat plasma, (B) Rat plasma spiked with 100 µg/mL CAPA and 20 µg/mL IS, (C) Rat plasma spiked with 100 µg/mL CAPE and 20 µg/mL IS

	Nominal Concentration (μg/ml)		
	2.5	**50**	**250**
Day 1	0.0449	0.915	5.904
	0.0448	0.970	5.822
	0.0436	1.001	5.793
	0.0478	0.965	5.635
	0.0470	0.984	6.012
Day 2	0.0512	0.995	6.058
	0.0504	1.018	6.045
	0.0517	1.038	6.149
	0.0518	1.013	6.057
	0.0544	1.025	6.100
Day 3	0.0517	1.012	6.048
	0.0510	1.012	6.077
	0.0456	0.995	5.999
	0.0562	1.010	5.918
	0.0521	0.993	6.058
AVG	0.0496	0.996	5.978
SD	0.0038	0.030	0.139
%RSD	7.6021	2.980	2.320

Table 4.2 – Inter-day precision values for CAPA. Analyte responses (CAPA : resveratrol signal ratio) are shown per concentration.

	Nominal Concentration (µg/ml)		
	2.5	**50**	**250**
	0.0381	1.130	5.554
	0.0339	1.113	5.270
Day 1	0.0349	1.126	5.435
	0.0333	1.135	5.331
	0.0348	1.112	5.370
	0.0322	1.164	5.381
	0.0304	1.220	5.329
Day 2	0.0388	1.163	5.128
	0.0299	1.143	5.618
	0.0355	1.196	5.480
	0.0315	1.056	5.247
	0.0300	1.127	5.352
Day 3	0.0316	1.103	5.369
	0.0400	1.117	5.362
	0.0335	1.112	5.353
AVG	0.0339	1.135	5.372
SD	0.0032	0.040	0.119
%RSD	9.3500	3.490	2.222

Table 4.3 – Inter-day precision values for CAPE. Analyte responses (CAPE : resveratrol signal ratio) are shown per concentration.

Nominal conc. (µg/mL)	Observed conc. (µg/mL) (AVG ± SD)	Intra-day precision (%RSD)	Inter-day precision (%RSD)	Accuracy (%Dev)	Absolute recovery (%RSD)
CAPA					
2.5	2.828 ± 0.022	2.87 – 7.41	7.60	13.12	85.2 (6.8)
50	52.28 ± 0.48	0.96 – 3.31	2.98	4.55	91.1 (4.5)
250	259.3 ± 1.9	0.71 – 2.39	2.32	3.73	99.8 (1.0)
CAPE					
2.5	2.382 ± 0.003	5.30 – 11.78	9.35	4.74	86.9 (5.1)
50	50.75 ± 2.33	0.93 – 2.59	3.49	1.51	99.9 (5.5)
250	248.6 ± 1.7	0.95 – 3.38	2.22	0.56	101.0 (4.1)

Table 4.4 – Intra-day precision, inter-day precision, accuracy and absolute recovery for CAPA and CAPE at 2.5, 50 and 250 µg/mL concentrations

4.3.2 – Stability Study

The natural logarithm (Ln) of the percent remaining of CAPA or CAPE was calculated and plotted against time. Linear regression was performed on these data points and the first order rate constant of decomposition was calculated from the slope of the linear regression line. Stability profiles of CAPA and CAPE are shown in Figure 4.2 and tabulated in Tables 4.5 and 4.6. An energy of activation (E_a) was calculated for both CAPA and CAPE by applying the Arrhenius equation. The correlation coefficients of the linear regression line from the Arrhenius plot were found to be $R^2 = 0.999$ for CAPA and $R^2 = 0.998$ for CAPE as shown in Figure 4.3. The activation energies for CAPA and CAPE were found to be 22.1 kcal/mol, and 14.1 kcal/mol, respectively. The half lives of CAPA and CAPE were found to be 10 hours and 0.13 hours at 37 °C, and 41.5 and 0.35 hours at 25 °C, respectively. The data is reported in Table 4.7. Plasma extracts of 100 μg/mL CAPA were recovered at 97.6% (3.5 %RSD) following three freeze thaw cycles when compared to samples analyzed prior to freezing. Long term stability samples were recovered at 97.4% (3.0 %RSD).

The stability of CAPE in rat plasma has been reported previously and it was shown that the decomposition of CAPE was similarly rapid [143]. Slight differences in decomposition rate constants may be attributed to variability in enzyme activity between different batches of plasma. Plasma stability is an important factor in drug discovery and development, as compounds which are highly labile in serum tend to have poor *in vivo* performance. Improved stability properties may lead to advantages in *in vivo* effects.

A)

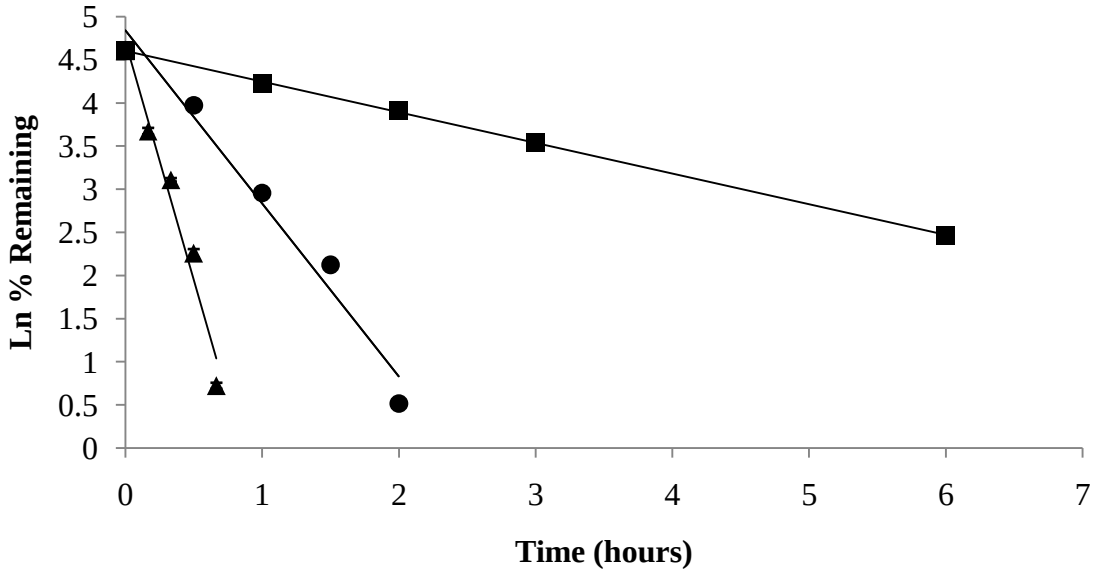

B)

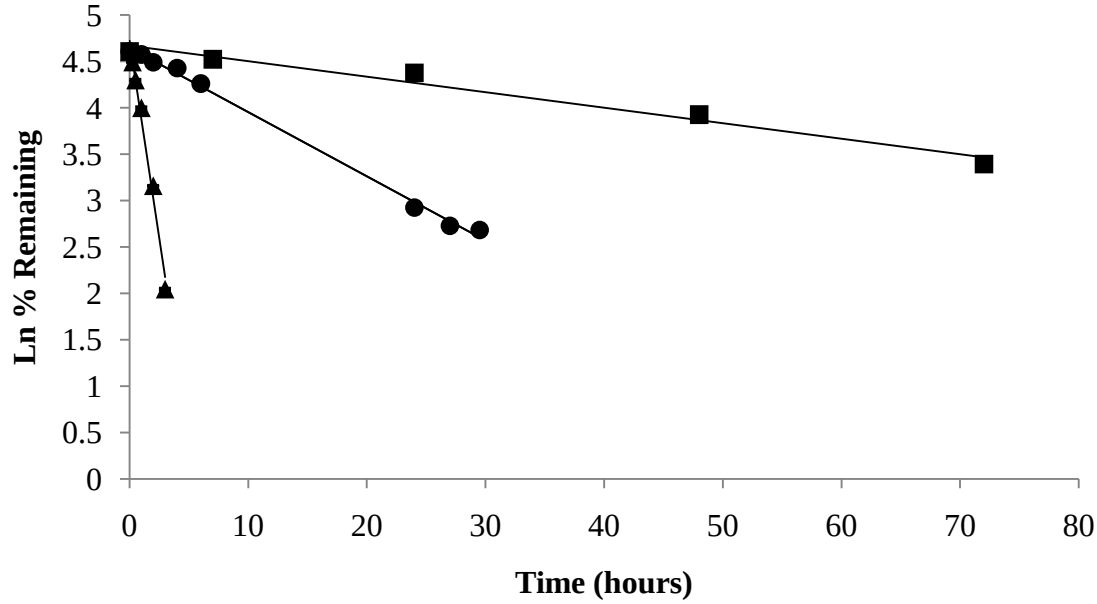

Figure 4.2 - (A) Stability profiles of CAPE (n=3 for all temps): 60 °C (▲ , R^2 = 0.987), 37 °C (● , R^2 = 0.997), and 25 °C (■ , R^2 = 0.975), (B) Stability profiles of CAPA (n=3 for all temps): 37 °C (■ , R^2 = 0.969), 25 °C (▲ , R^2 = 0.974), and 4 °C (● , R^2 = 0.999). Standard deviations are reported in Tables 4.5 and 4.6

Stability	% remaining of CAPA							
	0 h	0.25h	0.5 h	1 h	2 h	3 h		
	100.0	90.6	73.5	54.4	23.7	7.7		
60°C	100.0	86.3	71.8	53.5	22.8	7.6		
	100.0	91.0	75.3	55.7	24.1	7.9		
AVG		89.3	73.5	54.5	23.5	7.7		
SD		2.6	1.8	1.1	0.6	0.1		
%RSD		2.9	2.4	2.1	2.7	1.9		
	0 h	1 h	2 h	4 h	6 h	24 h	27 h	29.5h
	100.0	94.8	92.0	85.5	70.8	18.5	15.3	14.9
37°C	100.0	97.8	86.9	83.8	70.3	18.6	15.4	14.3
	100.0	97.7	88.1	81.6	71.0	18.7	15.1	14.7
AVG		96.8	89.0	83.6	70.7	18.6	15.3	14.6
SD		1.7	2.6	2.0	0.4	0.1	0.1	0.3
%RSD		1.8	3.0	2.3	0.5	0.6	0.8	2.4
	0 h	7 h	24 h	48 h	72 h			
	100.0	91.2	77.4	49.5	30.0			
25°C	100.0	93.0	79.9	51.7	30.2			
	100.0	91.9	81.0	50.8	29.1			
AVG		92.0	79.4	50.7	29.8			
SD		0.9	1.9	1.1	0.6			
%RSD		1.0	2.4	2.2	1.9			

Table 4.5 – Stability of CAPA at 60, 37 and 25 °C.

Stability	% remaining of CAPE				
	0h	0.17h	0.33h	0.50h	0.67h
	100.0	37.7	22.0	9.1	2.0
37°C	100.0	39.0	21.8	9.3	2.0
	100.0	41.6	23.5	10.3	2.2
AVG		39.4	22.4	9.6	2.1
SD		2.0	0.9	0.7	0.1
%RSD		5.0	4.2	7.0	5.5
	0h	0.5h	1h	1.5h	2h
	100.0	51.6	19.7	8.5	1.8
25°C	100.0	54.1	19.0	8.3	1.6
	100.0	53.9	19.1	8.3	1.6
AVG		53.2	19.3	8.4	1.7
SD		1.4	0.4	0.1	0.1
%RSD		2.6	1.9	1.1	7.6
	0h	1h	2h	3h	6h
	100.0	68.9	51.0	35.4	12.1
4°C	100.0	68.1	50.8	33.3	11.6
	100.0	67.7	49.1	35.5	11.5
AVG		68.2	50.3	34.7	11.7
SD		0.6	1.0	1.2	0.3
%RSD		0.9	2.1	3.5	2.4

Table 4.6 – Stability of CAPE at 37, 25 and 4 °C.

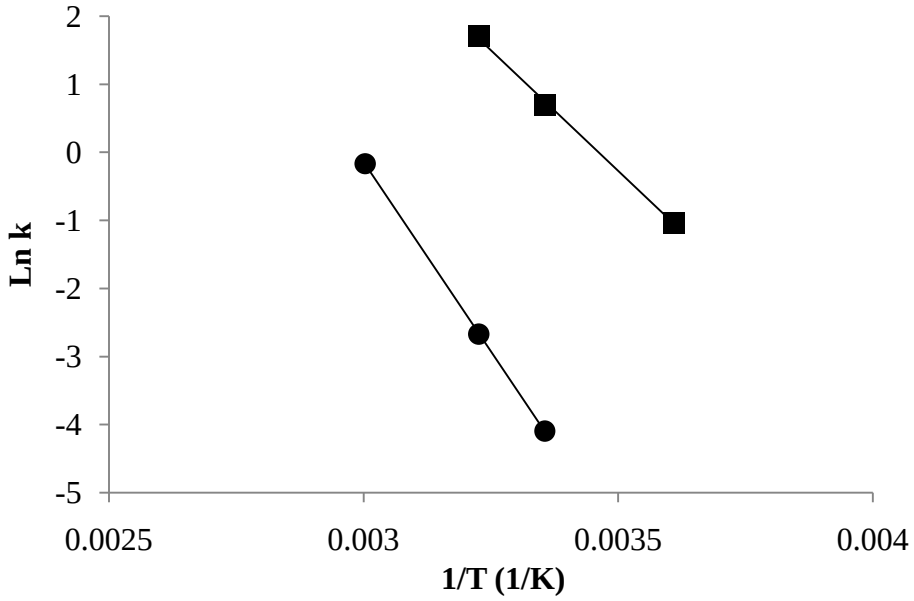

Figure 4.3 - Arrhenius plots for CAPA (●, $R^2 = 0.999$) and CAPE (■, $R^2 = 0.998$)

Temperature (°C)	k (h^{-1})	$t_{1/2}$ (h)	E_a (kcal/mol)
CAPA			
25	0.016	41.5	
37	0.069	10.0	22.1
60	0.85	0.82	
CAPE			
4	0.36	1.95	
25	2.01	0.35	14.1
37	5.51	0.13	

Table 4.7 - Rate constants, half lives, and activation energies of CAPA and CAPE

4.4 – Discussion and Conclusions

A simple HPLC method with UV detection was validated and used for the determination of plasma stability for CAPA and CAPE. The amide derivatization of CAPE significantly improves the stability of the compound in rat plasma as evidenced by CAPA's longer half-life at 25 °C (118 fold increase) and 37 °C (77 fold increase).

Chapter 5 – Pharmacokinetics of CAPA

5.1 – INTRODUCTION

The previously discussed stability studies show that CAPE is rapidly hydrolyzed in male Sprague-Dawley rat plasma, and that CAPA's half-life was significantly longer than CAPE's (Chapter 4). Similarly rapid hydrolysis of CAPE was seen in a previous investigation which compared the stability of CAPE to a fluorinated CAPE derivative. It has also been found that this rapid hydrolysis can be prevented by the addition of 0.4% NaF and 0.1M acetate buffer [143]. The purpose of the following study was to determine whether the improvement upon the *in vitro* stability of CAPE translates to increased elimination half-life of the compound *in vivo*. A validated liquid chromatography mass spectrometry (LCMS) method was developed and used for the quantitative determination of CAPA and CAPE following extraction from rat serum samples. The pharmacokinetic parameters of CAPA were investigated at 5, 10, and 20 mg/kg doses with CAPE investigated at 20 mg/kg using male Sprague-Dawley rats.

5.2 – MATERIALS AND METHODS

5.2.1 – Materials and Instrumentation

Materials

CAPE (≥ 98%) and trans-resveratrol (≥ 98%) were obtained from Cayman Chemical (Ann Arbor, MI). CAPA was previously synthesized in our laboratories [181]. Sodium fluoride, sodium acetate, propylene glycol, ethanol and acetic acid were purchased from Sigma-Aldrich (St Louis, MO). Lithium heparin blood collection vials were obtained from BD (Franklin Lakes, NJ). Water used in the procedures was passed through a Millipore (Billerica, MA, USA) Milli-Q water purification system (18.2MΩ). HPLC grade acetonitrile was obtained from VWR (Radnor, PA).

Animals

Jugular vein catheterized male Sprague-Dawley rats (290-350 g) were purchased from Charles River. The rats were housed in a temperature controlled room with 12 hour light/dark cycles following arrival to the facility. The rats were allowed to acclimate for a minimum of 3 days prior to the start of the experiments and were provided with food and water *ad libitum*. All animal experimental procedures were approved by the University of Texas Health Science Center at San Antonio and met the Institutional Animal Care and Use Committee (IACUC) guidelines.

LCMS Instrumentation

An Agilent 1100/1200 series LCMS was used for the quantitative determination of CAPA and CAPE. The system was comprised of a 1200 series degasser, binary pump, high performance autosampler and column thermostat. This was coupled to an 1100 series single quadrupole mass spectrometer with a multi-mode ESI/APCI ionization chamber. A Phenomenex (Torrance, CA) Synergi MAX-RP (150 mm x 2.0 mm i.d., 4.0 µm, 80 Å) column controlled at 35 °C was used for the separation of the compounds. The mobile phase consisted of water (solvent A) and acetonitrile (solvent B) being run at 500 µl/min. A gradient elution of 25%B to 98%B over 1 minute, with 98%B held for 4 minutes, was used to separate CAPA and CAPE from other plasma components and from the internal standard (resveratrol).

Electrospray ionization (ESI) was used in negative ion mode, with capillary voltage at 2000 V, fragmentor voltage at 70 V, nebulizer pressure at 60 psig, drying gas flow at 10 L/min, drying gas temperature at 300 °C and nebulizer temperature at 150 °C. Transitions of parent ion to major product ion were 282/135 m/z for CAPA, 283/133 m/z for CAPE and 227/143 m/z for resveratrol. Compound fragmentation was performed with the fragmentor set at 280 V.

5.2.2 – Pharmacokinetic Study

Solutions of CAPA and CAPE were made up in 45% propylene glycol, 40% sterile saline and 15% ethanol. Rats were divided into 4 groups of 5 rats each: 20 mg/kg CAPA, 10 mg/kg CAPA, 5 mg/kg CAPA and 20 mg/kg CAPE. The compounds were administered intravenously (~0.5 ml) over a 10 second period via jugular vein catheter with injection volumes normalized to body weight. The catheter was flushed with 0.1 ml of heparinized saline following injection to ensure complete delivery of the compounds as well as to prevent clotting of the catheter. Blood samples (0.4 ml) were drawn pre-injection as well as at 5 min, 30 min, 1 h, 2 h, 4 h, 6 h, and 8 h for CAPA and at 5 min, 15 min, 30 min, 1 h, 1.5 h, 2 h and 3 h for CAPE. Sterile saline (0.4 ml) was injected into the catheter following withdrawal of the blood with 0.1 ml of heparinized saline subsequently flushed into the catheter. Blood samples were collected in 0.5 ml lithium heparin blood collection vials and immediately centrifuged at 10,000 RCF for 5 minutes. The plasma layer (~200 µl) was removed and transferred to microtubes containing 50 µl of 2% sodium fluoride in 0.5 M acetate buffer (pH= 5). Once mixed, this provided a final solution of 0.4% NaF in 0.1M acetate buffer (pH = 5). This was done to prevent hydrolysis of CAPE during handling and storage. The plasma samples were frozen at -80 °C until assayed.

5.2.3 – LCMS assay validation

Extraction of CAPA and CAPE from plasma followed the procedure described in chapter 4. Briefly, 20 µl of the internal standard resveratrol (40 µg/ml) was introduced to the plasma samples immediately prior to extraction. The plasma samples were treated with 600 µl of ethyl acetate, vortexed for 5 minutes and then centrifuged at 13,000 RCF for 5 minutes. The organic layer was removed and the process repeated. The ethyl acetate layers were then pooled and concentrated via the Thermo Scientific SpeedVac (Waltham, MA) centrifugal vacuum. The samples were diluted 2X by reconstitution with 400 µl of MeOH, then vortexed and analyzed on the LCMS.

The LCMS method was qualified by generation of a calibration curve and establishment of selectivity, sensitivity, and both intra-day and inter-day precision and accuracy. Extraction recovery and stability of the compounds in plasma have been previously described. Analyte response was expressed as CAPA/resveratrol signal area ratio and CAPE/resveratrol signal area ratio.

Blank rat plasma was spiked with CAPA and CAPE at concentrations of 2, 20, 100, 500, 1000, and 2000 ng/ml using 5 replicates per concentration and quantified with the LCMS using the previously described conditions to construct a calibration curve. Selectivity was established by utilizing LCMS conditions such that analyte quantification was free from interferences. Sensitivity was established by determining the limit of detection (LOD) and the lower limit of quantification (LLOQ). The LOD was defined as the minimum concentration of analyte needed to produce a signal/noise ratio of 3:1, and the LLOQ was defined as the lowest concentration on the calibration curve that must produce a signal/noise ratio of at least 5:1. Precision was determined by spiking blank rat plasma with CAPA and CAPE at low, medium and high concentrations (20, 500, 2000

ng/ml) at five replicates per concentration and calculating the percent relative standard deviation (%RSD) of the analyte responses. Both intra-day and inter-day (3 consecutive days) precision measurements were performed. Precision was considered acceptable if %RSD did not exceed 15%. Accuracy was evaluated as percent deviation from the mean of the true value. The true value was defined as the analyte response obtained from the calibration curve standards. Accuracy was assessed at low, medium and high concentrations (20, 500, 2000 ng/ml) at 5 replicates per concentration and was considered acceptable if no value deviated more than 15% from the true value.

Quality control (QC) samples of known concentration were randomly inserted between rat plasma samples during LCMS analysis at a ratio of 1 QC sample per 8 plasma samples. LCMS runs were considered acceptable if the QC samples did not deviate more than 15% from the true value.

5.2.4 – Pharmacokinetic analysis

Plasma concentrations of CAPA and CAPE were modeled as a function of time using WinNonLin version 2.1 by Pharsight (Sunnyvale, CA). Pharmacokinetic parameters were obtained by non-compartmental analysis as well as through a non-linear fit to the bi-exponential equation. The first order elimination rate constant (λ_Z) was calculated during NCA using a log-linear regression of data points visually selected in the terminal phase of the plasma concentration-time plot. The calculation for half-life is shown in Equation 5.1. The area under the curve (AUC) was calculated using the linear trapezoidal rule, with AUC_∞ defined as the area under the plasma concentration-time curve from time zero (t_0) to time infinity (∞) (Equation 5.2). The calculation for the area under the plasma concentration first moment time curve from t_0 to ∞ ($AUMC_\infty$) is shown in Equation 5.3. The calculations for volume of distribution (Varea), total body clearance (Cl_T) and mean residence time (MRT) are shown in Equations 5.4, 5.5 and 5.6 respectively.

$$t_{1/2} = \frac{(ln2)}{\lambda_Z} \tag{5.1}$$

$$\mathrm{AUC}_\infty = \sum_{i=1}^{n} (C_i + C_{i-1})(t_i - t_{i-1})\left(\frac{1}{2}\right) + \frac{C_{last}}{\lambda_Z} \tag{5.2}$$

$$\mathrm{AUMC}_\infty = \sum_{i=1}^{n} (C_i * t_i + C_{i-1} * t_{i-1})(t_i - t_{i-1})\left(\frac{1}{2}\right) + \frac{C_{last} * t_{last}}{\lambda_Z} + \frac{C_{last}}{\lambda_Z^2} \tag{5.3}$$

$$V_{area} = \frac{Dose}{AUC_\infty * \lambda_Z} \tag{5.4}$$

$$Cl_T = \frac{Dose}{AUC_\infty} \quad \textbf{(5.5)}$$

$$MRT = \frac{AUMC_\infty}{AUC_\infty} \quad \textbf{(5.6)}$$

The plasma concentration-time data was also analyzed as a two-compartment model (Scheme 5.1) after observing a bi-exponential decline. The curve was fitted to Equation 5.7. The variables A, B, α and β were obtained from the intercepts and slopes of the distribution and elimination phases of the plasma concentration time curve, obtained by method of residuals. k_{10}, k_{12}, and k_{21} were defined as the first order elimination rate constant from the central compartment, first order transfer rate constant from the central compartment to the periphery and first order transfer rate constant from the periphery to the central compartment, respectively. The calculations for the following variables are shown below: Volume of the central compartment (Vc), volume of distribution at steady state (Vss), volume of distribution (Varea), area under the plasma concentration vs time curve from t_0 to ∞ (AUC_∞), area under the first moment time curve from t_0 to ∞ ($AUMC_\infty$), total clearance (Cl_T) and mean residence time (MRT).

Scheme 5.1

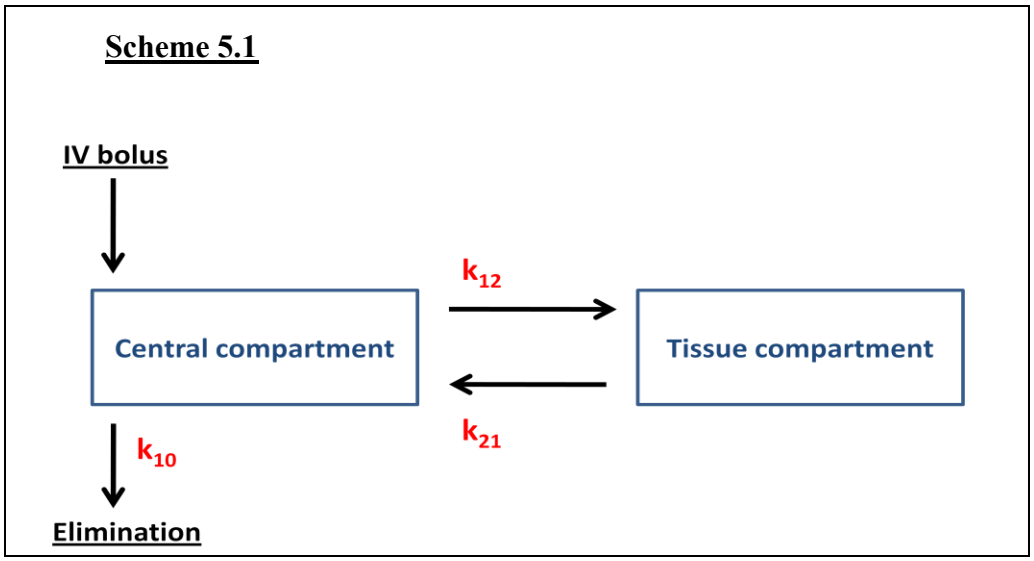

$$Cp = Ae^{-\alpha t} + Be^{-\beta t} \quad \textbf{(5.7)}$$

$$V_c = \frac{Dose}{(A+B)} \quad \textbf{(5.8)}$$

$$V_{ss} = MRT * Cl_T \quad \textbf{(5.9)}$$

$$V_\beta = \frac{Dose}{AUC_\infty * \beta} \quad \textbf{(5.10)}$$

$$AUC_\infty = \frac{A}{\alpha} + \frac{B}{\beta} \quad \textbf{(5.11)}$$

$$AUMC_\infty = \frac{A}{\alpha^2} + \frac{B}{\beta^2} \quad \textbf{(5.12)}$$

$$Cl_T = \frac{Dose}{AUC_\infty} \quad \textbf{(5.13)}$$

$$MRT = \frac{AUMC_{\infty}}{AUC_{\infty}} \quad \textbf{(5.14)}$$

$$\alpha + \beta = k_{10} + k_{12} + k_{12} \quad \textbf{(5.15)}$$

$$k_{10} = \frac{\alpha * \beta}{k_{21}} \quad \textbf{(5.16)}$$

$$k_{21} = \frac{A*\beta + B*\alpha}{A+B} \quad \textbf{(5.17)}$$

$$A = \frac{Dose}{V_c} * \frac{(k_{21} - \alpha)}{(\beta - \alpha)} \quad \textbf{(5.18)}$$

$$B = \frac{Dose}{V_c} * \frac{(k_{21} - \beta)}{(\alpha - \beta)} \quad \textbf{(5.19)}$$

The pharmacokinetic parameters were compared across dose groups using analysis of variance (ANOVA). Differences in values were considered significant at $p < 0.05$.

5.3 – RESULTS

5.3.1 – LCMS assay validation

LCMS chromatograms for CAPA (500 ng/ml), CAPE (500 ng/ml) and resveratrol (2000 ng/ml) are shown in Figure 5.1. The full scan mass spectra from 50-350 m/z of the CAPA, CAPE and resveratrol parent ions are shown in Figure 5.2. The full scan mass spectra from 50-350 m/z of the CAPA, CAPE and resveratrol product ions are shown in Figure 5.3. A non-linear analyte response to concentration relationship was observed for both CAPA and CAPE. The calibration curves in the range of 2-2000 ng/ml are shown in Figures 5.4 and 5.5 and were fit to the following quadratic equations describing the relationship between concentration (x) and analyte response (y):

For CAPA: $y = (-3.73 * 10^{-7})x^2 + (2.26 * 10^{-3})x + 0.0149$ ($R^2 = 0.999$)

For CAPE: $y = (-1.37 * 10^{-6})x^2 + (6.65 * 10^{-3})x + 0.141$ ($R^2 = 0.999$)

The LOD was found to be 1 ng/ml and the LLOQ was found to be 2 ng/ml for both CAPA and CAPE. Intra-day and inter-day precision values for both CAPA and CAPE did not exceed 15 %RSD at any concentration and are shown in Tables 5.1 and 5.2. Accuracy values did not exceed 15% deviation from the true value for both compounds at any tested concentrations. Precision and accuracy determinations are listed in Table 5.3. None of the quality control samples exceeded 15% deviation from the true concentration value.

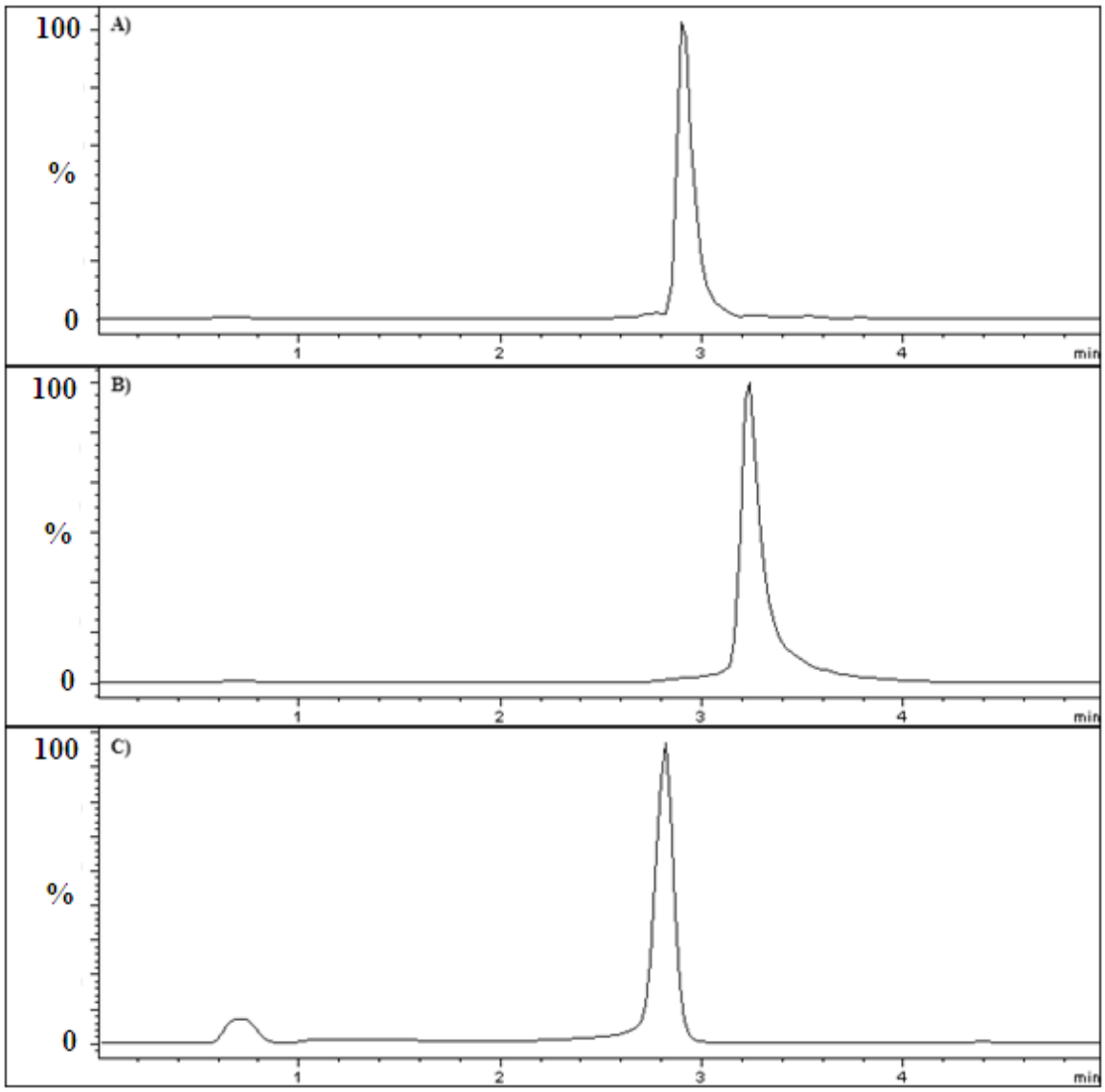

Figure 5.1 – Typical LCMS chromatograms of A) CAPA, B) CAPE and C) resveratrol

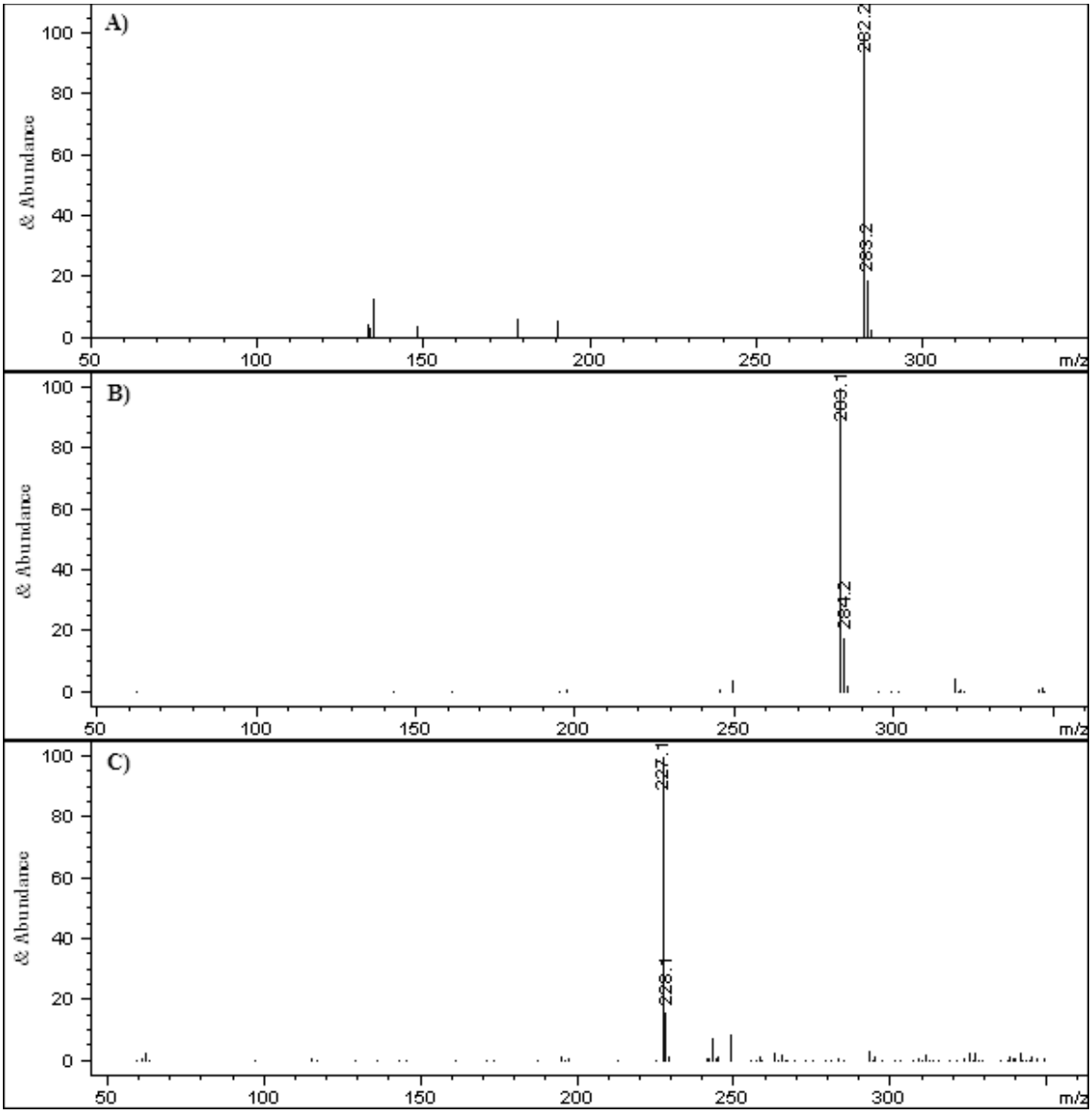

Figure 5.2 – Full scan mass spectra of parent ion from 50-350 m/z, 70V fragmentor: A) CAPA, B) CAPE, C) Resveratrol

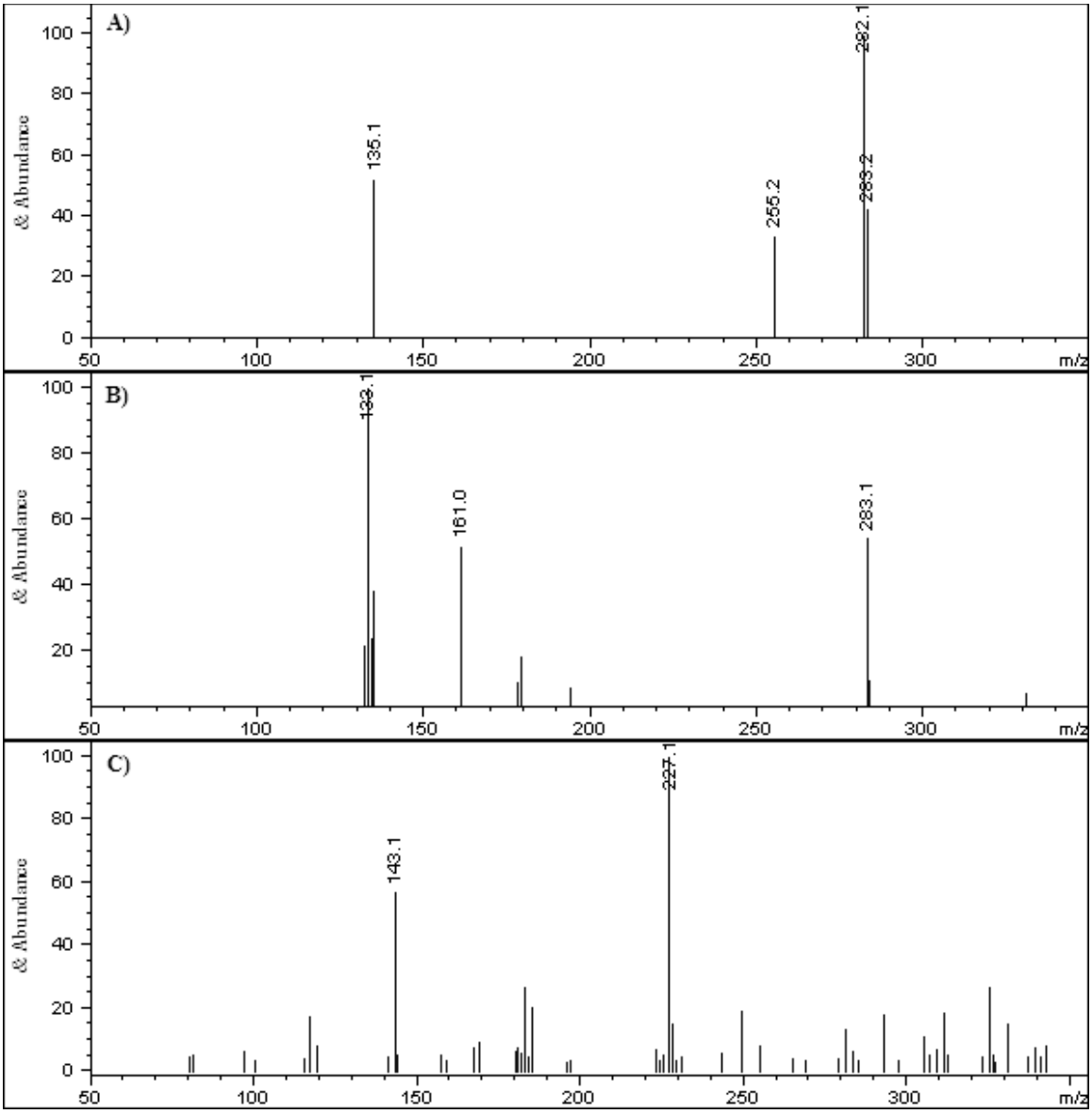

Figure 5.3 – Full scan mass spectra from 50-350 m/z of product ions, 280V fragmentor. A) CAPA, B) CAPE, C) Resveratrol

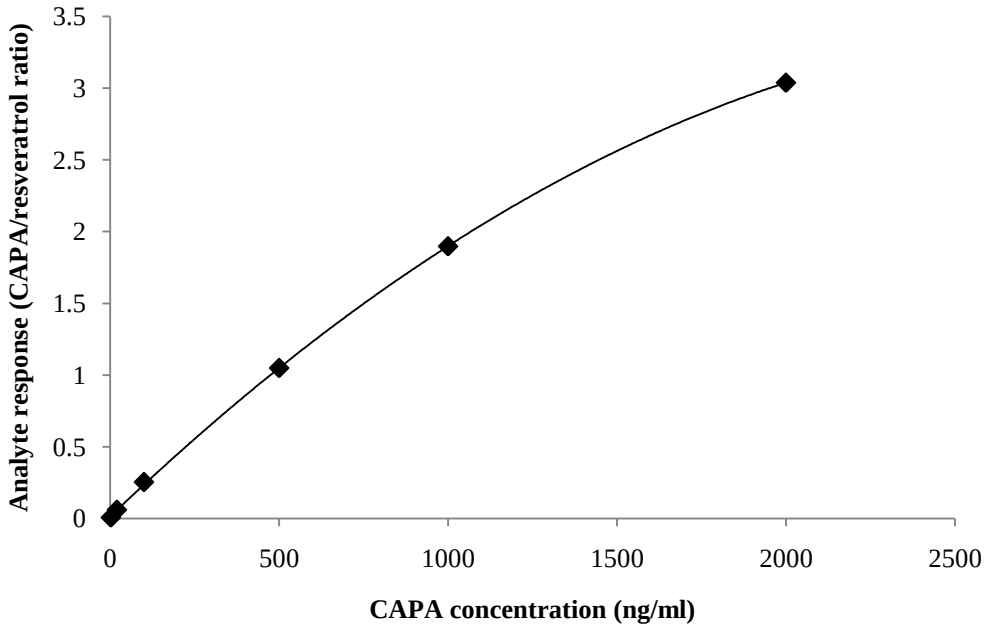

Figure 5.4 – CAPA calibration curve. Analyte response (CAPA / resveratrol signal ratio) is plotted against concentration (2-2000 ng/ml). Data points are fitted to the following equation: $y = (-3.73*10^{-7})x^2 + (2.26*10^{-3})x + 0.0149$, $R^2 = 0.999$

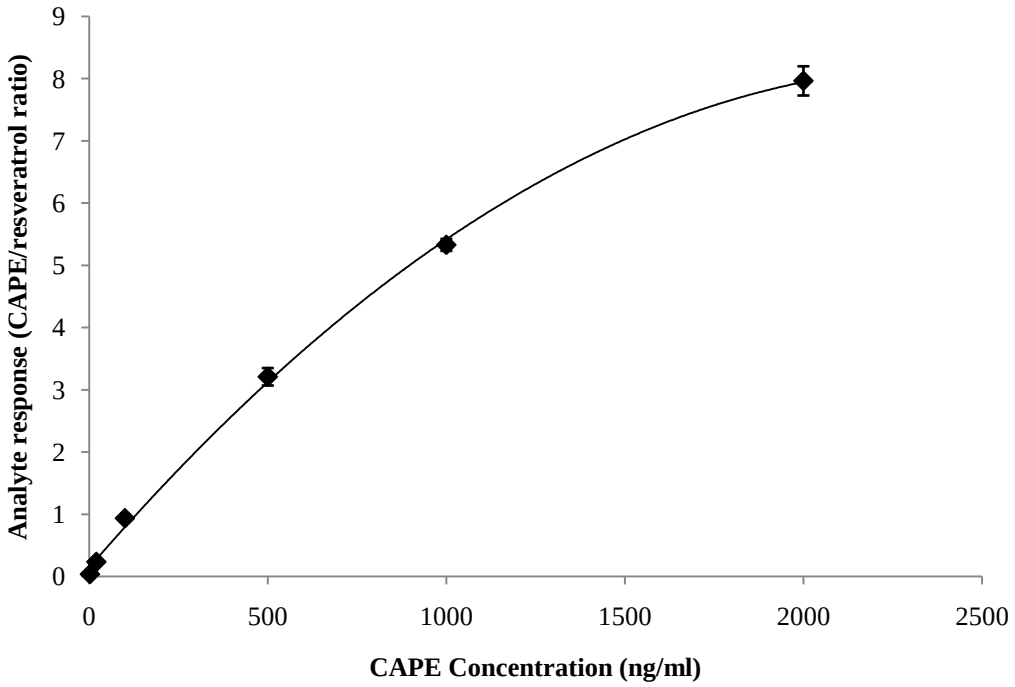

Figure 5.5 – CAPE calibration curve. Analyte response (CAPE / resveratrol signal ratio) is plotted against concentration (2-2000 ng/ml). The data points are fitted to the following equation: $y = (-1.37*10^{-6})x^2 + (6.65*10^{-3})x + 0.141$, $R^2 = 0.999$

CAPA conc.	**20 ng/ml**	**500 ng/ml**	**2000 ng/ml**
	Analyte response		
	0.0626	1.031	2.917
	0.0571	1.034	2.995
Day 1	0.0601	1.083	2.984
	0.0637	1.045	3.184
	0.0549	1.050	3.107
	nu	1.050	2.921
	0.0562	1.091	2.952
Day 2	0.0483	1.070	2.807
	0.0516	1.079	nu
	0.0512	1.038	2.275
	0.0561	1.093	3.063
	0.0452	1.053	3.049
Day 3	0.0458	1.100	3.057
	0.0505	1.076	3.187
	0.0510	1.054	3.141
AVG	0.0539	1.063	2.97
SD	0.0058	0.023	0.23
%RSD	10.74	2.14	7.69

Table 5.1 – Inter-day precision values for CAPA. Analyte response (CAPA/resveratrol signal ratio) is shown per concentration. nu = not usable for analysis.

CAPE conc.	**20 ng/ml**	**500 ng/ml**	**2000 ng/ml**
	Analyte response		
	0.2428	3.402	8.153
	0.2424	3.075	7.859
Day 1	0.2134	3.299	7.640
	0.2242	3.175	8.225
	0.2459	3.089	7.935
	0.2197	3.434	7.794
	0.2118	3.096	7.572
Day 2	0.2164	3.007	7.913
	0.2225	3.128	7.482
	0.2154	3.077	7.962
	0.2830	3.159	8.125
	0.2661	3.033	7.630
Day 3	0.2401	3.101	8.022
	0.2450	3.216	7.816
	0.2601	3.209	7.909
avg	0.2366	3.167	7.869
sd	0.0215	0.127	0.219
%RSD	9.08	4.01	2.78

Table 5.2 – Inter-day precision values for CAPE. Analyte response (CAPE/resveratrol signal ratio) is shown per concentration

Nominal Concentration (ng / ml)	Observed Concentration (ng/ml ± SD)	Intra-day precision (%RSD)	Inter-day precision (%RSD)	Accuracy (% deviation)
CAPA				
20	17.02 ± 1.51	6.17 – 8.86	10.74	14.9
500	510.4 ± 10.1	1.96 – 2.02	2.13	2.08
2000	1991 ± 61	1.98 – 4.20	3.63	0.47
CAPE				
20	20.37 ± 0.89	1.89 – 6.64	9.08	1.83
500	490.3 ± 19.3	2.45 – 5.26	4.01	1.94
2000	1965 ± 51	2.42 – 2.95	2.78	1.76

Table 5.3 – Assay qualification parameters for CAPA and CAPE

5.3.2 – Pharmacokinetics

The averaged plasma concentration (Cp) vs time profiles for the 3 doses of CAPA following intravenous bolus administration to male Sprague-Dawley rats are shown as a semi-logarithmic plot in Figure 5.6 and in Figure 5.7 for the 20 mg/kg CAPE dose group. The plasma concentration data for the individual rats in each CAPA dose group are presented in Tables 5.4-5.6 and plotted in Figures 5.7-5.9. Cp vs time data for individual rats treated with 20 mg/kg CAPE is shown in Table 5.7 and Figure 5.10.

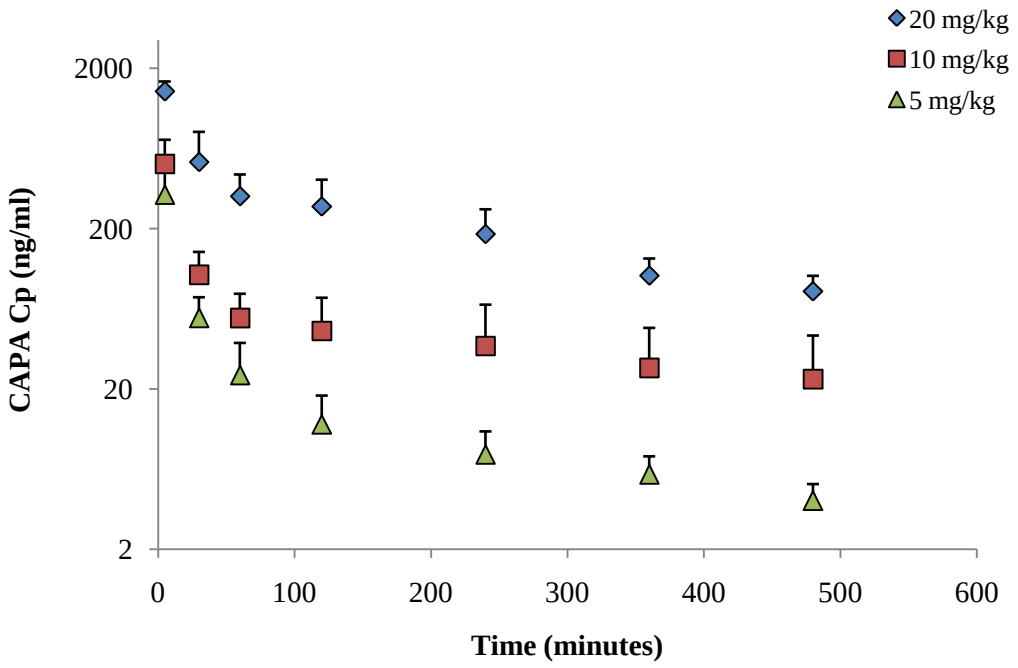

Figure 5.6 – Semi logarithmic representation of the averaged plasma concentration vs time profiles for CAPA administered at 20, 10 and 5 mg/kg doses via intravenous bolus to male Sprague Dawley rats. Error bars represent standard deviation

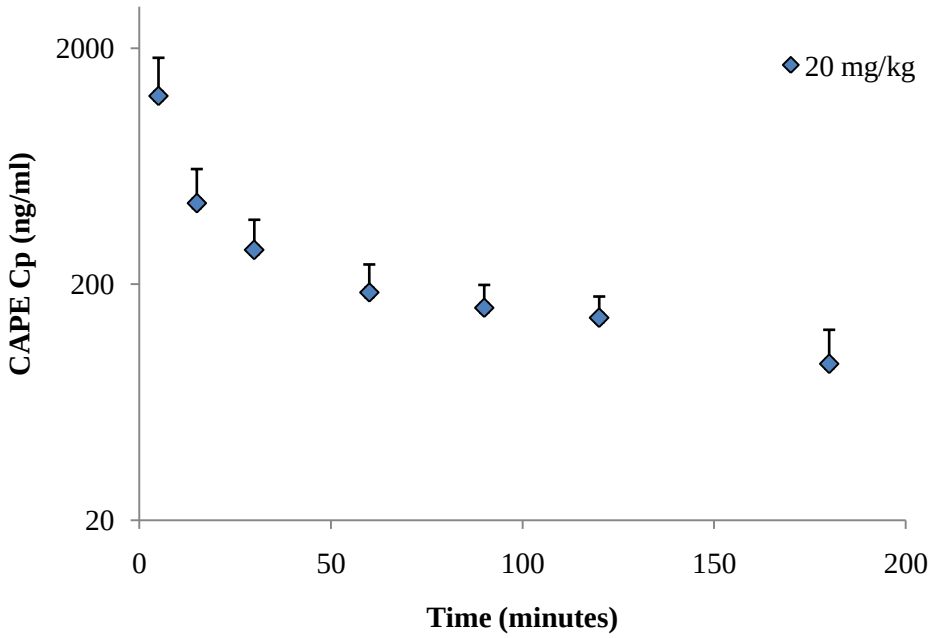

Figure 5.7 – Semi logarithmic representation of the averaged plasma concentration vs time profile for CAPE administered at 20 mg/kg via intravenous bolus to male Sprague Dawley rats. Error bars represent standard deviation

Time (min)	Rat 1	Rat 2	Rat 3	Rat 4	Rat 5	Mean	SD
5	1299	1726	1596	1194	1359	1435	220
30	903.5	672.8	505.1	182.4	339.3	520.6	281.6
60	414.0	440.3	305.4	147.9	284.8	318.5	116.6
120	384.1	425.3	238.4	111.2	214.9	274.8	128.7
240	293.3	234.9	169.2	103.4	124.6	185.1	78.7
360	103.0	138.8	118.5	76.7	71.1	101.6	28.4
480	70.48	86.78	114.18	65.20	70.12	81.35	20.08
Wt (g)	290	315	340	321	330	319	19
Dose (mg)	5.80	6.30	6.80	6.42	6.60	6.38	0.38

Table 5.4 – Observed individual CAPA plasma concentrations (ng/ml) following intravenous bolus administration of 20 mg/kg CAPA to male Sprague Dawley rats.

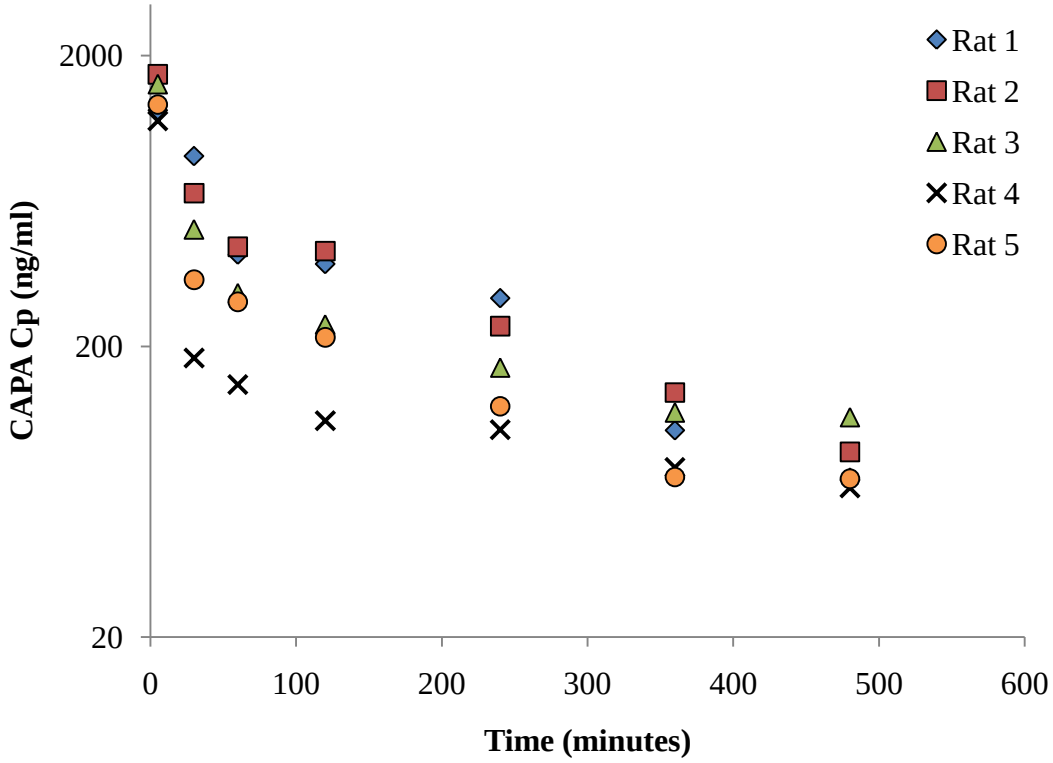

Figure 5.8 – Semi logarithmic representation of the individual plasma concentration vs time profiles for CAPA administered at 20 mg/kg via intravenous bolus to male Sprague Dawley rats

Time (min)	Rat 1	Rat 2	Rat 3	Rat 4	Rat 5	Mean	SD
5	nu	565.9	773.6	296.5	393.3	507.3	209.6
30	nu	163.7	81.17	89.11	81.46	103.9	40.06
60	nu	89.06	42.38	51.06	38.93	55.36	23.04
120	nu	86.06	27.99	48.08	22.38	46.13	28.82
240	nu	77.47	20.15	39.57	10.44	36.91	29.63
360	nu	52.39	13.69	35.18	6.95	27.05	20.74
480	nu	49.31	11.72	27.01	4.94	23.25	19.68
Wt (g)	341	325	338	302	303	317	18
Dose (mg)	3.41	3.25	3.38	3.02	3.03	3.17	0.18

Table 5.5 - Observed individual CAPA plasma concentrations (ng/ml) following intravenous bolus administration of 10 mg/kg CAPA to male Sprague Dawley rats. nu = not usable for analysis.

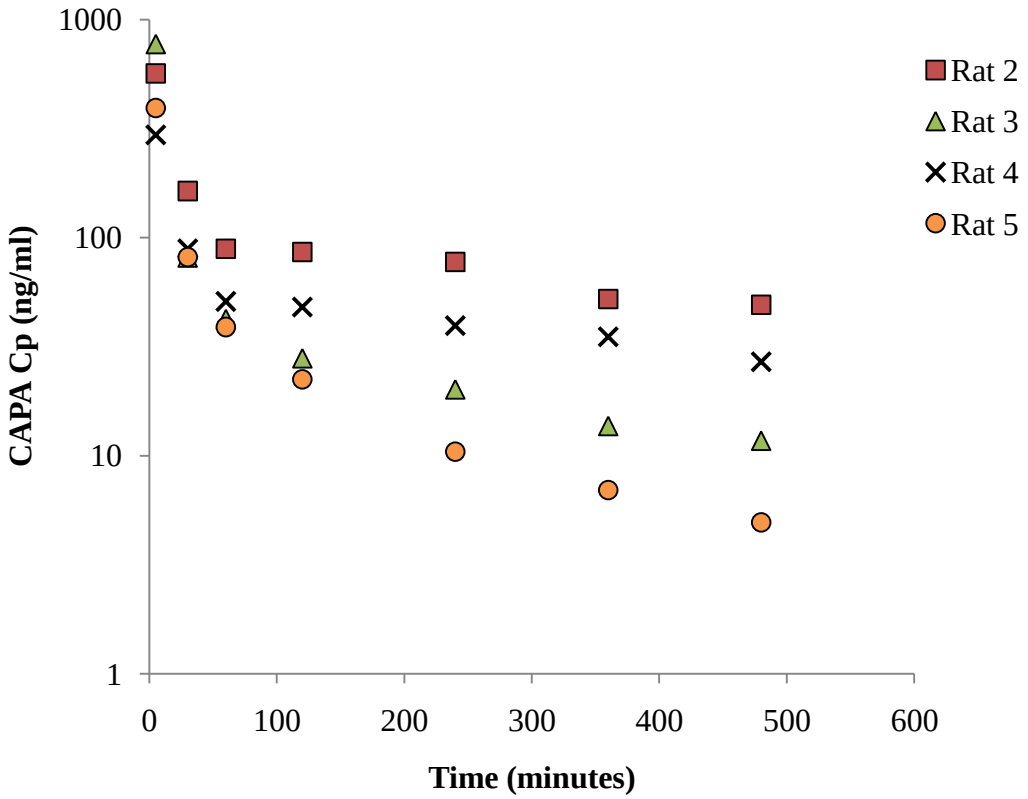

Figure 5.9 - Semi logarithmic representation of the individual plasma concentration vs time profiles for CAPA administered at 10 mg/kg via intravenous bolus to male Sprague Dawley rats

Time (min)	Rat 1	Rat 2	Rat 3	Rat 4	Rat 5	Mean	SD
5	408.1	197.6	447.8	174.2	nu	306.9	128.8
30	69.95	33.41	37.89	58.40	nu	49.92	19.22
60	23.19	12.84	25.72	12.26	nu	18.50	14.35
120	12.15	9.83	7.60	7.87	nu	9.36	6.16
240	11.13	7.17	5.57	4.81	nu	7.17	2.92
360	7.64	5.70	4.17	BLOQ	nu	5.84	1.74
480	5.09	4.04	2.91	BLOQ	nu	4.01	1.09
Wt (g)	318	324	347	344	296	326	21
Dose (mg)	1.59	1.62	1.74	1.72	1.48	1.63	0.10

Table 5.6 - Observed individual CAPA plasma concentrations (ng/ml) following intravenous bolus administration of 5 mg/kg CAPA to male Sprague Dawley rats. nu = not usable for analysis. BLOQ = below limit of quantification

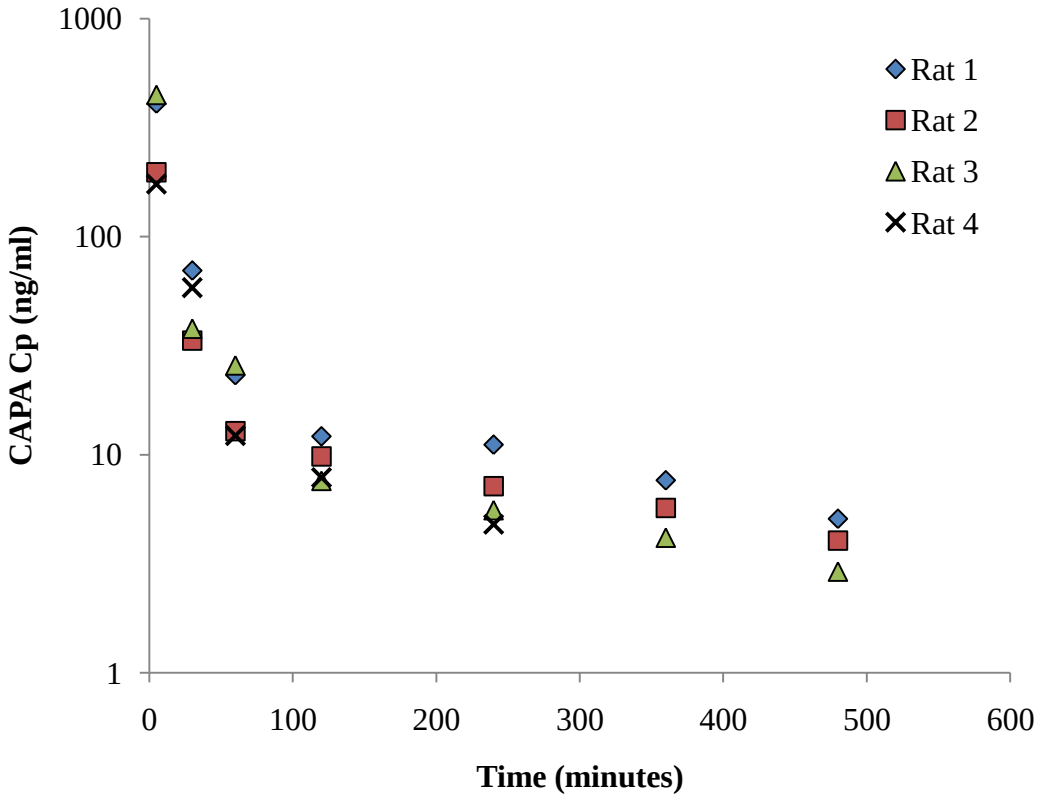

Figure 5.10 - Semi logarithmic representation of the individual plasma concentration vs time profiles for CAPA administered at 5 mg/kg via intravenous bolus to male Sprague Dawley rats

Time (min)	Rat 1	Rat 2	Rat 3	Rat 4	Rat 5	Mean	SD
5	1848.2	741.8	851.0	1890.1	941.0	1254.4	565.8
15	672.2	222.7	552.4	366.0	387.7	440.2	174.6
30	321.1	126.8	280.2	280.7	387.2	279.2	95.7
60	187.7	103.7	179.3	267.5	185.2	184.5	58.0
90	186.7	91.3	166.8	188.4	159.8	158.8	39.8
120	162.9	87.6	141.5	171.1	156.8	144.0	33.3
180	91.27	44.23	71.53	115.75	136.69	91.89	36.27
Wt (g)	322	314	314	310	321	316	5
Dose (mg)	6.44	6.28	6.28	6.20	6.42	6.32	0.10

Table 5.7 - Observed individual CAPE plasma concentrations (ng/ml) following intravenous bolus administration of 20 mg/kg CAPE to male Sprague Dawley rats.

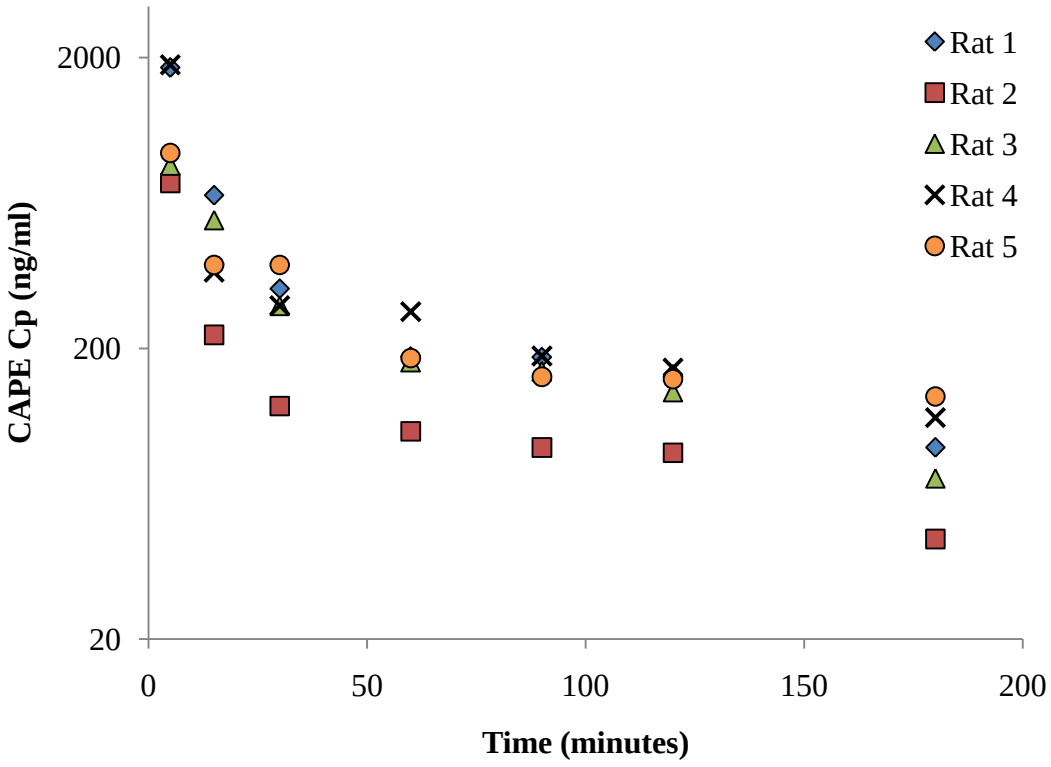

Figure 5.11 - Semi logarithmic representation of the individual plasma concentration vs time profiles for CAPE administered at 20 mg/kg via intravenous bolus to male Sprague Dawley rats

Non compartmental analysis

Non compartmental analysis (NCA) was performed on the plasma concentration time data for the CAPA and CAPE dose groups. The results of the NCA for the CAPA dose groups are summarized in Tables 5.8-5.10 and in Table 5.11 for the CAPE dose group. NCA was performed for individual plasma concentration time profiles as well as for the mean plasma concentration time profiles for each dose. The parameters obtained from NCA on the mean plasma concentration time curves are shown in Tables 5.12-5.13 and are seen to be in good agreement with the parameters calculated from the individual profiles. One way ANOVA was performed on select parameters obtained from the individual profiles from the 3 CAPA dose groups, shown in Table 5.14.

Non-linear pharmacokinetics were observed for CAPA, as clearance and volume of distribution decreased significantly ($P < 0.05$) with increasing dose. The AUC of CAPA also increased non-proportionally with increasing dose, as can be seen in Figure 5.12. There was no significant difference found in the first order elimination rate constant or the half-life of CAPA between the 3 doses. There was a significant difference found in the half-life calculated from the NCA between CAPA and CAPE at 20 mg/kg (255.1 minutes vs 92.3 minutes, $P < 0.05$).

Parameters	Rat 1	Rat 2	Rat 3	Rat 4	Rat 5	Mean	SD
Weight (g)	290	315	340	321	330	319	19
Dose (mg)	5.8	6.3	6.8	6.42	6.6	6.38	0.38
NCA							
λ_z (min^{-1})	0.0046	0.0041	0.0024	0.0018	0.0024	0.0031	0.0012
$t_{1/2}$ (min)	151.6	169.5	285.4	379.4	289.5	255.1	94.3
Cl_T (ml/min)	34.47	35.20	40.86	61.05	53.51	45.02	11.77
Varea (ml)	7541	8608	16820	33420	22350	17750	10670
AUC_∞ (µg*min/ml)	168.2	178.9	166.4	105.2	123.3	148.4	32.2
$AUMC_\infty$ (mg*min^2/ml)	31.81	37.11	59.14	46.67	38.44	42.63	10.65
MRT (min)	189.1	207.3	355.3	443.8	311.7	301.5	105.8

Table 5.8 – Pharmacokinetic parameters obtained from non-compartmental analysis (NCA) on the 20 mg/kg CAPA dose group.

Parameters	Rat 1	Rat 2	Rat 3	Rat 4	Rat 5	Mean	SD
Weight (g)	341	325	338	302	303	317	18
Dose (mg)	3.41	3.25	3.38	3.02	3.03	3.17	0.18
NCA							
λ_z (min^{-1})	nu	0.0019	0.0025	0.0022	0.0031	0.0024	0.0005
$t_{1/2}$ (min)	nu	368.2	277.4	314.9	222.5	295.8	61.4
Cl_T (ml/min)	nu	45.6	109	80.9	175	102.6	54.8
Varea (ml)	nu	24220	43980	36760	56470	40360	13490
AUC_∞ (µg*min/ml)	nu	71.29	30.75	37.33	17.22	39.15	23.01
$AUMC_\infty$ (mg*min^2/ml)	nu	33.75	6.18	16.50	2.45	14.72	14.01
MRT (min)	nu	473.4	200.9	442.0	142.0	314.6	167.5

Table 5.9 – Pharmacokinetic parameters obtained from non-compartmental analysis (NCA) on the 10 mg/kg CAPA dose group.

Parameters	Rat 1	Rat 2	Rat 3	Rat 4	Rat 5	Mean	SD
Weight (g)	318	324	347	344	296	325	20.8
Dose (mg)	1.59	1.62	1.74	1.72	1.48	1.63	0.10
NCA							
λ_z (min^{-1})	0.0026	0.0024	0.0027	0.0041	nu	0.0030	0.0008
$t_{1/2}$ (min)	265.2	284.9	253.7	168.8	nu	243.2	51.2
Cl_T (ml/min)	98.5	170.5	125.3	229.9	nu	156.1	57.5
Varea (ml)	37690	70120	45870	55990	nu	52420	13970
AUC_∞ (µg*min/ml)	16.14	9.50	13.84	7.48	nu	11.74	3.96
$AUMC_\infty$ (mg*min^2/ml)	2.758	2.234	1.543	0.815	nu	1.837	0.844
MRT (min)	170.9	235.2	111.5	108.9	nu	156.6	59.7

Table 5.10 – Pharmacokinetic parameters obtained from non-compartmental analysis (NCA) on the 5 mg/kg CAPA dose group.

Parameters	Rat 1	Rat 2	Rat 3	Rat 4	Rat 5	Mean	SD
Weight (g)	322	314	314	310	321	316	5.1
Dose (mg)	6.44	6.28	6.28	6.2	6.42	6.32	0.10
NCA							
λ_z (min^{-1})	0.0082	0.0085	0.0097	0.0066	0.0058	0.0078	0.0016
$t_{1/2}$ (min)	84.1	81.3	71.6	105.0	119.4	92.3	19.5
Cl_T (ml/min)	92.3	201.8	129.0	79.6	97.5	120.0	49.2
Varea (ml)	11230	23850	13360	12010	15950	15280	5110
AUC_∞ (µg*min/ml)	69.52	30.89	48.51	78.18	69.34	59.29	19.27
$AUMC_\infty$ (mg*min^2/ml)	5.96	2.84	4.34	8.68	11.02	6.57	3.30
MRT (min)	85.8	92.0	89.5	111.0	159.0	107.4	30.4

Table 5.11 – Pharmacokinetic parameters obtained from non-compartmental analysis (NCA) on the 20 mg/kg CAPE dose group.

Parameters	*20 mg/kg*		*10 mg/kg*		*5 mg/kg*	
	Mean ind.	Mean Cp	Mean ind.	Mean Cp	Mean ind.	Mean Cp
NCA						
λ_z (min^{-1})	0.0031	0.0035	0.0024	0.0019	0.0030	0.0033
$t_{1/2}$ (min)	255.1	200.4	295.8	359	243.2	207.7
Cl_T (ml/min)	45.02	44.90	102.6	79.3	156.1	124.0
Varea (ml)	17750	12980	40360	41150	52420	37330
AUC_∞ (µg*min/ml)	148.4	142.1	39.15	39.98	11.74	13.08
$AUMC_\infty$ (mg*min^2/ml)	42.63	34.51	14.72	15.73	1.837	1.818
MRT (min)	301.5	242.9	314.6	393.3	156.6	139

Table 5.12 – Pharmacokinetic parameters obtained from non-compartmental analysis (NCA) of the CAPA dose groups. Comparison between the average of the individually obtained pharmacokinetic parameters (mean ind.) and the parameters obtained from the averaged plasma concentration time profiles (mean Cp).

Parameters	Mean ind.	Mean Cp
NCA		
λ_z (min^{-1})	0.0078	0.0068
$t_{1/2}$ (min)	92.3	101.4
Cl_T (ml/min)	120.0	106.6
Varea (ml)	15280	15560
AUC_∞ (µg*min/ml)	59.29	59.48
$AUMC_\infty$ (mg*min^2/ml)	6.57	6.75
MRT (min)	107.4	113.4

Table 5.13 – Pharmacokinetic parameters obtained from non-compartmental analysis (NCA) of the 20 mg/kg CAPE dose group. Comparison between the average of the individually obtained pharmacokinetic parameters (mean ind.) and the parameters obtained from the averaged plasma concentration time profiles (mean Cp).

	20 mg/kg (AVG ± SD)	10 mg/kg (AVG ± SD)	5 mg/kg (AVG ± SD)	ANOVA P Value
NCA				
$t_{1/2}$ (min)	255.1 ± 94.3	295.75 ± 61.43	243.1 ± 51.2	> 0.05
Cl_T (ml/min)	45.02 ± 11.77	102.6 ± 54.8	156.1 ± 57.5	< 0.05
Varea (ml)	17750 ± 10670	40360 ± 13490	52420 ± 13980	< 0.05
AUC_∞ (µg*min/ml)	148.42 ± 32.21	39.15 ± 23.01	11.74 ± 3.96	< 0.05

Table 5.14 – Averaged pharmacokinetic parameters obtained from non-compartmental analysis (NCA) on the individual plasma concentration time profiles for the 3 CAPA dose groups. $P < 0.05$ was considered significant.

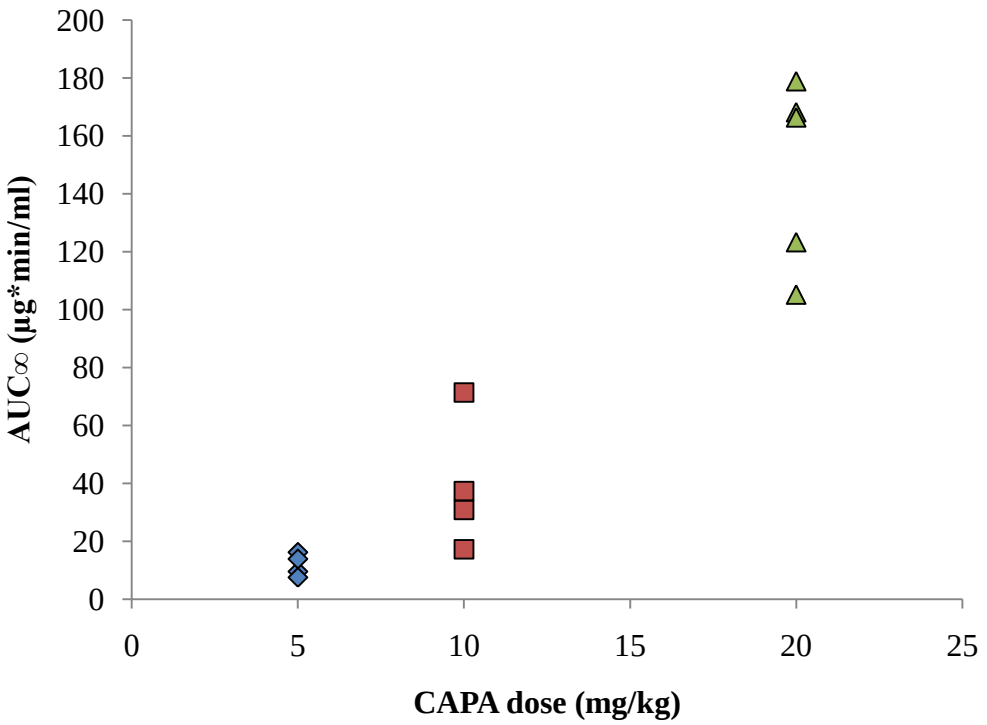

Figure 5.12 – Relationship between administered dose of CAPA and resulting AUC_{∞} calculated from the non-compartmental analysis (NCA)

Bi-exponential fit

The plasma concentration time data was analyzed as a two compartment model and fit to Equation 5.7. The fit of the average plasma concentration time profiles of the CAPA dose groups to the bi-exponential equation can be seen in Figures 5.13-5.15. Fit of the CAPE plasma concentration time profile to the bi-exponential equation can be seen in Figure 5.16. The pharmacokinetic parameters calculated from the compartmental analysis of the CAPA plasma concentration time profiles are summarized in Tables 5.15-5.17. Parameters obtained for CAPE are summarized in Table 5.18. Bi-exponential fit to Equation 5.7 was performed for individual plasma concentration time profiles as well as for the mean plasma concentration time profiles for each dose. The parameters obtained from the bi-exponential fit on the mean plasma concentration time curves of both CAPA and CAPE are shown in Tables 5.19-5.20 and are seen to be in good agreement with the parameters calculated from the individual profiles. One way ANOVA was performed on select parameters obtained from the individual profiles from the 3 CAPA dose groups; shown in Table 5.21.

Non-linear pharmacokinetics were observed for CAPA as clearance and volume of distribution decreased significantly ($P < 0.05$) with increasing dose. These trends were similar to what was observed in the same parameters obtained from NCA. The AUC of CAPA also increased non-proportionally with increasing dose, as can be seen in Figure 5.17, again similar to what was observed in the NCA. There was good agreement between the parameters obtained via NCA and parameters obtained via bi-exponential fit. A comparison of select pharmacokinetic parameters calculated via both methods is shown in Table 5.22 for the CAPA dose groups and in Table 5.23 for the 20 mg/kg CAPE dose group. It is seen again that the half-life of CAPA at 20 mg/kg is longer and

significantly different from the half-life of CAPE at 20 mg/kg (257.5 minutes for 20 mg/kg CAPA vs 98.9 minutes for 20 mg/kg CAPE, $P < 0.05$).

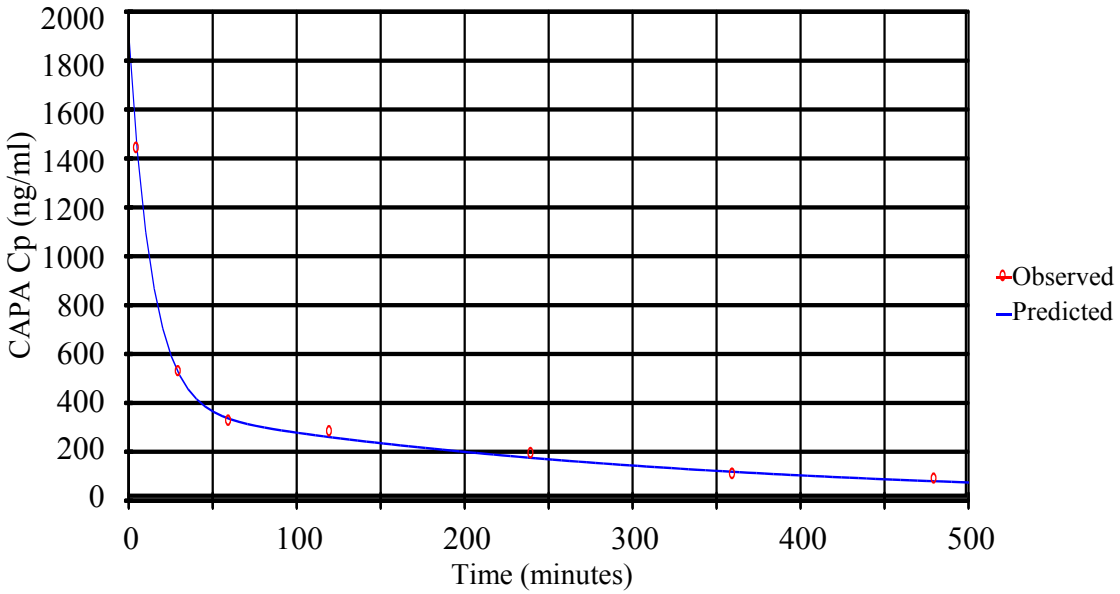

Figure 5.13 – Bi-exponential fit of the mean plasma concentration time profile of the 20 mg/kg CAPA dose group. Observed concentrations are shown along with the fitted line.

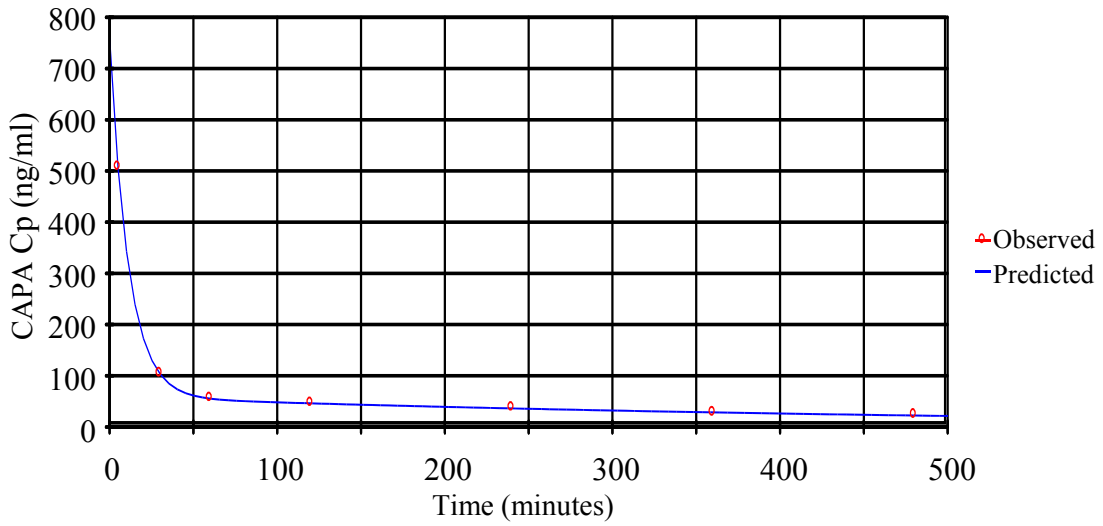

Figure 5.14 – Bi-exponential fit of the mean plasma concentration time profile of the 10 mg/kg CAPA dose group. Observed concentrations are shown along with the fitted line.

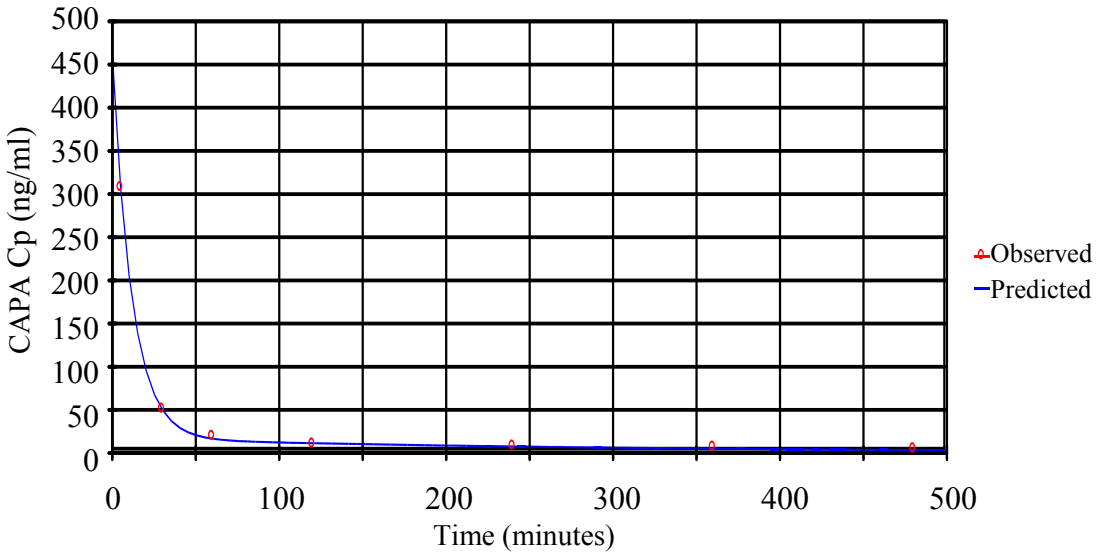

Figure 5.15 – Bi-exponential fit of the mean plasma concentration time profile of the 5 mg/kg CAPA dose group. Observed concentrations are shown along with the fitted line.

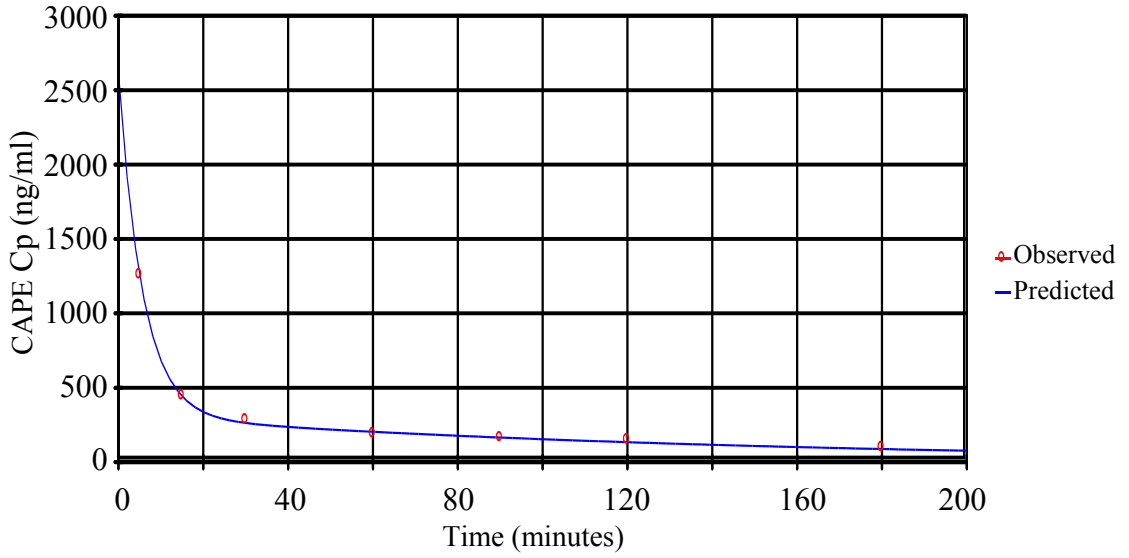

Figure 5.16 – Bi-exponential fit of the mean plasma concentration time profile of the 20 mg/kg CAPE dose group. Observed concentrations are shown along with the fitted line.

Parameters	Rat 1	Rat 2	Rat 3	Rat 4	Rat 5	Mean	SD
Weight (g)	290	315	340	321	330	319	19
Dose (mg)	5.8	6.3	6.8	6.42	6.6	6.38	0.38
Bi-exponential fit							
A (ng/ml)	918.2	1751	1837	2040	1824	1674	435
B (ng/ml)	563.1	589.4	320.6	155.3	289.0	383.5	186.8
α (min^{-1})	0.036	0.084	0.072	0.135	0.106	0.087	0.037
β (min^{-1})	0.0041	0.0038	0.0025	0.0019	0.0024	0.0029	0.0009
k_{10} (min^{-1})	0.0090	0.0132	0.0140	0.0220	0.0154	0.0147	0.0047
k_{12} (min^{-1})	0.0147	0.0510	0.0480	0.1030	0.0765	0.0586	0.0331
k_{21} (min^{-1})	0.0160	0.0240	0.0130	0.0110	0.0166	0.0161	0.0049
$t_{1/2}\alpha$ (min)	19.27	8.22	9.56	5.15	6.54	9.75	5.58
$t_{1/2}\beta$ (min)	169.1	183.3	278.4	367.9	288.8	257.5	82.1
Cl_T (ml/min)	35.61	35.67	44.12	65.79	47.96	45.83	12.38
Vc (ml)	3915	2692	3151	2925	3123	3161	459
Varea (ml)	8686	9388	17650	34620	19980	14900	10500
Vss (ml)	7479	8372	14910	29570	17540	15570	8910
AUC_∞ (µg*min/ml)	162.9	176.6	154.1	97.6	137.6	145.8	30.4
$AUMC_\infty$ (mg*min^2/ml)	34.21	41.06	51.65	43.14	50.34	44.08	7.14
MRT (min)	210.0	234.1	337.0	449.0	365.6	319.1	98.1

Table 5.15 - Pharmacokinetic parameters obtained from the plasma concentration time data of the 20 mg/kg CAPA dose group (bi-exponential fit).

Parameters	Rat 1	Rat 2	Rat 3	Rat 4	Rat 5	Mean	SD
Weight (g)	341	325	338	302	303	317	18
Dose (mg)	3.41	3.25	3.38	3.02	3.03	3.17	0.18
Bi-exponential fit							
A (ng/ml)	nu	689.9	1295	350.0	529.9	716.3	410.3
B (ng/ml)	nu	96.99	43.10	52.99	34.39	56.87	27.81
α (min^{-1})	nu	0.077	0.114	0.076	0.078	0.086	0.019
β (min^{-1})	nu	0.0019	0.0028	0.0021	0.0034	0.0026	0.0007
k_{10} (min^{-1})	nu	0.0130	0.0501	0.0140	0.0333	0.0276	0.0177
k_{12} (min^{-1})	nu	0.0546	0.0607	0.0530	0.0397	0.0520	0.0088
k_{21} (min^{-1})	nu	0.0111	0.0064	0.0118	0.0079	0.0093	0.0026
$t_{1/2}\,\alpha$ (min)	nu	9.00	6.06	9.12	8.90	8.27	1.48
$t_{1/2}\,\beta$ (min)	nu	364.8	247.6	330.1	203.9	286.6	73.9
Cl_T (ml/min)	nu	54.2	126.5	101.2	178.9	115.2	52.0
Vc (ml)	nu	4129	2525	7493	5369	4879	2096
Varea (ml)	nu	28500	45180	48190	52600	43620	10530
Vss (ml)	nu	24350	26500	40960	32340	31040	7420
AUC_∞ (µg*min/ml)	nu	60.00	26.72	29.84	16.94	33.38	18.59
$AUMC_\infty$ ($mg*min^2/ml$)	nu	26.98	5.59	12.07	3.06	11.93	10.73
MRT (min)	nu	449.7	209.5	404.7	180.8	311.2	135.7

Table 5.16 - Pharmacokinetic parameters obtained from the plasma concentration time data of the 10 mg/kg CAPA dose group (bi-exponential fit).

Parameters	Rat 1	Rat 2	Rat 3	Rat 4	Rat 5	Mean	SD
Weight (g)	318	324	347	344	296	325	20.8
Dose (mg)	1.59	1.62	1.74	1.72	1.48	1.63	0.10
Bi-exponential fit							
A (ng/ml)	580.8	284.5	587.7	215.0	nu	417.0	195.2
B (ng/ml)	20.02	12.99	9.52	4.79	nu	11.83	6.41
α (min^{-1})	0.081	0.086	0.058	0.047	nu	0.068	0.019
β (min^{-1})	0.0028	0.0024	0.0024	0.0058	nu	0.0034	0.0016
k_{10} (min^{-1})	0.0420	0.0340	0.0420	0.0407	nu	0.0397	0.0038
k_{12} (min^{-1})	0.0360	0.0480	0.0150	0.0054	nu	0.0261	0.0194
k_{21} (min^{-1})	0.0053	0.0061	0.0033	0.0067	nu	0.0054	0.0015
$t_{1/2}\,\alpha$ (min)	8.60	8.02	11.82	14.75	nu	10.80	3.12
$t_{1/2}\,\beta$ (min)	249.5	290.4	294.5	119.5	nu	238.5	81.9
Cl_T (ml/min)	110	185	123	319	nu	184	95
Vc (ml)	2646	5445	2905	7825	nu	4705	2433
Varea (ml)	39390	77250	51370	54920	nu	55730	15810
Vss (ml)	20520	49200	16570	14140	nu	25110	16280
AUC_∞ (µg*min/ml)	14.42	8.74	14.07	5.40	nu	10.66	4.36
$AUMC_\infty$ (mg*min^2/ml)	2.642	2.294	1.827	2.397	nu	1.751	1.061
MRT (min)	186.0	265.4	134.0	44.4	nu	157.4	92.7

Table 5.17 - Pharmacokinetic parameters obtained from the plasma concentration time data of the 5 mg/kg CAPA dose group (bi-exponential fit).

Parameters	Rat 1	Rat 2	Rat 3	Rat 4	Rat 5	Mean	SD
Weight (g)	322	314	314	310	321	316	5.1
Dose (mg)	6.44	6.28	6.28	6.2	6.42	6.32	0.10
Bi-exponential fit							
A (ng/ml)	3085	1677	845	3999	1639	2249	1268
B (ng/ml)	339.1	173.2	304.7	304.3	345.0	294.3	70.7
α (min^{-1})	0.141	0.214	0.080	0.192	0.201	0.166	0.055
β (min^{-1})	0.0074	0.0079	0.0081	0.0059	0.0063	0.0071	0.0009
k_{10} (min^{-1})	0.0506	0.0622	0.0240	0.0594	0.0312	0.0455	0.0171
k_{12} (min^{-1})	0.0775	0.1325	0.0370	0.1190	0.1352	0.1002	0.0422
k_{21} (min^{-1})	0.0207	0.0272	0.0270	0.0190	0.0405	0.0269	0.0085
$t_{1/2}\alpha$ (min)	4.90	3.24	8.66	3.61	3.45	4.77	2.27
$t_{1/2}\beta$ (min)	93.7	87.7	85.6	117.4	110.0	98.9	14.1
Cl_T (ml/min)	95.2	211.0	130.4	85.6	100.7	124.6	51.1
Vc (ml)	1881	3394	5461	1440	3228	3081	1575
Varea (ml)	12870	26710	16100	14500	15990	17230	5460
Vss (ml)	8930	19930	12920	10450	14010	13250	4240
AUC_∞ (µg*min/ml)	67.64	29.76	48.17	72.42	63.73	56.34	17.42
$AUMC_\infty$ (mg*min^2/ml)	6.346	2.812	4.775	8.843	8.860	6.327	2.622
MRT (min)	93.8	94.5	99.1	122.1	139.0	109.7	20.1

Table 5.18 - Pharmacokinetic parameters obtained from the plasma concentration time data of the 20 mg/kg CAPE dose group (bi-exponential fit).

Parameters	*20 mg/kg*		*10 mg/kg*		*5 mg/kg*	
	Mean ind.	Mean Cp	Mean ind.	Mean Cp	Mean ind.	Mean Cp
Bi-exponential fit						
A (ng/ml)	1674	1526	716.3	700.9	417.0	443.3
B (ng/ml)	383.5	384	56.87	58.68	11.83	16.97
α (min^{-1})	0.087	0.074	0.086	0.089	0.068	0.085
β (min^{-1})	0.0029	0.0033	0.0026	0.002	0.0034	0.0033
k_{10} (min^{-1})	0.0147	0.0140	0.0276	0.0205	0.0397	0.0445
k_{12} (min^{-1})	0.0586	0.0455	0.0520	0.0618	0.0261	0.0372
k_{21} (min^{-1})	0.0161	0.0170	0.0093	0.0087	0.0054	0.0063
$t_{1/2}\alpha$ (min)	9.75	9.42	8.27	7.79	10.80	8.18
$t_{1/2}\beta$ (min)	257.5	211.0	286.6	345.4	238.5	208.4
Cl_T (ml/min)	45.83	46.25	115.2	85.4	184	158
Vc (ml)	3161	3338	4879	4173	4705	3539
Varea (ml)	14900	14020	43620	40680	55730	47390
Vss (ml)	15570	12060	31040	33730	25110	24350
AUC_∞ (µg*min/ml)	145.8	137.9	33.38	37.12	10.66	10.33
$AUMC_\infty$ (mg*min^2/ml)	44.08	35.54	11.93	14.66	1.751	1.596
MRT (min)	319.1	260.7	311.2	394.9	157.4	154.5

Table 5.19 – Pharmacokinetic parameters obtained from the bi-exponential fit of the plasma concentration time profiles of the CAPA dose groups. Comparison between the average of the individually obtained pharmacokinetic parameters (mean ind.) and the parameters obtained from the averaged plasma concentration time profiles (mean Cp).

Parameters	Mean ind.	Mean Cp
Bi-exponential fit		
A (ng/ml)	2249	2305
B (ng/ml)	294.3	310.4
α (min^{-1})	0.166	0.176
β (min^{-1})	0.0071	0.0070
k_{10} (min^{-1})	0.0455	0.0450
k_{12} (min^{-1})	0.1002	0.1100
k_{21} (min^{-1})	0.0269	0.0270
$t_{1/2}\alpha$ (min)	4.77	3.92
$t_{1/2}\beta$ (min)	98.9	99.0
Cl_T (ml/min)	124.6	110.0
Vc (ml)	3081	2416
Varea (ml)	17230	15740
Vss (ml)	13250	12280
AUC_∞ (µg*min/ml)	56.34	57.38
$AUMC_\infty$ (mg*min^2/ml)	6.327	6.398
MRT (min)	109.7	111.5

Table 5.20 – Pharmacokinetic parameters obtained from the bi-exponential fit of the plasma concentration time profiles of the 20 mg/kg CAPE dose group. Comparison between the average of the individually obtained pharmacokinetic parameters (mean ind.) and the parameters obtained from the averaged plasma concentration time profiles (mean Cp).

	20 mg/kg (AVG ± SD)	10 mg/kg (AVG ± SD)	5 mg/kg (AVG ± SD)	ANOVA P Value
Bi-exponential fit				
$t_{1/2}$ (min)	257.5 ± 82.1	286.6 ± 73.9	238.5 ± 81.9	> 0.05
Cl_T (ml/min)	45.83 ± 12.38	115.2 ± 51.9	184.1 ± 95.4	< 0.05
Varea (ml)	14900 ± 10500	43620 ± 10530	55720 ± 15810	< 0.05
AUC_∞ (µg*min/ml)	145.8 ± 30.4	33.38 ± 18.59	10.66 ± 4.36	< 0.05
MRT (min)	319.1 ± 98.1	311.2 ± 135.7	157.4 ± 92.7	> 0.05

Table 5.21 – Averaged pharmacokinetic parameters obtained from the bi-exponential fit of the individual plasma concentration time profiles for the 3 CAPA dose groups. $P < 0.05$ was considered significant.

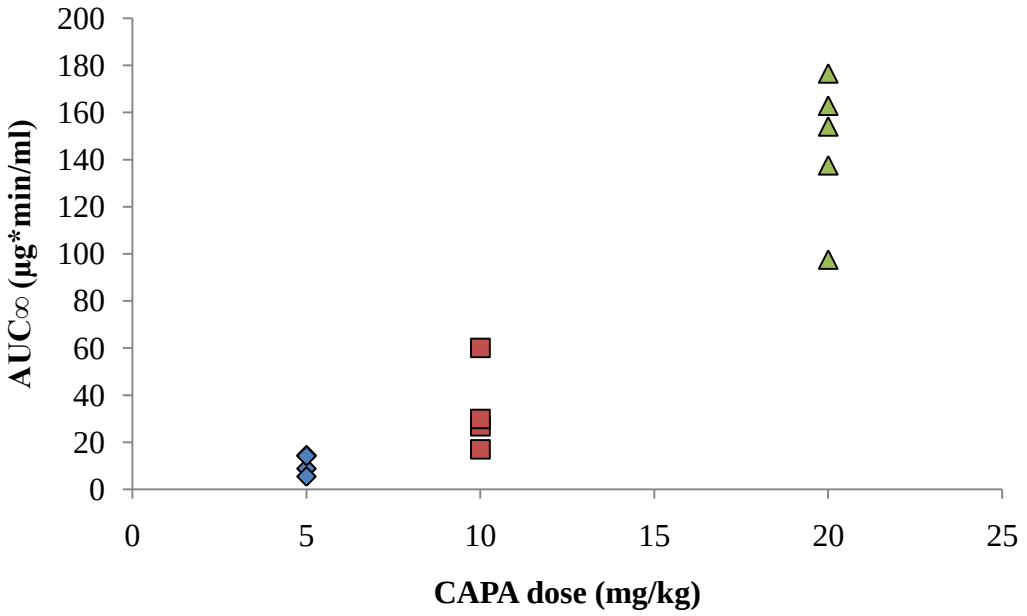

Figure 5.17 – Relationship between administered dose of CAPA and resulting AUC_{∞} calculated from the bi-exponential fit.

Parameters	*20 mg/kg* NCA	Fit	*10 mg/kg* NCA	Fit	*5 mg/kg* NCA	Fit
$t_{1/2}$ (min)	255.1	257.5	295.8	286.6	243.2	238.5
Cl_T (ml/min)	45.02	45.83	102.6	115.2	156.1	184
Varea (ml)	17750	14900	40360	43620	52420	55730
AUC_∞ (µg*min/ml)	148.4	145.8	39.15	33.38	11.74	10.66
MRT (min)	301.5	319.1	314.6	311.2	156.6	157.4

Table 5.22 – Mean pharmacokinetic parameters obtained via non-compartmental analysis (NCA) and bi-exponential fit to the two compartment model (Fit) of the CAPA plasma concentration time profiles. Elimination half-life ($t_{1/2}$), total clearance (Cl_T), volume of distribution (Varea), area under the curve from time zero to infinity (AUC_∞) and mean residence time (MRT) are shown.

Parameters	*CAPE 20 mg/kg* NCA	Fit
$t_{1/2}$ (min)	92.3	98.9
Cl_T (ml/min)	120.0	124.6
Varea (ml)	15280	17230
AUC_∞ (µg*min/ml)	59.29	56.34
MRT (min)	107.4	109.7

Table 5.23 – Mean pharmacokinetic parameters obtained via non compartmental analysis (NCA) and bi-exponential fit to the two compartment model (Fit) of the 20 mg/kg CAPE plasma concentration time profiles. Elimination half-life ($t_{1/2}$), total clearance (Cl_T), volume of distribution (Varea), area under the curve from time zero to infinity (AUC_∞) and mean residence time (MRT) are shown.

5.4 – DISCUSSION AND CONCLUSIONS

The pharmacokinetic properties of CAPA were investigated at 20 mg/kg, 10 mg/kg and 5 mg/kg doses. CAPE was investigated at 20 mg/kg. These doses were selected based on the previous pharmacokinetic investigation of CAPE. Dose proportionality was not observed for the three doses of CAPA. AUC_{∞} increased more than three-fold when dose increased from 5 to 10 mg/kg. A similar three-fold increase in AUC_{∞} was also seen when dose was raised from 10 to 20 mg/kg. Increases in dose were met with significant decreases in volume of distribution and in clearance. There were no significant differences seen in half-life of CAPA between the three doses. The lower volume of distribution at higher doses suggests that more of the compound is available in the central compartment and that distribution to the tissues is higher at lower concentrations. It is possible that there is significant tissue binding of CAPA in the periphery and that this binding is saturable. This would account for the higher volume of distribution at lower doses, as a higher proportion of CAPA would be bound in the tissues, preventing it from transferring back to the central compartment. If this binding is saturated at the higher doses, a higher proportion of CAPA would then be free to transfer back to the central compartment after the initial distribution, thus lowering the apparent volume of distribution. This possibility would also mean that the first order transfer rate constant from the periphery to the central compartment (k_{21}) would increase as dose is increased. This increase was observed in our experiments. There was a significant difference in k_{21} between the three tested doses of CAPA ($P < 0.05$). Further investigation is needed to determine whether this tissue binding is responsible for the non-linear pharmacokinetics observed.

When comparing the 20 mg/kg dose group of CAPA to the 20 mg/kg dose group of CAPE, it was seen that the half-life was CAPA was significantly higher than CAPE ($P < 0.05$). This was observed for both the non compartmental analysis and the 2 compartment analysis. CAPA has been shown to share a few of CAPE's multitude of beneficial properties. It is possible that CAPA's increased half-life over CAPE may allow it to exert its beneficial properties for a longer period of time. It remains to be seen if this improved half-life leads to improvements in efficacy.

Chapter 6 – Conclusions

CAPE has been shown to be an effective cytoprotectant against oxidative stress *in vitro* and against I/R injury *in vivo* despite having poor *in vitro* stability and short circulation half-life. CAPA is the amide analogue of CAPE and was synthesized to improve stability and to increase circulation half-life of the compound. An *in vitro* cytoprotection assay was developed and utilized to investigate whether CAPA retained CAPE's cytoprotective properties. Both compounds were then tested for *in vitro* stability in male Sprague-Dawley rat plasma. Finally a pharmacokinetic study was carried out in male Sprague Dawley rats to determine pharmacokinetic parameters for both CAPA and CAPE following intravenous bolus administration.

Synthesis and cytoprotective activity of CAPA and CAPA derivatives in HUVEC

CAPA and five catechol ring fluorinated derivatives were synthesized via Wittig reaction. CAPA and four of the derivatives showed no cytotoxicity in HUVEC up to 100 μM. CAPE showed significant toxicity when incubated in HUVEC at 20 μM for the same amount of time. This allows the possibility of higher dosing for CAPA over CAPE. CAPA was found to be the most cytoprotective derivative against hydrogen peroxide induced oxidative stress in HUVEC. Three of the fluorinated derivatives showed significant protective activity. Both CAPE and CAPA treated cells were able to significantly induce the expression of HO-1 over control with as little as 1 hour of exposure time. There were no significant differences found in HO-1 expression between cells treated with CAPE and CAPA beyond 2 hours of exposure time. These findings

suggest that the cells may not need to be continually exposed to CAPE or CAPA in order for a protective effect to be induced. There was no significant difference found in cytoprotective activity between CAPA and CAPE against hydrogen peroxide induced oxidative stress in HUVEC. These experiments show that amide derivatization does not compromise CAPE's protective activity in HUVEC.

Stability of CAPA in rat plasma

A validated HPLC method with UV detection was developed and used for the quantification of CAPA and CAPE following extraction from male Sprague-Dawley rat plasma. Stability of CAPA was tested at 25, 37 and 60 °C, and the stability of CAPE was tested at 4, 25 and 37 °C. CAPA exhibited a significantly longer half-life than CAPE at 25 °C (41.5 hours vs 0.35 hours) and 37 °C (10.0 hours vs 0.13 hours). CAPA was also shown to have a higher energy of activation than CAPE (22.1 kcal/mol vs 14.1 kcal/mol). It is hypothesized that the activity of esterase enzymes is responsible for CAPE's rapid decomposition and that CAPA's lack of an ester bond allowed for its longer half-life. CAPA showed only 8% decomposition after 7 hours at room temperature, suggesting that decomposition is negligible during sample handling (on ice) and sample storage (-80 °C). This information is useful for future pharmacokinetic studies as post collection compound stability is important for accurate analysis.

Pharmacokinetics of CAPA

Pharmacokinetic parameters of CAPA were investigated at 20 mg/kg, 10 mg/kg and 5 mg/kg following intravenous bolus administration to male Sprague-Dawley rats. The pharmacokinetic parameters of CAPE administered at 20 mg/kg were also determined. A LCMS method was developed, qualified and used for the quantification of CAPA and CAPE following extraction from rat blood samples. NCA and bi-exponential fit were employed to calculate the various pharmacokinetic parameters, with good agreement between the two analyses. Non linear pharmacokinetics were observed for CAPA as clearance and volume of distribution both decreased significantly with increasing dose. Dose proportionality was not observed for CAPA. It is possible that saturable tissue binding in the periphery is responsible for the non linear pharmacokinetics observed. There was no significant difference in half-life between the three doses of CAPA. CAPA at 20 mg/kg showed a significantly longer half-life than CAPE at 20 mg/kg (255 minutes vs 92 minutes, $P < 0.05$).

Summary

In conclusion, CAPA was synthesized in attempt to improve the stability of CAPE without compromising CAPEs cytoprotective activity. The cytoprotection studies show that amide derivatization did not alter CAPE's protective effects and that CAPA is transcriptionally active. The stability studies in rat plasma show that CAPA is indeed more stable than CAPE, evidenced by a significantly longer half-life at 25 °C and 37 °C. The pharmacokinetic studies show that CAPA remains in the circulation for a significantly longer period of time than CAPE. The longer elimination half-life from the systemic circulation of CAPA allows for extended exposure times compared to CAPE when administered at the same molar dose. Future studies should investigate the effect of CAPA and CAPE administration on animals experiencing I/R injury.

Bibliography

1. Murray, C.J., Lopez, A.D., *Alternative projections of mortality and disability by cause 1990-2020.* Global Burden of Disease Study, Lancet 349 (9064), 1997: p. 1498-1504.
2. Lopez, A.D., C.D. Mathers, M. Ezzati, D.T. Jamison, and C.J.L. Murray, *Measuring the Global Burden of Disease and Risk Factors, 1990-2001*. 2006.
3. Dorweiler, B., Pruefer, D., Andrasi, T.B., *Ischemia-Reperfusion Injury Pathophysiology and Clinical Implications.* European Journal of Trauma and Emergency Surgery, 2007. **33**: p. 600-612.
4. Jassem, W., S.V. Fuggle, M. Rela, D.D. Koo, and N.D. Heaton, *The role of mitochondria in ischemia/reperfusion injury.* Transplantation, 2002. **73**(4): p. 493-9.
5. Homer-Vanniasinkam, S., J.N. Crinnion, and M.J. Gough, *Post-ischaemic organ dysfunction: a review.* Eur J Vasc Endovasc Surg, 1997. **14**(3): p. 195-203.
6. Toledo-Pereyra, L.H., F. Lopez-Neblina, and A.H. Toledo, *Reactive oxygen species and molecular biology of ischemia/reperfusion.* Ann Transplant, 2004. **9**(1): p. 81-3.
7. Martindale, J.L. and N.J. Holbrook, *Cellular response to oxidative stress: Signaling for suicide and survival.* Journal of Cellular Physiology, 2002. **192**(1): p. 1-15.
8. Becker, L.B., *New concepts in reactive oxygen species and cardiovascular reperfusion physiology.* Cardiovascular Research, 2004. **61**(3): p. 461-470.
9. Flessas, II, A.E. Papalois, K. Toutouzas, F. Zagouri, and G.C. Zografos, *Effects of Lazaroids on Intestinal Ischemia and Reperfusion Injury in Experimental Models.* J Surg Res, 2010.
10. B. Dorweiler, e.a., *Ischemia-Reperfusion Injury Pathophysiology and Clinical Implications.* European Journal of Trauma and Emergency Surgery, 2007. **33**: p. 600-612.
11. Kilgore, K.S. and B.R. Lucchesi, *Reperfusion injury after myocardial infarction: the role of free radicals and the inflammatory response.* Clin Biochem, 1993. **26**(5): p. 359-70.
12. Hearse, D.J., *Reperfusion of the ischemic myocardium.* J Mol Cell Cardiol, 1977. **9**(8): p. 605-16.
13. Virmani, R., Kolodgie, F.D., Forman F.D., Farb, A., Jones, R.M., *Reperfusion injury in the ischemic myocardium.* Cardiovasc Pathol, 1992. **1**: p. 117-129.
14. Arumugam, T.V., I.A. Shiels, T.M. Woodruff, D.N. Granger, and S.M. Taylor, *The role of the complement system in ischemia-reperfusion injury.* Shock, 2004. **21**(5): p. 401-409.

15. Berthonneche, C., T. Sulpice, F. Boucher, L. Gouraud, J. de Leiris, S.E. O'Connor, J.M. Herbert, and P. Janiak, *New insights into the pathological role of TNF-alpha in early cardiac dysfunction and subsequent heart failure after infarction in rats.* Am J Physiol Heart Circ Physiol, 2004. **287**(1): p. H340-50.
16. Moro, C., M.G. Jouan, A. Rakotovao, M.C. Toufektsian, O. Ormezzano, N. Nagy, A. Tosaki, J. de Leiris, and F. Boucher, *Delayed expression of cytokines after reperfused myocardial infarction: possible trigger for cardiac dysfunction and ventricular remodeling.* Am J Physiol Heart Circ Physiol, 2007. **293**(5): p. H3014-9.
17. Gourdin, M.J., B. Bree, and M. De Kock, *The impact of ischaemia-reperfusion on the blood vessel.* Eur J Anaesthesiol, 2009. **26**(7): p. 537-47.
18. Arumugam, T.V., I.A. Shiels, T.M. Woodruff, D.N. Granger, and S.M. Taylor, *The role of the complement system in ischemia-reperfusion injury.* Shock, 2004. **21**(5): p. 401-9.
19. Shin, H.S., R. Snyderman, E. Friedman, A. Mellors, and M.M. Mayer, *Chemotactic and anaphylatoxic fragment cleaved from the fifth component of guinea pig complement.* Science, 1968. **162**(3851): p. 361-3.
20. Goldstein, I.M. and G. Weissmann, *Generation of C5-derived lysosomal enzyme-releasing activity (C5a) by lysates of leukocyte lysosomes.* J Immunol, 1974. **113**(5): p. 1583-8.
21. Sacks, T., C.F. Moldow, P.R. Craddock, T.K. Bowers, and H.S. Jacob, *Oxygen radicals mediate endothelial cell damage by complement-stimulated granulocytes. An in vitro model of immune vascular damage.* J Clin Invest, 1978. **61**(5): p. 1161-7.
22. Collard, C.D. and S. Gelman, *Pathophysiology, clinical manifestations, and prevention of ischemia-reperfusion injury.* Anesthesiology, 2001. **94**(6): p. 1133-8.
23. Sacks, T., C.F. Moldow, P.R. Craddock, T.K. Bowers, and H.S. Jacob, *Endothelial damage provoked by toxic oxygen radicals released from complement-triggered granulocytes.* Prog Clin Biol Res, 1978. **21**: p. 719-26.
24. Hess, M.L. and N.H. Manson, *Molecular oxygen: friend and foe. The role of the oxygen free radical system in the calcium paradox, the oxygen paradox and ischemia/reperfusion injury.* J Mol Cell Cardiol, 1984. **16**(11): p. 969-85.
25. Park, J.L. and B.R. Lucchesi, *Mechanisms of myocardial reperfusion injury.* Ann Thorac Surg, 1999. **68**(5): p. 1905-12.
26. Ambrosio, G. and I. Tritto, *Reperfusion injury: experimental evidence and clinical implications.* Am Heart J, 1999. **138**(2 Pt 2): p. S69-75.
27. Weisfeldt, M.L., J. Zweier, G. Ambrosio, L.C. Becker, and J.T. Flaherty, *Evidence that free radicals result in reperfusion injury in heart muscle.* Basic Life Sci, 1988. **49**: p. 911-9.
28. Becker, L.B., *New concepts in reactive oxygen species and cardiovascular reperfusion physiology.* Cardiovasc Res, 2004. **61**(3): p. 461-70.

29. Boveris, A. and B. Chance, *The mitochondrial generation of hydrogen peroxide. General properties and effect of hyperbaric oxygen.* Biochem J, 1973. **134**(3): p. 707-16.
30. Forman, H.J. and J.A. Kennedy, *Role of superoxide radical in mitochondrial dehydrogenase reactions.* Biochem Biophys Res Commun, 1974. **60**(3): p. 1044-50.
31. Weisiger, R.A. and I. Fridovich, *Mitochondrial superoxide simutase. Site of synthesis and intramitochondrial localization.* J Biol Chem, 1973. **248**(13): p. 4793-6.
32. Ichas, F. and J.P. Mazat, *From calcium signaling to cell death: two conformations for the mitochondrial permeability transition pore. Switching from low- to high-conductance state.* Biochimica Et Biophysica Acta, 1998. **1366**(1-2): p. 33-50.
33. Dubinsky, J.M. and Y. Levi, *Calcium-induced activation of the mitochondrial permeability transition in hippocampal neurons.* Journal of Neuroscience Research, 1998. **53**(6): p. 728-41.
34. McCully, J.D., H. Wakiyama, Y.J. Hsieh, M. Jones, and S. Levitsky, *Differential contribution of necrosis and apoptosis in myocardial ischemia-reperfusion injury.* Am J Physiol Heart Circ Physiol, 2004. **286**(5): p. H1923-35.
35. Luetjens, C.M., N.T. Bui, B. Sengpiel, G. Munstermann, M. Poppe, A.J. Krohn, E. Bauerbach, J. Krieglstein, and J.H. Prehn, *Delayed mitochondrial dysfunction in excitotoxic neuron death: cytochrome c release and a secondary increase in superoxide production.* J Neurosci, 2000. **20**(15): p. 5715-23.
36. Yang, J., X. Liu, K. Bhalla, C.N. Kim, A.M. Ibrado, J. Cai, T.I. Peng, D.P. Jones, and X. Wang, *Prevention of apoptosis by Bcl-2: release of cytochrome c from mitochondria blocked.* Science, 1997. **275**(5303): p. 1129-32.
37. Kluck, R.M., E. Bossy-Wetzel, D.R. Green, and D.D. Newmeyer, *The release of cytochrome c from mitochondria: a primary site for Bcl-2 regulation of apoptosis.* Science, 1997. **275**(5303): p. 1132-6.
38. Jiang, X. and X. Wang, *Cytochrome C-mediated apoptosis.* Annu Rev Biochem, 2004. **73**: p. 87-106.
39. Li, C. and R.M. Jackson, *Reactive species mechanisms of cellular hypoxia-reoxygenation injury.* Am J Physiol Cell Physiol, 2002. **282**(2): p. C227-41.
40. Berry, C.E. and J.M. Hare, *Xanthine oxidoreductase and cardiovascular disease: molecular mechanisms and pathophysiological implications.* J Physiol, 2004. **555**(Pt 3): p. 589-606.
41. Chambers, D.E., D.A. Parks, G. Patterson, R. Roy, J.M. McCord, S. Yoshida, L.F. Parmley, and J.M. Downey, *Xanthine oxidase as a source of free radical damage in myocardial ischemia.* J Mol Cell Cardiol, 1985. **17**(2): p. 145-52.
42. Schaffer, S.W., R.S. Roy, and J.M. McMcord, *Possible role for calmodulin in calcium paradox-induced heart failure.* Eur Heart J, 1983. **4 Suppl H**: p. 81-7.
43. Granger, D.N., M.E. Hollwarth, and D.A. Parks, *Ischemia-reperfusion injury: role of oxygen-derived free radicals.* Acta Physiol Scand Suppl, 1986. **548**: p. 47-63.

44. Jassem, W., S.V. Fuggle, M. Rela, D.D.H. Koo, and N.D. Heaton, *The role of mitochondria in ischemla/reperfusion injury.* Transplantation, 2002. **73**(4): p. 493-499.
45. Hensley, K., K.A. Robinson, S.P. Gabbita, S. Salsman, and R.A. Floyd, *Reactive oxygen species, cell signaling, and cell injury.* Free Radic Biol Med, 2000. **28**(10): p. 1456-62.
46. Dhalla, N.S., A.B. Elmoselhi, T. Hata, and N. Makino, *Status of myocardial antioxidants in ischemia-reperfusion injury.* Cardiovasc Res, 2000. **47**(3): p. 446-56.
47. Ceconi, C., A. Cargnoni, E. Pasini, E. Condorelli, S. Curello, and R. Ferrari, *Evaluation of phospholipid peroxidation as malondialdehyde during myocardial ischemia and reperfusion injury.* Am J Physiol, 1991. **260**(4 Pt 2): p. H1057-61.
48. Dixon, I.M., M. Kaneko, T. Hata, V. Panagia, and N.S. Dhalla, *Alterations in cardiac membrane Ca2+ transport during oxidative stress.* Mol Cell Biochem, 1990. **99**(2): p. 125-33.
49. Maxwell, S.R. and G.Y. Lip, *Reperfusion injury: a review of the pathophysiology, clinical manifestations and therapeutic options.* Int J Cardiol, 1997. **58**(2): p. 95-117.
50. Winquist, R.J. and S. Kerr, *Cerebral ischemia-reperfusion injury and adhesion.* Neurology, 1997. **49**(5 Suppl 4): p. S23-6.
51. Choudhury, N.A., S. Sakaguchi, K. Koyano, A.F. Matin, and H. Muro, *Free radical injury in skeletal muscle ischemia and reperfusion.* J Surg Res, 1991. **51**(5): p. 392-8.
52. Homer-Vanniasinkam S, G.M., *The Role of Leukotrienes in Controlling Post-Ischemic Skeletal Muscle Function.* Vasc Surg, 1991. **27**: p. 585–90.
53. Ceyran, H., F. Narin, N. Narin, H. Akgun, A.B. Ceyran, F. Ozturk, and Y. Akcali, *The effect of high dose melatonin on cardiac ischemia- reperfusion Injury.* Yonsei Med J, 2008. **49**(5): p. 735-41.
54. Rodriguez-Reynoso, S., C. Leal, E. Portilla-de Buen, J.C. Castillo, and F. Ramos-Solano, *Melatonin ameliorates renal ischemia/reperfusion injury.* J Surg Res, 2004. **116**(2): p. 242-7.
55. Korkmaz, A., *et al*., *The Protective Effects of Ascorbic Acid against Renal Ischemia-Reperfusion Injury in Male Rats* Renal Failure, 2009. **31**(1): p. 36-42.
56. Portella, A.O., E.F. Montero, L.F. Poli de Figueiredo, A.S. Bueno, A.A. Thurow, and F.G. Rodrigues, *Effects of N-acetylcysteine in hepatic ischemia-reperfusion injury during hemorrhagic shock.* Transplant Proc, 2004. **36**(4): p. 846-8.
57. Erturk, E., B. Cekic, S. Geze, M. Kosucu, I. Coskun, A. Eroglu, H. Ulusoy, A. Mentese, C. Karahan, and S. Kerimoglu, *Comparison of the effect of propofol and N-acetyl cysteine in preventing ischaemia-reperfusion injury.* Eur J Anaesthesiol, 2009. **26**(4): p. 279-84.
58. Korkmaz, A. and D. Kolankaya, *Protective Effect of Rutin on the Ischemia/Reperfusion Induced Damage in Rat Kidney.* J Surg Res, 2009.

59. Sehirli, A.O., G. Sener, and F. Ercan, *Protective Effects of Pycnogenol against Ischemia Reperfusion-Induced Oxidative Renal Injury in Rats.* Renal Failure, 2009. **31**(8): p. 690-697.
60. Cho, J.Y., I.S. Kim, Y.H. Jang, A.R. Kim, and S.R. Lee, *Protective effect of quercetin, a natural flavonoid against neuronal damage after transient global cerebral ischemia.* Neurosci Lett, 2006. **404**(3): p. 330-5.
61. Singh, D., V. Chander, and K. Chopra, *The effect of quercetin, a bioflavonoid on ischemia/reperfusion induced renal injury in rats.* Arch Med Res, 2004. **35**(6): p. 484-94.
62. Bartekova, M., S. Carnicka, D. Pancza, M. Ondrejcakova, A. Breier, and T. Ravingerova, *Acute treatment with polyphenol quercetin improves postischemic recovery of isolated perfused rat hearts after global ischemia.* Can J Physiol Pharmacol, 2010. **88**(4): p. 465-71.
63. Ray, P.S., G. Maulik, G.A. Cordis, A.A. Bertelli, A. Bertelli, and D.K. Das, *The red wine antioxidant resveratrol protects isolated rat hearts from ischemia reperfusion injury.* Free Radic Biol Med, 1999. **27**(1-2): p. 160-9.
64. Jiang, J., W. Wang, Y.J. Sun, M. Hu, F. Li, and D.Y. Zhu, *Neuroprotective effect of curcumin on focal cerebral ischemic rats by preventing blood-brain barrier damage.* Eur J Pharmacol, 2007. **561**(1-3): p. 54-62.
65. Jung, W.K., I. Choi, D.Y. Lee, S.S. Yea, Y.H. Choi, M.M. Kim, S.G. Park, S.K. Seo, S.W. Lee, C.M. Lee, Y.M. Park, and I.W. Choi, *Caffeic acid phenethyl ester protects mice from lethal endotoxin shock and inhibits lipopolysaccharide-induced cyclooxygenase-2 and inducible nitric oxide synthase expression in RAW 264.7 macrophages via the p38/ERK and NF-kappaB pathways.* Int J Biochem Cell Biol, 2008. **40**(11): p. 2572-82.
66. Kulisz, A., N. Chen, N.S. Chandel, Z. Shao, and P.T. Schumacker, *Mitochondrial ROS initiate phosphorylation of p38 MAP kinase during hypoxia in cardiomyocytes.* Am J Physiol Lung Cell Mol Physiol, 2002. **282**(6): p. L1324-9.
67. Samavati, L., M.M. Monick, S. Sanlioglu, G.R. Buettner, L.W. Oberley, and G.W. Hunninghake, *Mitochondrial K(ATP) channel openers activate the ERK kinase by an oxidant-dependent mechanism.* Am J Physiol Cell Physiol, 2002. **283**(1): p. C273-81.
68. Zhuang, S. and R.G. Schnellmann, *A death-promoting role for extracellular signal-regulated kinase.* J Pharmacol Exp Ther, 2006. **319**(3): p. 991-7.
69. Liu, J. and A. Lin, *Role of JNK activation in apoptosis: a double-edged sword.* Cell Res, 2005. **15**(1): p. 36-42.
70. Miwa, K., A. Igawa, K. Nakagawa, T. Hirai, and H. Inoue, *Consumption of vitamin E in coronary circulation in patients with variant angina.* Cardiovasc Res, 1999. **41**(1): p. 291-8.
71. Persad, S., S. Takeda, V. Panagia, and N.S. Dhalla, *Beta-adrenoceptor-linked signal transduction in ischemic-reperfused heart and scavenging of oxyradicals.* J Mol Cell Cardiol, 1997. **29**(2): p. 545-58.

72. Marchioli, R., *Antioxidant vitamins and prevention of cardiovascular disease: laboratory, epidemiological and clinical trial data.* Pharmacol Res, 1999. **40**(3): p. 227-38.
73. Tribble, D.L., *AHA Science Advisory. Antioxidant consumption and risk of coronary heart disease: emphasison vitamin C, vitamin E, and beta-carotene: A statement for healthcare professionals from the American Heart Association.* Circulation, 1999. **99**(4): p. 591-5.
74. Land, W., H. Schneeberger, S. Schleibner, W.D. Illner, D. Abendroth, G. Rutili, K.E. Arfors, and K. Messmer, *The beneficial effect of human recombinant superoxide dismutase on acute and chronic rejection events in recipients of cadaveric renal transplants.* Transplantation, 1994. **57**(2): p. 211-7.
75. Flaherty, J.T., B. Pitt, J.W. Gruber, R.R. Heuser, D.A. Rothbaum, L.R. Burwell, B.S. George, D.J. Kereiakes, D. Deitchman, N. Gustafson, and *et al*., *Recombinant human superoxide dismutase (h-SOD) fails to improve recovery of ventricular function in patients undergoing coronary angioplasty for acute myocardial infarction.* Circulation, 1994. **89**(5): p. 1982-91.
76. Sanhueza, J., J. Valdes, R. Campos, A. Garrido, and A. Valenzuela, *Changes in the xanthine dehydrogenase/xanthine oxidase ratio in the rat kidney subjected to ischemia-reperfusion stress: preventive effect of some flavonoids.* Res Commun Chem Pathol Pharmacol, 1992. **78**(2): p. 211-8.
77. Necas, J., L. Bartosikova, T. Florian, J. Klusakova, V. Suchy, E.M. Naggar, E. Janostikova, T. Bartosik, and M. Liskova, *[Protective effects of the flavonoids osajin and pomiferin on heart ischemia-reperfusion]*. Ceska Slov Farm, 2006. **55**(4): p. 168-74.
78. Zhang, D.L., Y.T. Zhang, J.J. Yin, and B.L. Zhao, *Oral administration of Crataegus flavonoids protects against ischemia/reperfusion brain damage in gerbils.* J Neurochem, 2004. **90**(1): p. 211-9.
79. Viuda-Martos, M., Y. Ruiz-Navajas, J. Fernandez-Lopez, and J.A. Perez-Alvarez, *Functional properties of honey, propolis, and royal jelly.* J Food Sci, 2008. **73**(9): p. R117-24.
80. Salatino, A., C.C. Fernandes-Silva, A.A. Righi, and M.L. Salatino, *Propolis research and the chemistry of plant products.* Nat Prod Rep, 2011. **28**(5): p. 925-36.
81. Ozer, M.K., H. Parlakpinar, and A. Acet, *Reduction of ischemia--reperfusion induced myocardial infarct size in rats by caffeic acid phenethyl ester (CAPE).* Clin Biochem, 2004. **37**(8): p. 702-5.
82. Huang, S.S., S.M. Liu, S.M. Lin, P.H. Liao, R.H. Lin, Y.C. Chen, C.L. Chih, and S.K. Tsai, *Antiarrhythmic effect of caffeic acid phenethyl ester (CAPE) on myocardial ischemia/reperfusion injury in rats.* Clin Biochem, 2005. **38**(10): p. 943-7.
83. Shi, Y., X. Wu, Y. Gong, Y. Qiu, H. Zhang, Z. Huang, and K. Su, *Protective effects of caffeic acid phenethyl ester on retinal ischemia/reperfusion injury in rats.* Curr Eye Res, 2010. **35**(10): p. 930-7.

84. Roso, N.C., R.R. Correa, Y.M. Castiglia, L.R. Carvalho, L.M. Scatena, A.V. de Souza, C.C. de Oliveira, and P.T. Vianna, *Caffeic acid phenethyl ester effects in the kidney during ischemia and reperfusion in rats anesthetized with isoflurane.* Transplant Proc, 2012. **44**(5): p. 1211-3.
85. Ilhan, A., U. Koltuksuz, S. Ozen, E. Uz, H. Ciralik, and O. Akyol, *The effects of caffeic acid phenethyl ester (CAPE) on spinal cord ischemia/reperfusion injury in rabbits.* Eur J Cardiothorac Surg, 1999. **16**(4): p. 458-63.
86. Koltuksuz, U., S. Ozen, E. Uz, M. Aydinc, A. Karaman, A. Gultek, O. Akyol, M.H. Gursoy, and E. Aydin, *Caffeic acid phenethyl ester prevents intestinal reperfusion injury in rats.* J Pediatr Surg, 1999. **34**(10): p. 1458-62.
87. Koltuksuz, U., M.K. Irmak, A. Karaman, E. Uz, A. Var, H. Ozyurt, and O. Akyol, *Testicular nitric oxide levels after unilateral testicular torsion/detorsion in rats pretreated with caffeic acid phenethyl ester.* Urol Res, 2000. **28**(6): p. 360-3.
88. Natarajan, K., S. Singh, T.R. Burke, Jr., D. Grunberger, and B.B. Aggarwal, *Caffeic acid phenethyl ester is a potent and specific inhibitor of activation of nuclear transcription factor NF-kappa B.* Proc Natl Acad Sci U S A, 1996. **93**(17): p. 9090-5.
89. Abdel-Latif, M.M., H.J. Windle, B.S. Homasany, K. Sabra, and D. Kelleher, *Caffeic acid phenethyl ester modulates Helicobacter pylori-induced nuclear factor-kappa B and activator protein-1 expression in gastric epithelial cells.* Br J Pharmacol, 2005. **146**(8): p. 1139-47.
90. Lee, Y., D.H. Shin, J.H. Kim, S. Hong, D. Choi, Y.J. Kim, M.K. Kwak, and Y. Jung, *Caffeic acid phenethyl ester-mediated Nrf2 activation and IkappaB kinase inhibition are involved in NFkappaB inhibitory effect: structural analysis for NFkappaB inhibition.* Eur J Pharmacol, 2010. **643**(1): p. 21-8.
91. Ang, E.S., N.J. Pavlos, L.Y. Chai, M. Qi, T.S. Cheng, J.H. Steer, D.A. Joyce, M.H. Zheng, and J. Xu, *Caffeic acid phenethyl ester, an active component of honeybee propolis attenuates osteoclastogenesis and bone resorption via the suppression of RANKL-induced NF-kappaB and NFAT activity.* Journal of Cellular Physiology, 2009. **221**(3): p. 642-9.
92. Fitzpatrick, L.R., J. Wang, and T. Le, *Caffeic acid phenethyl ester, an inhibitor of nuclear factor-kappaB, attenuates bacterial peptidoglycan polysaccharide-induced colitis in rats.* J Pharmacol Exp Ther, 2001. **299**(3): p. 915-20.
93. Song, J.J., J.G. Cho, S.J. Hwang, C.G. Cho, S.W. Park, and S.W. Chae, *Inhibitory effect of caffeic acid phenethyl ester (CAPE) on LPS-induced inflammation of human middle ear epithelial cells.* Acta Otolaryngol, 2008. **128**(12): p. 1303-7.
94. Motawi, T.K., H.A. Darwish, and A.M. Abd El Tawab, *Effects of caffeic acid phenethyl ester on endotoxin-induced cardiac stress in rats: a possible mechanism of protection.* J Biochem Mol Toxicol, 2011. **25**(2): p. 84-94.
95. Chen, M.F., P.C. Keng, P.Y. Lin, C.T. Yang, S.K. Liao, and W.C. Chen, *Caffeic acid phenethyl ester decreases acute pneumonitis after irradiation in vitro and in vivo.* BMC Cancer, 2005. **5**: p. 158.

96. Tan, J., Z. Ma, L. Han, R. Du, L. Zhao, X. Wei, D. Hou, B.H. Johnstone, M.R. Farlow, and Y. Du, *Caffeic acid phenethyl ester possesses potent cardioprotective effects in a rabbit model of acute myocardial ischemia-reperfusion injury.* Am J Physiol Heart Circ Physiol, 2005. **289**(5): p. H2265-71.
97. Cakir, T., E. Ozkan, E. Dulundu, U. Topaloglu, A.O. Sehirli, F. Ercan, E. Sener, and G. Sener, *Caffeic acid phenethyl ester (CAPE) prevents methotrexate-induced hepatorenal oxidative injury in rats.* J Pharm Pharmacol, 2011. **63**(12): p. 1566-71.
98. Michaluart, P., J.L. Masferrer, A.M. Carothers, K. Subbaramaiah, B.S. Zweifel, C. Koboldt, J.R. Mestre, D. Grunberger, P.G. Sacks, T. Tanabe, and A.J. Dannenberg, *Inhibitory effects of caffeic acid phenethyl ester on the activity and expression of cyclooxygenase-2 in human oral epithelial cells and in a rat model of inflammation.* Cancer Res, 1999. **59**(10): p. 2347-52.
99. Watanabe, M.A., M.K. Amarante, B.J. Conti, and J.M. Sforcin, *Cytotoxic constituents of propolis inducing anticancer effects: a review.* J Pharm Pharmacol, 2011. **63**(11): p. 1378-86.
100. Grunberger, D., R. Banerjee, K. Eisinger, E.M. Oltz, L. Efros, M. Caldwell, V. Estevez, and K. Nakanishi, *Preferential cytotoxicity on tumor cells by caffeic acid phenethyl ester isolated from propolis.* Experientia, 1988. **44**(3): p. 230-2.
101. Lee, K.J., J.H. Choi, Y.P. Hwang, Y.C. Chung, and H.G. Jeong, *Protective effect of caffeic acid phenethyl ester on tert-butyl hydroperoxide-induced oxidative hepatotoxicity and DNA damage.* Food Chem Toxicol, 2008. **46**(7): p. 2445-50.
102. Chen, M.J., W.H. Chang, C.C. Lin, C.Y. Liu, T.E. Wang, C.H. Chu, S.C. Shih, and Y.J. Chen, *Caffeic acid phenethyl ester induces apoptosis of human pancreatic cancer cells involving caspase and mitochondrial dysfunction.* Pancreatology, 2008. **8**(6): p. 566-76.
103. Lin, W.L., W.H. Liang, Y.J. Lee, S.K. Chuang, and T.H. Tseng, *Antitumor progression potential of caffeic acid phenethyl ester involving p75(NTR) in C6 glioma cells.* Chem Biol Interact, 2010. **188**(3): p. 607-15.
104. Szliszka, E., Z.P. Czuba, J. Bronikowska, A. Mertas, A. Paradysz, and W. Krol, *Ethanolic Extract of Propolis Augments TRAIL-Induced Apoptotic Death in Prostate Cancer Cells.* Evid Based Complement Alternat Med, 2011. **2011**: p. 535172.
105. Lee, Y.J., P.H. Liao, W.K. Chen, and C.Y. Yang, *Preferential cytotoxicity of caffeic acid phenethyl ester analogues on oral cancer cells.* Cancer Lett, 2000. **153**(1-2): p. 51-6.
106. Chen, H.J., Ho, C.T., *Antioxidant Activities of Caffeic Acid and Its Related Hydroxycinnamic Acid Compounds.* Journal of Agricultural and Food Chemistry, 1997. **45**: p. 2374-2378
107. Gocer, H. and I. Gulcin, *Caffeic acid phenethyl ester (CAPE): correlation of structure and antioxidant properties.* Int J Food Sci Nutr, 2011. **62**(8): p. 821-5.

108. Lien, E.J., S. Ren, H.H. Bui, and R. Wang, *Quantitative structure-activity relationship analysis of phenolic antioxidants.* Free Radic Biol Med, 1999. **26**(3-4): p. 285-94.
109. Wang, T., L. Chen, W. Wu, Y. Long, and R. Wang, *Potential cytoprotection: antioxidant defence by caffeic acid phenethyl ester against free radical-induced damage of lipids, DNA, and proteins.* Can J Physiol Pharmacol, 2008. **86**(5): p. 279-87.
110. Bhimani, R.S., W. Troll, D. Grunberger, and K. Frenkel, *Inhibition of oxidative stress in HeLa cells by chemopreventive agents.* Cancer Res, 1993. **53**(19): p. 4528-33.
111. Gokalp, O., E. Uz, E. Cicek, H.R. Yilmaz, M.K. Ozer, A. Altunbas, and N. Ozcelik, *Ameliorating role of caffeic acid phenethyl ester (CAPE) against isoniazid-induced oxidative damage in red blood cells.* Mol Cell Biochem, 2006. **290**(1-2): p. 55-9.
112. Wang, X., S. Stavchansky, P.D. Bowman, and S.M. Kerwin, *Cytoprotective effect of caffeic acid phenethyl ester (CAPE) and catechol ring-fluorinated CAPE derivatives against menadione-induced oxidative stress in human endothelial cells.* Bioorg Med Chem, 2006. **14**(14): p. 4879-87.
113. Bolli, R., L. Becker, G. Gross, R. Mentzer, Jr., D. Balshaw, and D.A. Lathrop, *Myocardial protection at a crossroads: the need for translation into clinical therapy.* Circulation Research, 2004. **95**(2): p. 125-34.
114. Pasupathy, S. and S. Homer-Vanniasinkam, *Ischaemic preconditioning protects against ischaemia/reperfusion injury: emerging concepts.* Eur J Vasc Endovasc Surg, 2005. **29**(2): p. 106-15.
115. Zeynalov, E., Z.A. Shah, R.C. Li, and S. Dore, *Heme oxygenase 1 is associated with ischemic preconditioning-induced protection against brain ischemia.* Neurobiol Dis, 2009. **35**(2): p. 264-9.
116. Panchenko, M.V., H.W. Farber, and J.H. Korn, *Induction of heme oxygenase-1 by hypoxia and free radicals in human dermal fibroblasts.* Am J Physiol Cell Physiol, 2000. **278**(1): p. C92-C101.
117. Christou, H., N. Bailey, M.S. Kluger, S.A. Mitsialis, and S. Kourembanas, *Extracellular acidosis induces heme oxygenase-1 expression in vascular smooth muscle cells.* Am J Physiol Heart Circ Physiol, 2005. **288**(6): p. H2647-52.
118. Gozzelino, R., V. Jeney, and M.P. Soares, *Mechanisms of cell protection by heme oxygenase-1.* Annu Rev Pharmacol Toxicol, 2010. **50**: p. 323-54.
119. Alam, J., D. Stewart, C. Touchard, S. Boinapally, A.M. Choi, and J.L. Cook, *Nrf2, a Cap'n'Collar transcription factor, regulates induction of the heme oxygenase-1 gene.* J Biol Chem, 1999. **274**(37): p. 26071-8.
120. Choi, D., J. Han, Y. Lee, J. Choi, S. Han, S. Hong, H. Jeon, Y.M. Kim, and Y. Jung, *Caffeic acid phenethyl ester is a potent inhibitor of HIF prolyl hydroxylase: structural analysis and pharmacological implication.* J Nutr Biochem, 2010. **21**(9): p. 809-17.

121. Scapagnini, G., R. Foresti, V. Calabrese, A.M. Giuffrida Stella, C.J. Green, and R. Motterlini, *Caffeic acid phenethyl ester and curcumin: a novel class of heme oxygenase-1 inducers.* Mol Pharmacol, 2002. **61**(3): p. 554-61.
122. Wu, M.L., Y.C. Ho, and S.F. Yet, *A central role of heme oxygenase-1 in cardiovascular protection.* Antioxid Redox Signal, 2011. **15**(7): p. 1835-46.
123. Chen, M.C., Y.Y. Ye, G. Ji, and J.W. Liu, *Hesperidin upregulates heme oxygenase-1 to attenuate hydrogen peroxide-induced cell damage in hepatic L02 cells.* J Agric Food Chem, 2010. **58**(6): p. 3330-5.
124. Ke, B., X.D. Shen, F. Gao, B. Qiao, H. Ji, R.W. Busuttil, H.D. Volk, and J.W. Kupiec-Weglinski, *Small interfering RNA targeting heme oxygenase-1 (HO-1) reinforces liver apoptosis induced by ischemia-reperfusion injury in mice: HO-1 is necessary for cytoprotection.* Human Gene Therapy, 2009. **20**(10): p. 1133-42.
125. Takagi, T., Y. Naito, H. Okada, T. Ishii, K. Mizushima, S. Akagiri, S. Adachi, O. Handa, S. Kokura, H. Ichikawa, K. Itoh, M. Yamamoto, H. Matsui, and T. Yoshikawa, *Lansoprazole, a proton pump inhibitor, mediates anti-inflammatory effect in gastric mucosal cells through the induction of heme oxygenase-1 via activation of NF-E2-related factor 2 and oxidation of kelch-like ECH-associating protein 1.* J Pharmacol Exp Ther, 2009. **331**(1): p. 255-64.
126. Hwang, Y.P., H.J. Yun, H.K. Chun, Y.C. Chung, H.K. Kim, M.H. Jeong, T.R. Yoon, and H.G. Jeong, *Protective mechanisms of 3-caffeoyl, 4-dihydrocaffeoyl quinic acid from Salicornia herbacea against tert-butyl hydroperoxide-induced oxidative damage.* Chem Biol Interact, 2009. **181**(3): p. 366-76.
127. Amersi, F., R. Buelow, H. Kato, B. Ke, A.J. Coito, X.D. Shen, D. Zhao, J. Zaky, J. Melinek, C.R. Lassman, J.K. Kolls, J. Alam, T. Ritter, H.D. Volk, D.G. Farmer, R.M. Ghobrial, R.W. Busuttil, and J.W. Kupiec-Weglinski, *Upregulation of heme oxygenase-1 protects genetically fat Zucker rat livers from ischemia/reperfusion injury.* J Clin Invest, 1999. **104**(11): p. 1631-9.
128. Katori, M., R. Buelow, B. Ke, J. Ma, A.J. Coito, S. Iyer, D. Southard, R.W. Busuttil, and J.W. Kupiec-Weglinski, *Heme oxygenase-1 overexpression protects rat hearts from cold ischemia/reperfusion injury via an antiapoptotic pathway.* Transplantation, 2002. **73**(2): p. 287-92.
129. Tsuchihashi, S., T. Tamaki, M. Tanaka, A. Kawamura, T. Kaizu, A. Ikeda, and A. Kakita, *Pyrrolidine dithiocarbamate provides protection against hypothermic preservation and transplantation injury in the rat liver: the role of heme oxygenase-1.* Surgery, 2003. **133**(5): p. 556-67.
130. Tullius, S.G., M. Nieminen-Kelha, U. Bachmann, A. Reutzel-Selke, S. Jonas, J. Pratschke, W.O. Bechstein, P. Reinke, R. Buelow, P. Neuhaus, and H. Volk, *Induction of heme-oxygenase-1 prevents ischemia/reperfusion injury and improves long-term graft outcome in rat renal allografts.* Transplant Proc, 2001. **33**(1-2): p. 1286-7.
131. Ollinger, R. and J. Pratschke, *Role of heme oxygenase-1 in transplantation.* Transpl Int, 2010. **23**(11): p. 1071-81.

132. Fenton, H., *Oxidation of tartaric acid in the presence of iron.* J Chem Soc. (London), 1894. **65**: p. 899-910.
133. Soares, M.P., Y. Lin, J. Anrather, E. Csizmadia, K. Takigami, K. Sato, S.T. Grey, R.B. Colvin, A.M. Choi, K.D. Poss, and F.H. Bach, *Expression of heme oxygenase-1 can determine cardiac xenograft survival.* Nat Med, 1998. **4**(9): p. 1073-7.
134. Soares, M.P., M.P. Seldon, I.P. Gregoire, T. Vassilevskaia, P.O. Berberat, J. Yu, T.Y. Tsui, and F.H. Bach, *Heme oxygenase-1 modulates the expression of adhesion molecules associated with endothelial cell activation.* J Immunol, 2004. **172**(6): p. 3553-63.
135. Silva, G., A. Cunha, I.P. Gregoire, M.P. Seldon, and M.P. Soares, *The antiapoptotic effect of heme oxygenase-1 in endothelial cells involves the degradation of p38 alpha MAPK isoform.* J Immunol, 2006. **177**(3): p. 1894-903.
136. Stocker, R., Y. Yamamoto, A.F. McDonagh, A.N. Glazer, and B.N. Ames, *Bilirubin is an antioxidant of possible physiological importance.* Science, 1987. **235**(4792): p. 1043-6.
137. Xie, C., N. Zhang, H. Zhou, J. Li, Q. Li, T. Zarubin, S.C. Lin, and J. Han, *Distinct roles of basal steady-state and induced H-ferritin in tumor necrosis factor-induced death in L929 cells.* Mol Cell Biol, 2005. **25**(15): p. 6673-81.
138. Zhang, X., P. Shan, D. Jiang, P.W. Noble, N.G. Abraham, A. Kappas, and P.J. Lee, *Small interfering RNA targeting heme oxygenase-1 enhances ischemia-reperfusion-induced lung apoptosis.* J Biol Chem, 2004. **279**(11): p. 10677-84.
139. Ali, F., S.S. Hamdulay, A.R. Kinderlerer, J.J. Boyle, E.A. Lidington, T. Yamaguchi, M.P. Soares, D.O. Haskard, A.M. Randi, and J.C. Mason, *Statin-mediated cytoprotection of human vascular endothelial cells: a role for Kruppel-like factor 2-dependent induction of heme oxygenase-1.* J Thromb Haemost, 2007. **5**(12): p. 2537-46.
140. Shen, X.D., B. Ke, Y. Zhai, F. Gao, R.W. Busuttil, G. Cheng, and J.W. Kupiec-Weglinski, *Toll-like receptor and heme oxygenase-1 signaling in hepatic ischemia/reperfusion injury.* American Journal of Transplantation, 2005. **5**(8): p. 1793-800.
141. Bhaskaran, M., N. Radhakrishnan, H. Patni, P. Singh, A.N. Chaudhary, and P.C. Singhal, *Dialysis membrane-induced oxidative stress: role of heme oxygenase-1.* Nephron Exp Nephrol, 2007. **105**(1): p. e24-32.
142. Wang, X., S. Stavchansky, B. Zhao, J.A. Bynum, S.M. Kerwin, and P.D. Bowman, *Cytoprotection of human endothelial cells from menadione cytotoxicity by caffeic acid phenethyl ester: the role of heme oxygenase-1.* Eur J Pharmacol, 2008. **591**(1-3): p. 28-35.
143. Wang, X., P.D. Bowman, S.M. Kerwin, and S. Stavchansky, *Stability of caffeic acid phenethyl ester and its fluorinated derivative in rat plasma.* Biomed Chromatogr, 2007. **21**(4): p. 343-50.
144. Wang, X., J. Pang, J.A. Maffucci, D.S. Pade, R.A. Newman, S.M. Kerwin, P.D. Bowman, and S. Stavchansky, *Pharmacokinetics of caffeic acid phenethyl ester*

and its catechol-ring fluorinated derivative following intravenous administration to rats. Biopharm Drug Dispos, 2009. **30**(5): p. 221-8.
145. *Lange's Handbook of Chemistry, 15th ed.*, ed. J.A. Dean. 1999, New York: McGraw-Hill.
146. Hagmann, W.K., *The many roles for fluorine in medicinal chemistry.* J Med Chem, 2008. **51**(15): p. 4359-69.
147. Shah, P. and A.D. Westwell, *The role of fluorine in medicinal chemistry.* J Enzyme Inhib Med Chem, 2007. **22**(5): p. 527-40.
148. Mira, L., M.T. Fernandez, M. Santos, R. Rocha, M.H. Florencio, and K.R. Jennings, *Interactions of flavonoids with iron and copper ions: a mechanism for their antioxidant activity.* Free Radic Res, 2002. **36**(11): p. 1199-208.
149. Sestili, P., G. Diamantini, A. Bedini, L. Cerioni, I. Tommasini, G. Tarzia, and O. Cantoni, *Plant-derived phenolic compounds prevent the DNA single-strand breakage and cytotoxicity induced by tert-butylhydroperoxide via an iron-chelating mechanism.* Biochem J, 2002. **364**(Pt 1): p. 121-8.
150. Son, S., Lewis B., *Free Radical Scavenging and Antioxidative Activity of Caffeic Acid Amide and Ester Analogues: Structure-Activity Relationship.* J. Agric. Food Chem., 2002. **50**(3): p. 468-472.
151. Naito, Y., M. Sugiura, Y. Yamaura, C. Fukaya, K. Yokoyama, Y. Nakagawa, T. Ikeda, M. Senda, and T. Fujita, *Quantitative structure-activity relationship of catechol derivatives inhibiting 5-lipoxygenase.* Chem Pharm Bull (Tokyo), 1991. **39**(7): p. 1736-45.
152. Rajan, P., I. Vedernikova, P. Cos, D.V. Berghe, K. Augustyns, and A. Haemers, *Synthesis and evaluation of caffeic acid amides as antioxidants.* Bioorg Med Chem Lett, 2001. **11**(2): p. 215-7.
153. Nishioka, T., *Isolation and Activity of N-p-Coumaroyltyramine, an α-Glucosidase In hibitor in Welsh Onion (Allium fistulosum).* Biosci. Biotech. Biochem., 1997. **61**(7): p. 1138-1141.
154. Chen, M., Cho SD., *et al*., *One-Pot Synthesis of Pyridazino[1,4]oxazin-3-ones* Synthetic Communications, 2004. **34**(8): p. 1399-1405.
155. Laurent, S., Boissier, J.. *et al*, *Synthesis of "Trioxaquantel" Derivatives as Potential New Antischistosomal Drugs.* Eur. J. Org. Chem., 2008(5).
156. Boyle, E.M., Jr., T.H. Pohlman, C.J. Cornejo, and E.D. Verrier, *Endothelial cell injury in cardiovascular surgery: ischemia-reperfusion.* Ann Thorac Surg, 1996. **62**(6): p. 1868-75.
157. Arun K. Singhal, J.D.S., Sihem Boudina, Bharat Jaishy and Yan-Ting E. Shiu, *Role of Endothelial Cells in Myocardial Ischemia-Reperfusion Injury.* Vascular Disease Prevention, 2010. **7**: p. 1-14.
158. Frangogiannis, N.G., C.W. Smith, and M.L. Entman, *The inflammatory response in myocardial infarction.* Cardiovasc Res, 2002. **53**(1): p. 31-47.
159. Coudray, C., S. Pucheu, F. Boucher, J. de Leiris, and A. Favier, *Ischemia and reperfusion injury in isolated rat heart: effect of reperfusion duration on xanthine*

oxidase, lipid peroxidation, and enzyme antioxidant systems in myocardium. Basic Res Cardiol, 1992. **87**(5): p. 478-88.
160. Zweier, J.L., P. Kuppusamy, S. Thompson-Gorman, D. Klunk, and G.A. Lutty, *Measurement and characterization of free radical generation in reoxygenated human endothelial cells.* Am J Physiol, 1994. **266**(3 Pt 1): p. C700-8.
161. Davidson, S.M. and M.R. Duchen, *Endothelial mitochondria: contributing to vascular function and disease.* Circulation Research, 2007. **100**(8): p. 1128-41.
162. Quintero, M., S.L. Colombo, A. Godfrey, and S. Moncada, *Mitochondria as signaling organelles in the vascular endothelium.* Proc Natl Acad Sci U S A, 2006. **103**(14): p. 5379-84.
163. Pober, J.S., W. Min, and J.R. Bradley, *Mechanisms of endothelial dysfunction, injury, and death.* Annu Rev Pathol, 2009. **4**: p. 71-95.
164. Fedalen, P.A., V. Piacentino, 3rd, V. Jeevanandam, C. Fisher, J. Greene, K.B. Margulies, S.R. Houser, S. Furukawa, A.K. Singhal, and B.I. Goldman, *Pharmacologic pre-conditioning and controlled reperfusion prevent ischemia-reperfusion injury after 30 minutes of hypoxia/ischemia in porcine hearts.* J Heart Lung Transplant, 2003. **22**(11): p. 1234-44.
165. Mohara, J., I. Aguilera, B.I. Goldman, C.A. Fisher, J.P. Gaughan, J.R. Libonati, S. Furukawa, and A.K. Singhal, *Effects of nutrient and hemoglobin enriched cell free perfusates upon ex vivo isolated rat heart preparation.* ASAIO J, 2005. **51**(3): p. 288-95.
166. Mold, C. and C.A. Morris, *Complement activation by apoptotic endothelial cells following hypoxia/reoxygenation.* Immunology, 2001. **102**(3): p. 359-64.
167. Therade-Matharan, S., E. Laemmel, J. Duranteau, and E. Vicaut, *Reoxygenation after hypoxia and glucose depletion causes reactive oxygen species production by mitochondria in HUVEC.* Am J Physiol Regul Integr Comp Physiol, 2004. **287**(5): p. R1037-43.
168. Zhao, H., M. Miller, K. Pfeiffer, J.A. Buras, and G.L. Stahl, *Anoxia and reoxygenation of human endothelial cells decrease ceramide glucosyltransferase expression and activates caspases.* Faseb Journal, 2003. **17**(6): p. 723-4.
169. Wang, H.Y., X.L. Liu, and B.M. Jiang, *[Changes of nucleolin expression and cellular localization during HUVEC apoptosis induced by hydrogen peroxide]*. Zhong Nan Da Xue Xue Bao Yi Xue Ban, 2008. **33**(6): p. 488-93.
170. Chen, T., Z.P. Guo, X.Y. Jiao, Y.H. Zhang, J.Y. Li, and H.J. Liu, *Protective effects of peoniflorin against hydrogen peroxide-induced oxidative stress in human umbilical vein endothelial cells.* Can J Physiol Pharmacol, 2011. **89**(6): p. 445-53.
171. Zhang, L., Z.Z. Ma, Y.Y. Che, N. Li, and P.F. Tu, *Protective effect of a new amide compound from Pu-erh tea on human micro-vascular endothelial cell against cytotoxicity induced by hydrogen peroxide.* Fitoterapia, 2011. **82**(2): p. 267-71.

172. Chen, J., Y. Gu, Z. Shao, J. Luo, and Z. Tan, *Propofol protects against hydrogen peroxide-induced oxidative stress and cell dysfunction in human umbilical vein endothelial cells.* Mol Cell Biochem, 2010. **339**(1-2): p. 43-54.
173. Kumar, S., X. Sun, D.A. Wiseman, J. Tian, N.S. Umapathy, A.D. Verin, and S.M. Black, *Hydrogen peroxide decreases endothelial nitric oxide synthase promoter activity through the inhibition of Sp1 activity.* DNA Cell Biol, 2009. **28**(3): p. 119-29.
174. Kunduzova, O.R., P. Bianchi, A. Parini, and C. Cambon, *Hydrogen peroxide production by monoamine oxidase during ischemia/reperfusion.* Eur J Pharmacol, 2002. **448**(2-3): p. 225-30.
175. Li, W.M., H.T. Liu, X.Y. Li, J.Y. Wu, G. Xu, Y.Z. Teng, S.T. Ding, and C. Yu, *The effect of tetramethylpyrazine on hydrogen peroxide-induced oxidative damage in human umbilical vein endothelial cells.* Basic Clin Pharmacol Toxicol, 2010. **106**(1): p. 45-52.
176. Liu, H.T., W.M. Li, G. Xu, X.Y. Li, X.F. Bai, P. Wei, C. Yu, and Y.G. Du, *Chitosan oligosaccharides attenuate hydrogen peroxide-induced stress injury in human umbilical vein endothelial cells.* Pharmacol Res, 2009. **59**(3): p. 167-75.
177. Kirk, K.L., O. Olubajo, K. Buchhold, G.A. Lewandowski, F. Gusovsky, D. McCulloh, J.W. Daly, and C.R. Creveling, *Synthesis and adrenergic activity of ring-fluorinated phenylephrines.* J Med Chem, 1986. **29**(10): p. 1982-8.
178. Bakalbassis, E.G., A.T. Lithoxoidou, and A.P. Vafiadis, *Theoretical insights, in the liquid phase, into the antioxidant mechanism-related parameters in the 2-monosubstituted phenols.* J Phys Chem A, 2006. **110**(38): p. 11151-9.
179. Russo, A., R. Longo, and A. Vanella, *Antioxidant activity of propolis: role of caffeic acid phenethyl ester and galangin.* Fitoterapia, 2002. **73 Suppl 1**: p. S21-9.
180. Wang, J., Bell, L., *ADME-Enabling Technologies in Drug Design and Development*, ed. Z. D. 2012: Wiley.
181. Yang, J., G.A. Marriner, X. Wang, P.D. Bowman, S.M. Kerwin, and S. Stavchansky, *Synthesis of a series of caffeic acid phenethyl amide (CAPA) fluorinated derivatives: comparison of cytoprotective effects to caffeic acid phenethyl ester (CAPE).* Bioorg Med Chem, 2010. **18**(14): p. 5032-8.

Vita

John enrolled at the University of Texas at Arlington in 2003 and transferred to the University of Texas at Austin in 2004. Following completion of his Bachelor's of Science degree in Biochemistry in 2007, John joined the research laboratory of Dr Nicholas A. Peppas in the Department of Chemical Engineering as an undergraduate research assistant. He developed an interest in pharmaceutical research while working in this position. John joined the Pharmaceutics department at UT Austin in the summer of 2008 under the guidance of Professor Salomon Stavchansky. John has also worked on collaborative research projects with Dr Phillip D Bowman of the US Army Institute of Surgical Research. During his graduate studies, John has presented work at various national scientific meetings, published two manuscripts and has an additional manuscript submitted for publication.

Email contact - john.yang@utexas.edu

This dissertation was typed by the author